INSIGHTS INTO SOLUTE TRAFFICKING VIA THE MENINGEAL LYMPHATIC SYSTEM

BY

JAMES R. GOODMAN

A DISSERTATION

PRESENTED TO THE PROGRAM OF PHYSIOLOGY AND PHARMACOLOGY
AND THE OREGON HEALTH & SCIENCE UNIVERSITY SCHOOL OF MEDICINE
IN PARTIAL FULFILLMENT OF THE
REQUIREMENTS FOR THE DEGREE OF
DOCTOR OF PHILOSOPHY
MAY 2019

School of Medicine

Oregon Health & Science University

CERTIFICATE OF APPROVAL

This is to certify that the PhD dissertation of

James Robert Goodman

has been approved

Mentor: Jeffrey J. Iliff, PhD

Committee Chair: Daniel L. Marks, MD, PhD

Member: Amanda W. Lund, PhD

Member: Ian Martin, PhD

Member: Sue A. Aicher, PhD

Acknowledgments

In producing this dissertation, I am indebted to many individuals who selflessly shared their time, energy, and financial resources to aid me in my scientific endeavors.

First, I would like to thank my mentor, Dr. Jeff Iliff, who taught me to craft a narrative, to ask important questions, and to pursue the truth in all things. His guidance and mentorship greatly accelerated my ability to critically interpret scientific findings and to understand the framework of modern scientific inquiry. I would like to thank the other members of the Iliff lab, both past and present, including Matt Simon and Natalie Roese, Drs. Thierno Madjou Bah, Marquitta Smith, Marie Wang, Erin Boespflug, Selda Yildiz, and Eugene Cilento. Their good humor and scientific insights made the lab a wonderful place to work.

My scientific development was greatly aided by the advice and oversight of my Dissertation Advisory Committee, composed of Drs. Dan Marks, Amanda Lund, Ian Martin, and Jeff Iliff. In addition to their expertise in whole animal physiology, lymphatic biology, and neurodegeneration, they provided me with thoughtful feedback that improved the quality of my experiments and my scientific reasoning.

I would also like to thank all of the members of the Anesthesiology and Perioperative Medicine department, most of whom provided direct mentorship and scientific insight into my graduate studies, including Drs. Ines Koerner, Anusha Mishra, Wenri Zhang, Carmen Methner, Mike Hutchens. Their aid provided me with the conceptual and technical understanding of human and mouse physiology that was mission critical to my dissertation.

I must also acknowledge the invaluable scientific and career mentorship that I received from Drs. Edward Neuwelt and Leslie Muldoon, along with the past and present members of the Neuwelt Lab, including Drs. Prakash Ambady and Ramon Barajas, Cymon Kersch, Jessica Bills, Josh Robertson, Dan Schwartz, and Dree Anna Morris. Together, they embody a truly translational research program and ensure that there is never a dull moment on the 5th floor of Mackenzie Hall.

I am grateful for the expertise of Drs. Stefanie Kaech-Petrie, Aurelie Snyder, and Crystal Chaw, who invited me into the world of light microscopy, tolerated my wild experimental ideas, and moved a fluorescence dissection microscope across the OHSU campus so that I could accomplish a technically demanding experiment. Their enthusiasm for science is contagious and their esoteric knowledge of light microscopy knows no bounds.

I owe a great deal to the leadership of the MD/PhD program, Drs. David Jacoby and Dan Marks, who made themselves available at every moment that I sought their advice, who advocated for me when challenges arose, and who gave me the confidence to navigate the open waters of graduate school. I would also like to thank Johanna Colgrove and Alexis Young, the past and present coordinators of the MD/PhD program. Their meticulous attention to detail and thoughtful guidance kept me from disaster on too many occasions to count. I would also like to thank my physician-scientist comrades in my MD/PhD cohort, Sam Huang, Rachel Drake, and Ali Pincus, as well as Brad Weaver at the University of Utah. They made my experiments better through their ideas, listened keenly to my practice talks, and cheered me on through the highs and lows of graduate school.

An acknowledgements section would not be complete without mentioning my father and mother, Greg and Kathy, my siblings Emily and Dan, and grandparents Barbara, Robert, Peggy, and Pete. They've supported my growth as a person and physician scientist unconditionally, inspired me to push forward when I stalled, and reminded me to enjoy the journey.

Most importantly I would like to thank my wife, Jaiya Choles, who has always given me shelter from the storm. Throughout my graduate studies, I tested her patience through my singlemindedness and consistent lack of punctuality, which she suffered with grace. Without her unyielding encouragement and honest feedback, this work would have gone unfinished.

“The truth knocks on the door and you say, "Go away, I'm looking for the truth,"

and so it goes away. Puzzling.”

- Robert Pirsig

Zen and the Art of Motorcycle Maintenance

List of Abbreviations

AAV	Adeno-associated virus
Aβ	Amyloid beta
AD	Alzheimer's dementia
APP	Amyloid precursor protein
AQP1	Aquaporin-1
AQP4	Aquaporin-4
BBB	Blood Brain Barrier
CERAD	Consortium to Establish a Registry for Alzheimer's Dementia
CBF	Cerebral blood flow
CNS	Central nervous system
CSF	Cerebrospinal fluid
DCLN	Deep cervical lymph nodes
ECS	Extracellular space
eGFP	Enhanced green fluorescence protein
ELISA	Enzyme-linked immunosorbent assay
GFAP	Glial fibrillary acidic protein
ICP	Intracranial pressure
ISF	Interstitial fluid
LRP1	Low density lipoprotein receptor 1
LYVE1	Lymphatic vessel endothelial hyaluronan receptor 1
MRI	Magnetic resonance imaging
PDPN	Podoplanin
PROX1	Prospero homeobox 1
PS1	Presenilin
PVS	Perivascular space
SAS	Subarachnoid space
VEGFC	Vascular endothelial growth factor C
VEGFR3	Vascular endothelial growth factor receptor

Table of Contents

List of Tables

List of Figures

Abstract

Historically, the complex anatomical landscape of the central nervous system and the physiology that governs it presented a challenge for scientists interested in elucidating fundamental properties of solute trafficking in the central nervous system. This resulted in a wide range of conflicting models of fundamental physiological processes, such as the production and reabsorption of cerebrospinal fluid in the cranium. Major advances were recently made in the study of solute trafficking between the brain and cerebrospinal fluid, and the reabsorption of cerebrospinal fluid and solutes therein. These findings challenge the previous assumptions about where cerebrospinal fluid (CSF) circulates through the cranium and how it is reabsorbed. One such finding is the characterization of differentiated lymphatic vessels in the dura mater of the mouse. Discovered independently by two different groups, this revealed a new potential pathway for the efflux of macromolecules, cells, and fluid out of the central nervous system. Although interest in this putative pathway between the intracranial space and deep cervical lymph nodes (DCLNs) was invigorated by these findings, several important gaps in our current knowledge exist. First and foremost is the translational relevance of this finding to human anatomy. Although robust characterizations were carried out in the rodent, it remains unclear if the human meninges contain analogous lymphatic structures. Second, since the discovery of a lymphatic network in the meninges, there was widespread speculation that it plays a role in the development of neurological disease, particularly in Alzheimer's dementia. While this is possible, foundational studies examining the trafficking of amyloid beta along this pathway do not yet exist. Third, there is a paucity of data in the literature concerning the physiological parameters that mediate the lymphatic absorption of solutes in the brain and cerebrospinal fluid. The work described in

this dissertation aims to address these knowledge gaps using a combination of light microscopy, transgenic animal models, and experimental manipulation of physiological parameters that act on this biological system.

To examine the translational importance of the meningeal lymphatic system, we began by examining sections of the human meninges with a combined approach of spectral unmixing and immunofluorescence. We found that, like in the rodent meninges, lymphatic vessels also populate the human meninges and express similar molecular signatures. Unlike the rodent, however, we identified vessels with variable morphology that may belong to distinct subpopulations of lymphatic vasculature. To begin to examine the role of the meningeal lymphatic system in Alzheimer's dementia, we examined meningeal samples collected from subjects with Alzheimer's dementia and control subjects. We did not identify any significant deposition of amyloid beta in the meninges of Alzheimer's dementia or control subjects.

Because the nature of this experiment was limited to associations between amyloid beta immunoreactivity and lymphatic vessels in the human meninges, we next infused a fluorescently-labeled species of amyloid beta into the brain and cerebrospinal fluid of mice to identify if it can be trafficked out of these compartments via the lymphatic system. Indeed, we found that exogenous amyloid beta was trafficked out of both compartments via the lymphatic system, suggesting that this previously unstudied pathway contributes to the clearance of amyloid beta from intracranial compartments. If this efflux pathway was responsible for reduced amyloid beta efflux observed in aging and Alzheimer's dementia patients, we would anticipate an age-related reduction in lymphatic function. We tested this hypothesis by measuring the efflux rate of solutes, including amyloid beta, from the CSF in

young and aged mice. We noted a significant reduction in lymphatic solute efflux in the aged group compared to the young group. This supports the hypothesis that a reduction in lymphatic solute efflux from the cranium contributes to the accumulation of amyloid beta in the brain of aging and Alzheimer's dementia patients.

Finally, to determine the physiological controls on lymphatic efflux from the cranium, we considered the known mediators of lymphatic solute uptake in peripheral systems. In the peripheral lymphatic system, arousal state is a potent regulator of lymphatic flow, with multiple reports of anesthesia reducing lymphatic uptake and flow velocity. Therefore, to test whether lymphatic solute uptake in the intracranial space is affected by anesthesia, we considered lymphatic drainage in awake and anesthetized mice. Similar to the peripheral lymphatic system, the rate of lymphatic drainage from the brain was markedly reduced in anesthetized mice compared to waking mice. However, we discovered that without intubation and ventilation, anesthetized mice rapidly develop a respiratory acidosis, hypoxemia, and oxygen desaturation. Correction of normal physiological values with intubation and mechanical ventilation resulted in recovery of lymphatic solute drainage, suggesting that hypoxemia, hypercapnia, and/or respiratory rate affect this process. Using different ventilation parameters and hypercapnic challenge with CO_2, we determined that hypercapnia, not respiratory rate or hypoxia, is responsible for the majority of impairment of lymphatic drainage in anesthetized and non-intubated mice.

Together, these findings confirm that humans have an analogous lymphatic network in the meninges, that lymphatic drainage of amyloid beta and other solutes is impaired in aging rodents, and that arterial CO_2 tension modulates lymphatic drainage of the cranium.

These findings may inform future studies of Alzheimer's dementia and provide valuable insight into lymphatic reabsorption in different physiological states.

Chapter One: Introduction

The Anatomy and Physiology of the Body's "Third Circulation"

An Overview of the Intracranial Topography

The intracranial space in humans features a landscape of bone, meninges, gray and white matter, cerebral blood vessels, and cerebrospinal fluid. This complexity is reflected in the diversity of interfaces between the tissues found within the cranium and has complicated centuries of investigations focused in this region. Broadly, the intracranial space is defined by the bony boundaries of the skull that can be roughly divided into the superior and inferior aspects called the calvarium and skull base. Immediately deep to the skull is the meninges, composed of three layers called the dura, arachnoid, and pia mater (Figure 1). Together, the meningeal layers completely ensheathe the cerebrospinal fluid and brain. Cerebral blood vessels traverse the meningeal layers, with arteries passing through the subarachnoid space and running along the pia mater before entering into the cortex. The gyrencephalic human brain features cortical gyri and sulci perfused by these penetrating arteries and arterioles (Figure 1). The majority of venous blood is drained into the venous sinuses via bridging veins, which also traverse the pia, arachnoid, and inner aspect of the dura mater. In the skull base, cranial nerves pass across the meninges and through ventral fossa in the skull. The interfaces between these features, especially the cerebral vasculature and cranial nerves that pass across the meningeal boundaries, give rise to a convoluted pathway for fluid and solutes that are trafficked through the intracranial space. Special consideration to the key features of fluid movement and solute trafficking in the CNS will be discussed in the following sections.

The Ventricular System

The cerebral ventricular system is composed of four cavernous and connected fluid-filled spaces called ventricles. These ventricles are characterized anatomically by their location within the brain, forming two lateral ventricles, a third ventricle, and a fourth ventricle. The lateral ventricles are connected to the third ventricle via the foramen of Monro and the third ventricle is connected to the fourth ventricle via the cerebral aqueduct. Interestingly, the entire ventricular system is lined with ciliated ependymal cells that actively beat, generating small currents near the surface of the ventricle (Faubel et al., 2016). Each ventricle features a specialized vascular CSF-secreting organ called the choroid plexus, which will be discussed in greater detail below. Historically, the ventricular system was considered to be central to human consciousness with each ventricle containing a *spiritus animalis* that performed specific cognitive and spiritual functions. Indeed, the Roman physician Galen of Pergamon described the ventricular-pneumatic system, whereby the human spirit and the source of cognitive function was seated within the ventricles (Manzoni, 1998). Since then, the attributed purpose of the ventricular system has changed, with most modern models asserting that the principle functions of the ventricular system are the production of CSF and the circulation of neuroendocrine signaling molecules. Much attention was dedicated to pathological changes in the ventricular system in different disease states, including hydrocephalus which features volumetric changes in the ventricles due to obstruction of outflow tracts and yet unknown etiologies.

Subarachnoid, cisternal, and perivascular spaces

The subarachnoid space (SAS) is continuous with the ventricular system, connected via the foramina of Luschka and Magendie. The patency of these apertures facilitates the

movement of fluid between the ventricular system and the SAS, as characterized in detail by Key and Retzius in 1875 (Key and Retzius, 1875). The SAS contains the majority of CSF within the CNS and allows for CSF circulation around the entire brain. Due to variations in neuroanatomy, several regions called cisterns host relatively large volumes of CSF in the SAS. These interconnected cisterns also must remain patent for effective CSF circulation.

In some regions of the brain, including the space between the corpus callosum and the thalamus, the pia mater invaginates around dense vascular structures, forming an anatomical region called the tela choroidea (Tubbs et al., 2008). This is perhaps best characterized in the velum interpositum, which forms a cisternal space in close proximity to the quadrigeminal cistern shown in Figure 1. Although this anatomical region is known clinically for its tendency to form cysts and expand in hydrocephalus (Rhoton, 2002; Zohdi and Elkheshin, 2012), the association between these layers of pia mater with the choroidal structures in the third ventricle demonstrate the diversity of the meningeal topography within the cranium. As previously noted, large intracranial arteries and veins generally enter into the SAS, passing through ventral cisterns before passing through the pia and into the cortex. Interestingly, as they penetrate into the cortex, the single layer of the pia mater at the cortical surface continuously ensheathes the blood vessels. Deeper in the cortex, this pial sheath becomes increasingly discontinuous and eventually there is direct contact between the basement membrane of the blood vessels and the surrounding astrocytic endfeet within the brain (Morris et al., 2014; Zhang et al., 1990). Between the vascular basement membrane and the astrocytic endfoot is a fluid-filled space commonly called the perivascular space (PVS). This space is thought to exist around both arteries and veins, but there are conflicting reports regarding the continuity of this space around capillaries (Lam et al., 2017; Pizzo et al.,

2018). The fluid in the PVS is thought to be similar in character to CSF, owing to the fact that the SAS and PVS are continuous (Abbott et al., 2018; Bedussi et al., 2017; Ichimura et al., 1991). There is also evidence that fluid in the PVS exchanges with the interstitial fluid (ISF) in the brain (Cserr, 1983; Iliff et al., 2012; Rennels et al., 1990, 1985). These studies led some to speculate that the CSF and ISF compartments are in equilibrium, however the specific gravity of the fluid in these compartments is 1.003 and 1.040, respectively, suggesting that the soluble constituents in these compartments are different (Bradley, 1970a).

Cerebrospinal fluid

CSF is a clear fluid that fills the ventricular system and SAS. Many functions are ascribed to CSF, including distribution of neuroendocrine signaling molecules such as hormone signaling factors and melatonin (Leston et al., 2010; Skinner and Malpaux, 1999), buffering the CNS (Shibata et al., 1976; Swanson and Rosengren, 1962), and protecting the brain from the rigid bone of the cranium during changes in ICP and head movement. CSF is essentially isotonic relative to serum, but contains far less proteinaceous material (0.6 g/L and 70 g/L, respectively). Because the parenchyma of the brain lacks a traditional lymphatic system, the relative paucity of protein and other macromolecules in the CSF led many to speculate that the CSF serves as a sink for solutes that extravasate from the bloodstream or that are produced in the brain. This is evidenced by the appearance of brain-derived amyloid beta, tau, and alpha synuclein in the CSF, which vary with the progression of neurodegenerative disease (Kang et al., 2013; Mattsson et al., 2009; Noguchi-Shinohara et al., 2009).

Pathologically, the obstruction of CSF circulation can lead to accumulation of CSF in the ventricular system, a condition called hydrocephalus. Congenital hydrocephalus affects

roughly 1 in 1000 infants (Tully and Dobyns, 2014), which is currently treated either with ventricular shunts or endoscopic third ventriculostomy, both of which have relatively poor success rates. Thus, the production, circulation, and reabsorption of CSF were of interest to the neurological and neurosurgical communities for decades. In this section, these aspects of CSF physiology are discussed.

Production

It is widely believed that the majority of CSF is formed by the choroid plexus, though claims of transependymal and pial CSF production exist in the literature (Hammerstad et al., 1969; Pollay and Curl, 1967; Sato et al., 1972). However, because of the technical complexity of experiments that report extrachoroidal CSF production, it is difficult to conclude that these mechanisms of CSF production occur under physiological conditions. The choroid plexus is a specialized vascular organ found in each of the ventricles and features a single layer of cuboidal epithelium overlying a basement membrane and blood vessels (Figure 1). Arterial blood supplying the choroid plexus varies by location, with the anterior choroidal artery supplying the lateral and third ventricles, while the posterior inferior cerebellar artery and anterior inferior arteries often supply the choroid plexus of the fourth ventricle (Sharifi et al., 2005). Although the production of CSF was suspected at the choroid plexus, the scientific community lacked empirical evidence until a series of experiments were performed by Walter Dandy and Kenneth Blackfan. To test this hypothesis, they surgically obstructed one of the lateral ventricles in the dog. Following the procedure, the dogs displayed symptoms of hydrocephalus, including lethargy and vomiting. Examination of the gross brain demonstrated ventriculomegaly and the authors concluded that CSF must be formed in the ventricles, speculating that the source was the choroid plexus because of its

unique vascular structure (Dandy and Blackfan, 1913). This experiment precipitated much interest in the formation of CSF at the choroid plexus.

Decades later, a series of inhibitors including ouabain were used to demonstrate that CSF production was dependent on Na^+-K^+ ATPase (Davson and Segal, 1970; Pollay et al., 1985) and microdissections of the choroid plexus were found to contain multiple subunits of the Na^+-K^+ ATPase heterodimer (Zlokovic et al., 1993). Similar experimental approaches were undertaken to demonstrate the presence of other ion cotransporters in the choroid plexus, including inhibition of $Na^+K^+2Cl^-$ with butmetanide (Bairamian et al., 1991; Keep et al., 1994), $Na^+HCO_3^-$ with dihydrogen-4,4'-diisothiocyanatostilbene-2,2'-disulfonic acid (Praetorius et al., 2004), and Na^+H^+ with amiloride (Murphy and Johanson, 1989). In addition to these ion cotransporters, a critical role for carbonic anhydrase was shown in the choroid plexus. Indeed, the carbonic anhydrase inhibitor acetazolamide reduces CSF production in multiple species, and is currently used to reduce intracranial pressure in humans (Carrion et al., 2001; Faraci et al., 1990; Uldall et al., 2017). The potent effect of carbonic anhydrase inhibition on CSF production suggests that the handling of HCO_3^- is critically important for the production of new CSF at the choroid plexus. Another critical aspect of CSF production is the transportation of water from the intravascular to the intraventricular compartment. In the choroid plexus, the molecular water channel aquaporin-1 (AQP1) is abundantly expressed at the apical membrane. Interestingly, there appears to be a lack of AQP1 expressed in the basolateral membrane, raising the question of how water movement is facilitated into the choroidal epithelium (Nielsen et al., 1993). In addition to the lateralization of AQP1 in the choroid plexus, several other observations raised questions about the mechanism of CSF production beyond passive movement of water after secretion

of ions into the ventricles. For instance, in 2001 Oshio et al. reported that the deletion and subsequent loss of AQP1 in the choroid plexus only reduced CSF production by 25% (Oshio et al., 2005). Although this experiment clearly demonstrates a relationship between AQP1 and the magnitude of CSF production, it also challenges the assertion that transmembrane water channels are required for this critical process. Were hydrostatic pressure gradients between the intravascular and intraventricular compartments responsible for the production of CSF, one would expect that experimental manipulation of arterial blood pressure would alter the rate of CSF secretion. However, when this experiment was performed, it was found that CSF production was unchanged at varying hydrostatic pressures between -10 and +30 cm H_2O (Heisey et al., 1962). Thus, the mechanisms governing water transport in the choroid plexus, and therefore CSF production are incompletely understood.

In mammals, the estimated rate of CSF secretion is remarkably similar, ranging from 0.18-0.625 μL $minute^{-1}mg^{-1}$(as reviewed by Cserr, 1971). Interestingly, the rate of CSF secretion in humans is subject to diurnal fluctuation, with maximum and minimum CSF production at approximately 0200 and 1800, respectively (Nilsson et al., 1992b). Although the total volume of CSF in humans ranges from 150-200 mL, the total daily volume of CSF produced in the human is estimated at 650 mL, therefore CSF turnover occurs several times per day (Nilsson et al., 1992b).

Circulation

CSF circulation has been a subject of great interest since modern models were first proposed by Harvey Cushing and Lewis Weed in the early 20th century (Cushing, 1914; Weed, 1917). Early studies demonstrated a hydrostatic pressure gradient between the

ventricles and the subarachnoid space, which led investigators to postulate that this hydrostatic gradient enabled directional circulation of CSF from the choroid plexus toward sites of reabsorption (Tourtelloutte, 1968). Indeed, magnetic resonance imaging (MRI) revealed net CSF flow through the cerebral aqueduct and out of the ventricular system (Nilsson et al., 1992b). This study further demonstrated that cranial/caudal movement of CSF was actually bidirectional and entrained to the cardiac cycle, with caudal CSF flow during the systolic phase and cranial CSF flow during the diastolic phase. Despite the large bidirectional flux of CSF, a small net movement in the caudal direction was still found. Thus, these findings suggest that CSF flows out of the ventricles and into the SAS before being reabsorbed. However, it was also recognized early on that the cardiac and respiratory cycles also contributed to the movement of CSF (Bradley, 1970b). In 2011, these findings were later confirmed using cine phase contrast MRI by Sweetman and Linninger, who simultaneously measured the heart rate, cerebral blood flow, and CSF flow in a human subject to model three-dimensional CSF movement in the cranium (Sweetman and Linninger, 2011). Their model predicted pressure waves generated during cardiac systole that originate in the ventral cisterns and tracked superiorly into the lateral ventricles. The authors observed that this small but reproducible 10% phase lag results in biphasic systolic expansion of the cerebral vasculature. They concluded that this may be due to the expansion of proximal arteries in the ventral SAS that travels distally and superiorly into the brain, eventually compressing the dorsal SAS and ventricles. Since then, it was further clarified that while both the cardiac and respiratory cycle contribute to CSF movement, the magnitude of CSF movement entrained with the respiratory cycle was greater than the cardiac cycle (Dreha-Kulaczewski et al., 2015).

Along with the net movement of fluid, solutes within the CSF are trafficked by bulk flow throughout the ventricular system, SAS, and PVS. As mentioned above, this observation led many to speculate about exchange of solutes between the CSF and ISF compartments at the PVS as a means of neuroendocrine signaling, electrolyte homeostasis, and removal of macromolecules produced in the brain (Cserr et al., 1981; Rennels et al., 1990, 1985; Scott et al., 1977). Though some models integrate PVS fluid movement as part of CSF circulation, a quantitative fraction of total CSF that 'circulates' through this pathway is not currently known.

Reabsorption

Multiple sites of CSF reabsorption are known, including efflux at the cribriform plate, arachnoid granulations, perineural sheaths, and into the cervical lymphatic trunk, which drains into the deep cervical lymph nodes (DCLNs). These efflux pathways were elucidated by infusing ink, gelatin, or polymers into the subarachnoid space (Dandy and Blackfan, 1913; Hill, 1896; Johnston et al., 2004; Weed, 1914a). In the absence of noninvasive techniques, these studies provided exceptional insight into the intracranial distribution of soluble materials infused into the CSF. Early reports were often inconsistent, with some groups only observing reabsorption in the arachnoid granulations and others observing reabsorption in the skull base. These incongruent findings raised much contention in the field and are likely due to inconsistent methods. For instance, some early studies considered tracer infusion into cadaveric human heads while others infused tracers into the SAS of dogs, rabbits, sheep, or rats. These experiments were also criticized for their use of supraphysiological infusion pressures, toxic substances, and, in some cases, being carried out in deceased animals. Importantly, the type of tracer, anesthesia used, and time between the

infusion and sacrificing the animals was also inconsistent between these studies, all of which may contribute to the conflicting results that were reported.

Regardless of the inconsistencies, there is evidence for CSF reabsorption at the arachnoid granulations, which are valvular diverticula of the arachnoid mater that pass across the dura mater and into the lumen of the dural venous sinuses (Gomez et al., 1974a). The arachnoid granulations are thought to play a functional role as one-way valves that allow for direct efflux of CSF from the SAS into the venous sinuses or tributary veins. Interestingly, the microscopic architecture of the arachnoid granulations is state-dependent. Indeed, in physiological states wherein hydrostatic pressure in the SAS exceeds that of the venous sinuses, microvilli on these granulations are observable with scanning electron microscopy (Gomez et al., 1974b). However, the microvilli appear to collapse when the venous pressure exceeds that of the SAS, which is thought to reduce the likelihood of blood cells and plasma passing into the SAS. (Gomez and Potts, 1974). On the luminal side, the arachnoid granulations are lined with vascular endothelial cells, and most studies examining the ultrastructural quality of the arachnoid granulations reported that the luminal endothelial lining is continuous (Shabo and Maxwell, 1968; Upton and Weller, 1985). This raises questions about the mechanism of CSF reabsorption at this interface, however the abundance of pinocytotic vesicles in the arachnoid and endothelial cells led some to speculate that pinocytosis may be the dominant mechanism by which CSF enters into the blood stream. In terms of functional studies, Lewis Weed performed multiple experiments in the early 20th century showing that infusion of ferrocyanide and iron-ammonium citrate into the SAS resulted in accumulation of these tracers in the arachnoid granulations (Weed, 1914b, 1914a). Weed's interpretation of this finding was that the arachnoid granulations

provided a direct path for reabsorption of CSF into the bloodstream (Weed, 1938). Other reports from independent labs reported similar findings (Dandy and Blackfan, 1913; Gomez et al., 1974b; Hill, 1896), and provided the foundation for the central dogma stating that the arachnoid granulations are the dominant pathway by which CSF irreversibly escapes from the cranium.

Throughout early studies of CSF reabsorption, lymphatic drainage of tracers infused into the SAS was noted, but considered to be a delayed and relatively minor efflux pathway (Weed, 1938). Later in the 20th century, multiple studies renewed interest in lymphatic drainage of CSF. Specifically, the use of radiolabeled solutes allowed for quantitative measurement of lymphatic CSF efflux and it was found that between 15 and 50% of radiolabeled proteins exited the cranium via the lymphatic pathway in animal models (Bradbury et al., 1981; Bradbury and Cole, 1980; Bradbury and Westrop, 1983a; Cserr et al., 1992). These reports challenged the existing models of CSF reabsorption and returned scientific focus on the lymphatic component of CSF efflux. Perhaps what is most surprising about the observation that lymphatic pathways are a major drainage route for solute clearance from the brain is that the brain parenchyma lacks a differentiated lymphatic network. Though it was clear that solutes in the interstitial space eventually exit the cranium via the cervical lymphatic vasculature, the intracranial trafficking pathway remained unclear. To investigate a putative connection between the SAS and the cervical lymphatic trunk, several groups infused polymers or ink into the SAS of rodents, sheep, and nonhuman primates (Boulton et al., 1999, 1998; Johnston et al., 2004; Kida et al., 1993; Zakharov et al., 2004). In these studies, the intracranial tracer distribution was reported in close proximity to the cribriform plate and around cranial nerves exiting the anterior skull base. Upon

dissecting or sectioning the head, the tracers were found to traverse the cribriform plate and deposited in the nasal turbinates, which are known to contain dense lymphatic networks. The interpretation of this finding was that efflux via the cribriform plate and cranial nerves in the anterior skull base is one pathway by which the CSF exits the cranium and is trafficked into the cervical lymphatic trunk. Another pathway for CSF efflux was recently addressed by two groups, who independently described a network of differentiated lymphatic tissues in the rodent meninges that absorb solutes injected into the brain and CSF (Aspelund et al., 2015; Iliff et al., 2015; Louveau et al., 2015). These studies will be discussed in greater detail in the section entitled "The Meningeal Lymphatic System."

Other pathways for CSF efflux were proposed by Elman in the early 20th century, including along nerve roots in the spinal cord and the spinal arachnoid granulations (Elman, 1923). Although Elman's studies were not quantitative in nature, he observed relatively less ferrocyanide tracer accumulation in the spinal than in the cranial arachnoid granulations and concluded that the spinal arachnoid granulations likely played a minor role in CSF reabsorption under physiological states. Nevertheless, they may perform a critical supplementary role if the function of the intracranial granulations is compromised. Perhaps the earliest suggestion of this was by Lewis Weed who critiqued a study performed by Walter Dandy, wherein Dandy surgically separated the intracranial dural sinuses from the arachnoid granulations in dogs (Dandy, 1929). Dandy reported that the dogs did not develop pathology associated with this presumed blockage of CSF reabsorption. Weed argued that since the spinal arachnoid granulations were not separated, that they may compensate for CSF efflux in the setting of impairment of the intracranial arachnoid granulations (Weed, 1938).

Together, these are the known pathways for CSF reabsorption. Although there is much contention in the literature regarding the dominant site of reabsorption, it is clear that multiple sites exist and likely contribute in this essential function. Because there are undoubtedly differences between CSF efflux in humans and other mammals, further clarification of CSF reabsorption using noninvasive and quantitative neuroimaging in humans is needed.

Solute Trafficking in the CNS

The movement of ions, small molecules, and macromolecular solutes through the CNS is restricted at multiple barriers and interfaces, including the blood-brain barrier (BBB), the blood-CSF barriers, and the interface between the PVS and brain parenchyma. Many physiochemical properties affect the movement of these solutes, including lipophilicity, molecular weight, hydrodynamic radius, and charge. In the following sections, the mechanisms of passive and active transport at these interfaces will be discussed. Once a solute enters into the ISF, PVS, or SAS, there is evidence that several forces may act on solutes including diffusion, advection, convection, and dispersion. Diffusion is defined as the net movement of solutes down a chemical concentration gradient. It is a phenomenon driven by the stochastic movement of solutes in a solvent, thus it is temperature-dependent and is inversely related to the molecular weight of the solute. The diffusion process is generally isotropic, or non-directional with exception to the chemical gradient. Despite this, the rate of net movement of solutes via diffusion depends on the tortuosity of the path and apparent anisotropic diffusion can be observed in highly organized and linear pathways. This feature of diffusion is particularly evident in the extracellular space (ECS) of the human

brain, which features dense and highly tortuous neuronal and glial cell bodies in gray matter as well as parallel bundles of myelinated white matter tracts. Alternatively, multiple reports demonstrated the action of advection, or bulk flow, in the movement of solutes in the brain. Advection is defined as the net movement of solutes in a medium secondary to the movement of the medium. Unlike diffusion, solute advection occurs without respect to the physiochemical properties of the solute and the motive force for bulk flow is a hydrostatic pressure gradient. As a consequence, the rate of solute movement by bulk flow is generally much higher than that of diffusion. It is important to note that advection and convection are used interchangeably in referring to bulk flow within the neurophysiology literature. More specifically, the term convection actually describes both advection and diffusion together. Throughout this work, the terms advection and bulk flow will be used interchangeably, whereas the term convection will be used to describe both bulk flow and diffusion. Finally, it is also thought that dispersion contributes to solute movement in the CNS. Similar to advection, solute transport due to dispersion occurs via movement of water generated by hydrostatic pressure gradients. However, instead of net solute and solvent movement, net solute movement occurs in the absence of net solvent movement. As discussed in the previous section, the magnitude of CSF movement in the ventricular system, SAS, and PVS is large, yet the net movement of CSF is comparatively small due to reversal of the vector during cardiac diastole and expiration. In the sections to follow, the evidence for these mechanisms of solutes movement in the brain will be discussed in greater detail.

Solute influx into the brain's extracellular space

Soluble proteins, lipids, and carbohydrates are either trafficked into the brain across the blood-brain, blood-CSF barriers, and fenestrated endothelium in circumventricular

organs or they are produced within the brain parenchyma. Passive movement across the BBB favors nonpolar molecules due to tight junctions between continuous endothelial cells, but several mechanisms including receptor-mediated transcytosis exist to transport polarized solutes such as glucose and amino acids into the brain. In terms of fluid movement, the majority of water in the blood stream crosses the BBB with every pass, despite the tight junctions between the cerebral endothelium. This leads to a staggering volume of water exchange across the BBB. As outlined by Hladky and Barrand, if cerebral blood flow in man is estimated to be 800 mL min^{-1}, adjusting for leukocyte and erythrocyte volume in the blood, we might expect to see ~680 L of water exchanged at the BBB on a daily basis (Hladky and Barrand, 2016). However, net water movement from the intravascular to the interstitial compartments is very low due to very similar rates of water influx and efflux across the BBB due to Starling forces (Sweet et al., 1950). The blood-CSF barrier is composed of at least two interfaces; the choroid plexus and the arachnoid membrane. Unfortunately, besides structural studies, very little is known about solute movement at the CSF-arachnoid interface (Vandenabeele et al., 1996). It is clear, however, that the arachnoid mater contains a significant barrier to solute and fluid movement in the form of arachnoid cells joined together by tight junctions (Nabeshima et al., 1975). Unlike most of the brain, the endothelium at the choroid plexus is fenestrated. Despite its fenestrations, movement of most polar molecules across the choroidal epithelium requires transcellular transport mechanisms, similar to the BBB. Interestingly, while these barriers express similar transport proteins for solute trafficking, the actual solutes vary between the interfaces. For instance, higher levels of transthyretin and insulin-like growth factor-II are secreted into the CSF at the choroid plexus than the BBB, while more glucose and amino acids are trafficked across

the BBB than the blood-CSF barrier (Nilsson et al., 1992a). Together, these selective barriers tightly regulate the movement of solutes into the brain at the blood-CSF and BBB. Several brain regions called the circumventricular organs feature a fenestrated endothelium which allows direct passage of solutes in the bloodstream into the ISF. Although there is documented heterogeneity of vascular permeability in these organs, most are permissive to the passage of dextrans up to 3 kDa (Morita et al., 2016; Willis et al., 2007). A size-based exclusion of molecules over 10 kDa is still noted, however, which appears to be related to the integrity of the basement membrane (Willis et al., 2007). Although the vascular permeability facilitates the secretion of neuroendocrine signaling molecules into the blood stream, its significance in the physiological absorption of solutes from the bloodstream into the ISF is relatively understudied.

Mechanisms governing solute behavior into, and efflux out of, the extracellular space

The fate of solutes that arrive in the fluid-filled ECS of the brain, either by crossing the BBB or being secreted into the ISF from the intracellular space of neurons, glia, or pericytes, has been intensely studied for several decades. In the living rodent, the ECS ranges from 38-64 nm in width (Thorne and Nicholson, 2006) and contains not only ISF, but matrices of extracellular proteins, including heparin sulfate and chondroitin sulfate (Thorne et al., 2008). Using integrative optical imaging, Thorne and colleagues demonstrated that solutes with a hydrodynamic radius of up to 35 nm can diffuse through the ECS, and interact with proteins in the ECS (Thorne et al., 2008). Interestingly, the diffusion of solutes through this space is dependent on the tortuosity and the density of the extracellular matrix (Nicholson and Phillips, 1981). This finding is used as a mechanistic underpinning of the observation that myelinated white matter tracts display higher fractional anisotropy than gray

matter on diffusion tensor imaging magnetic resonance imaging (Basser et al., 1994; Basser and Pierpaoli, 1996).

In addition to isotropic diffusion due to Brownian motion, multiple groups believe that convective fluid movement occurs in the ECS of the brain (Cserr et al., 1977; Iliff et al., 2012; Ray et al., 2019; Rennels et al., 1990, 1985; Rosenberg et al., 1980). Fluid convection consists of both diffusion and bulk fluid movement and although the rate of solute movement via diffusion is dependent on concentration gradient and molecular weight, bulk fluid movement transports molecules without respect to molecular weight or concentration gradient. Perhaps the first evidence underpinning this claim was provided by Cserr and colleagues in 1977, which featured the injection of triturated polyethylene glycol (4 kDa) and dextrans (70 kDa) in the rat caudate nucleus and measurement of their rate of efflux. Four hours after the initial tracer injection, the authors reported that there was no difference in the quantity of tracer remaining in the caudate, indicating that advection contributed to their efflux from the ECS (Cserr et al., 1977). Shortly after this work was published, another group used ventricular perfusion of triturated sucrose in the cat to calculate apparent diffusion constants in white and gray matter with respect to time (Rosenberg and Kyner, 1980). They found that their initial model, which assumed no advection occurred in the brain parenchyma, accurately predicted the movement of sucrose through the striatal gray matter but not the periventricular white matter. Once they factored advection into the modeling equation, it predicted both accurately. The authors concluded that advection contributes to solute movement in the white matter, but not gray matter. Thus, although advection in the brain was reported by both groups, conflicting findings in different brain subregions emerged in even the earliest investigations. Since these studies were published,

several conflicting reports on advection in the gray matter were also reported. The observation that solutes of different molecular weights have similar clearance rates in the gray matter was reproduced by the same lab (Cserr et al., 1981) as well as more recently by two independent groups (Groothuis et al., 2007; Iliff et al., 2012). Using an orthogonal approach, Smith and colleagues co-injected 10, 70, and 2000 kDa dextrans into the mouse striatum and measured the tracer distribution using confocal microscopy (Smith et al., 2017). They report a strong size-dependence on solute distribution around the injection site. These authors also investigated whether solute movement in the cortical gray matter is directional, which would support the notion of advection. To accomplish this, they employed a light-microscopy based technique called fluorescence recovery after photobleaching, where a 500 kDa tracer distributed throughout the mouse cortex in equilibrium was photobleached and the rate of fluorescence recovery in the photobleached region was subsequently measured. The authors reported that fluorescence recovery was not directional, further suggesting that solute movement in the ECS of gray matter is not influenced by bulk flow. Based on these findings, the authors of this study concluded that diffusive forces, not advection, dominate in the gray matter. In an attempt to reconcile these discrepant findings, multiple groups attempted to model ISF movement in the brain. To date, most of these models support the notion that diffusion or dispersion, but not bulk flow dominates in moving solutes in the gray matter (Asgari et al., 2016; Faghih and Sharp, 2018; Holter et al., 2017a; Jin et al., 2016). Notwithstanding the differences in the gray matter, it is generally agreed that advection occurs in the ventricular system, SAS, PVS, and in white matter tracts.

The thoughtful work of Cserr and colleagues also demonstrated that solutes injected into the brain parenchyma escaped into the CSF, which reinvigorated scientific interest in

the mechanisms underlying molecular efflux from the brain (Cserr, 1983; Cserr et al., 1981, 1977). Indeed, multiple groups demonstrated that solutes of varying molecular size are rapidly transported both into and out of the PVS at rates that far surpass diffusion (J. Iliff et al., 2013; Iliff et al., 2012; Rennels et al., 1990, 1985).

Until recently, however, physiological controls on exchange between the CSF and ISF were not clearly described. In an effort to generate a unified model of solute exchange between the ISF and CSF, a brain-wide perivascular system for exchange of fluid and solutes was recently proposed (Iliff et al., 2012). This study found that CSF-ISF exchange at the perivascular interface requires perivascular localization of the aquaporin-4 (AQP4) water channel expressed at the astroglial endfoot throughout the brain, therefore this system was called the "glymphatic system" (Iliff et al., 2012). Follow up studies characterizing this physiology suggest that the motive force for exchange between these compartments is, in part, due to arterial pulsation (Iliff et al., 2013b). These findings were interpreted in the context of prior studies that suggested that parenchymal solutes escape from the brain via convective flow (N. J. Abbott, 2004; Cserr, Cooper, Suri, & Patlak, 1981). Together, these studies provided mechanistic insight into the trafficking of solutes and fluid into and out of the brain. Shortly after the initial characterization of the glymphatic system, reductions in the magnitude of ISF-CSF exchange were reported in states of aging and disease (Gaberel et al., 2014; Goulay et al., 2017; Iliff et al., 2014; Kress et al., 2014; Wang et al., 2017).

Other studies have questioned mechanistic elements of the glymphatic system, including the claim that AQP4 is required for molecular exchange between the compartments and arterial pulsations establish the motive force for fluid movement (Faghih and Sharp, 2018; Smith et al., 2017). In 2017, Smith and colleagues attempted to reproduce

the key findings described by Iliff et al. in 2012; namely that bulk flow facilitates solute movement in a brain-wide fashion, that parenchymal bulk flow was dependent on AQP4 expression at the astrocytic endfoot, and that hydrodynamic pressure waves from arterial pulsations provided the motive force for parenchymal bulk flow (Smith et al., 2017). To test these questions, Smith and colleagues measured solute (dextrans of varying hydrodynamic radii) influx and movement throughout the gray matter, CSF-ISF exchange in transgenic AQP4 knockout mice and rats, fluorescence recovery after photobleaching, and measured CSF-ISF exchange in mice moments after euthanasia. In each of these approaches, the authors reported conflicting results compared to those found by Iliff et al. These conflicting experimental findings are supported by modeling studies that suggest that diffusion, not bulk flow, is the dominant mechanism acting on solutes in the gray matter (Faghih and Sharp, 2018; Holter et al., 2017b). Together, these studies have brought major elements of the glymphatic system into question. Notwithstanding the conflicting reports focused on the mechanisms driving CSF-ISF exchange, there is essentially no contention in the literature that solutes can exchange between the CSF and ISF compartments.

Although the glymphatic system is still under active study and our understanding of its underlying mechanisms is still being refined (Abbott et al., 2018; Holter et al., 2017a; Smith et al., 2017), there is much interest in developing methods for non-invasive measurement of CSF-ISF exchange in rodents and humans. After the initial characterization of the glymphatic system using fluorescent tracers and multiphoton microscopy, steps were quickly taken to develop robust magnetic resonance imaging protocols with gadolinium-based contrast enhanced cisternography to measure the magnitude of CSF-ISF exchange in the rodent (Iliff et al., 2013; Yang et al., 2013). Shortly thereafter, an elegant case study was

published by Eide and Ringstad recapitulating these preclinical studies in a human subject with suspected CSF leakage (Eide and Ringstad, 2015). Through repeated imaging of the brain after intrathecal infusion of gadobutrol in this subject, the authors concluded that ISF-CSF exchange exists in the human as well as the rodent. Further work by Eide and Ringstad confirmed these findings in 30 patients with suspected CSF leaks and/or normal pressure hydrocephalus (Eide and Ringstad, 2018). Together, these studies provide confirmation that exchange between the CSF and ISF occurs in the human, and that this process may be impaired in the setting of pathology.

Physiological aspects of solute efflux from the brain

Because the brain parenchyma lacks a traditional lymphatic system, the physiological mediators of solute efflux from the brain, including across the BBB and CSF-ISF exchange are of great interest to physiologists focused on efflux of solutes, including drugs, from the brain. Several important efforts to elucidate the physiological controls on exchange between these two compartments exist in the literature. First, in an elegant study by Groothuis and colleagues, the relative contribution of transcapillary, diffusion, and convection was measured in different physiological states of almost 500 rats (Groothuis et al., 2007). In the first arm of this study, the authors measured the half-life and total efflux constant of molecules that are passively transported through the brain like urea, inulin, and sucrose, 10-70 kDa dextrans. They also measured these parameters in several actively transported molecules like para-aminohippuric acid, cytosine arabinoside, azidothymidine, and a 6 kDa oligonucleotide. This data set proved to be exceptionally useful for estimating the relative contribution of diffusion across the BBB, transporter-mediated efflux, and convective efflux.

For example, to measure these parameters for para-aminohippuric acid, the authors relied on the following equation,

$$k_{eff} = k_p + k_{csf} + k_x \qquad (1)$$

where k_{eff} represents the total rate of solute efflux, k_p represents diffusion across the BBB, k_{csf} represents convective solute efflux, and k_x represents yet transporter-mediated clearance mechanisms. For para-aminohippuric acid, the rate of diffusional influx (k_p', 0.012 g mL^{-1} hr^{-1}) and efflux across the BBB was assumed to be equal, but the magnitude of the constant was strongly dependent on the volume of the ECS (0.16 mL g^{-1}) and the size and lipophilicity of the molecule based on previous studies (Fenstermacher and Rapoport, 1984). Because there are no known molecular changes in para-aminohippuric acid, the authors therefore calculated k_p from equation 1 using the following equation,

$$k_p = k_p' \,/\, \text{Volume of ECS} \qquad (2)$$

to generate a BBB diffusion constant of 0.075 hr^{-1}. Because the rate of convective efflux is independent of a molecule's chemical properties, k_{csf} was generated by simply averaging the measured k_{eff} for the solutes that are passively transported and not metabolized (0.3 hr^{-1}). From this arm of the study, the authors concluded that the relative contribution of convection to solute efflux from the brain was strongly dependent on magnitude of k_p and specifically highlighted the variability of solute lipophilicity, though they assumed the ECS volume and other physiological characteristics were held constant.

The second arm of this study focused on physiological parameters that may affect convective efflux. To test this, they compared the rate of ^{14}C-sucrose clearance in rats that

were either awake and freely behaving or restrained, anesthetized with pentobarbital or ketamine/xylazine, treated with adenosine or epinephrine or induced hypovolemia. These conditions allowed for the examination of movement, cardiovascular dynamics, and cerebral metabolic demand on the rate of convection in the brain. They reported that the only physiological conditions associated with a change in sucrose clearance were the adenosine- and pentobarbital-treated rats, increasing and decreasing the rate of efflux, respectively. Similar hemodynamic changes were measured in both treatment groups, including a reduction in mean blood pressure which led the authors to conclude that this effect may involve cerebral metabolic demands. Also included in their study without remark from the authors was a clear increase in clearance of ^{14}C-sucrose in animals anesthetized with ketamine/xylazine compared to awake and restrained mice (0.2657 ± 0.04 hr^{-1} and 0.15 ± 0.06 hr^{-1}, respectively). Together, the experiments in this arm of their study suggest that different anesthetic agents have different effects on solute clearance via bulk flow.

The work of Xie and colleagues aimed to interrogate several additional physiological mediators of parenchymal solute movement with orthogonal approaches, including two-photon light microscopy and real-time tetramethylammonium iontophoresis to study changes in the volume of the ECS (Xie et al., 2013). To accomplish this, the authors infused a fluorescent tracer into the SAS and measured its influx into the cortex as a proxy for CSF-ISF exchange in sleeping and waking mice. In this technically impressive experiment, the authors measured the influx of a tracer into the cortex of the same animal while sleeping and awake. They noted a striking reduction in the tracer penetration in the waking state compared to the sleeping state. Given the changes in the dominant neuronal oscillations during sleep, the authors measured brain activity with electroencephalography and were able

to recapitulate these firing patterns with ketamine-xylazine anesthesia. When the multiphoton experiments were repeated comparing cortical tracer penetration before and after ketamine-xylazine anesthesia, they observed a similar increase in tracer penetration when the animals were anesthetized. The authors went on to demonstrate that rapid changes in the volume of the ECS occur between sleeping and waking states, with an increase of over 60% in the ECS volume of sleeping mice. The mechanism underlying the rapid structural remodeling was inhibited by a cocktail of adrenergic inhibitors, including prazosin, atipamezole, and propranolol. These findings suggest that adrenergic tone in the CNS may also have a strong effect on parenchymal solute movement. It is important to note that the systemic effects of the adrenergic inhibition were not controlled in this experiment. Therefore, adrenergic inhibition may have confounding effects on the cardiovascular system that also contribute to CSF-ISF exchange, such as modulating vascular pulsatility(J. Iliff et al., 2013).

Physiological aspects of solute efflux from the cerebrospinal fluid

Once in the SAS, molecules may escape via several efflux pathways outlined in the "Cerebrospinal fluid" section above, or may remain in the CSF if efflux from this compartment is impaired. Because of the dominant notion that CSF reabsorption occurs via bulk efflux across the arachnoid granulations, early studies of CSF reabsorption attempted to measure the "resistance" to reabsorption using a formula developed by Davson (Czosnyka et al., 2003; Ekstedt, 1978),

$$ICP_{baseline} = R_{CSF} \times \text{Rate of CSF Production} + P_{ss} \qquad (3)$$

Where R_{CSF} is the resistance of bulk CSF efflux and P_{ss} is the pressure in the superior sagittal sinus. Following this logic, many studies measure the resistance to CSF efflux by infusing

artificial CSF or saline into the intrathecal space and monitoring changes in ICP. This led to the derivation of the following equation, which facilitates experimental estimation of the R_{CSF} parameter,

$$ICP_{Post\text{-}infusion} - ICP_{baseline} = R_{CSF} \times \text{Rate of Infusion} \qquad (4)$$

Where $ICP_{Post\text{-}infusion}$ is the steady state ICP achieved after constant intrathecal infusion. This model relies on several assumptions, including that the only bulk reabsorption occurs in the dural venous sinuses, that CSF formation is constant across the course of the intrathecal infusion, and that CSF absorption is proportional to the pressure difference between the venous sinuses and the ICP (Boon et al., 1997; Ekstedt, 1978; Vastola, 1980). Despite these very limiting assumptions, this technique was used widely to study neurological diseases thought to be associated with reduced CSF reabsorption such as normal pressure hydrocephalus and communicating hydrocephalus.

Studies focused on the physiological mediators of lymphatic CSF reabsorption are remarkably few. In fact, to date the only studies available on this subject were described in the 1983 by Bradbury and colleagues (Bradbury and Westrop, 1983). The authors infused radioiodinated albumin into the lateral ventricle of the rabbit, cannulated the cervical lymphatic trunk, and measured the rate of tracer efflux into the lymph. The authors included several groups, including different head positions, infusion rates, and mechanical or chemical obstruction of the olfactory fossa with kaolin or cyanoacrylate glue. Together, these experimental groups allowed the authors to test the effect of CSF flow rate, intracranial pressure, and the anatomical importance of the nasal turbinates in the lymphatic drainage of solutes in the CSF. Interestingly, they found that chemical or mechanical obstruction of the cribriform plate markedly reduced the rate of radiolabeled albumin into the lymphatic trunk.

This suggests that the olfactory fossa or olfactory nerve endings that extend across the cribriform plate provide an important contribution to lymphatic drainage of solutes in the CSF. The effect of head positioning was tested by performing the tracer infusion into the rabbit in a prone position with the head either elevated or lowered twenty degrees from the control position. While the lowered head position was not associated with a significant change in lymphatic drainage, the elevated head position markedly reduced the rate of lymphatic drainage. From these data, the authors concluded that this was not particularly surprising and suggested that gravitational effects likely contributed to this observation. However, in the context of more recent findings regarding fluid movement, it is also likely that the altered tracer efflux may also be due to changes in cerebral blood flow and intracranial pressure associated with postural changes. As noted above, this study stands alone as the only study to evaluate physiological factors that influence solute efflux into the cervical lymphatic vasculature.

Lymphatic Biology and the Meningeal Lymphatic System

The molecular determinants governing lymphatic vascular biology have received little attention in the past. Indeed, until the end of the 20th century there was still a paucity of insight into critical signaling pathways that govern proliferation and development of lymphatic vessels in the mammal (Jeltsch et al., 1997; Joukov et al., 1998). Similarly, relatively few studies investigate the physiological properties that govern the function of lymphatic vessels. This section will highlight the major elements of lymphatic biology established in the peripheral lymphatic system and comprehensively outline the known literature describing the meningeal lymphatic vasculature at the commencement of the work in this dissertation.

The structure and function of lymphatic vessels in peripheral tissues

Lymphatic vessels are broadly classified into two categories: initial lymphatic vessels, also called lymphatic capillaries, and collecting vessels. Initial lymphatic vessels are blind-ending capillaries that interdigitate into capillary beds throughout the body. These vessels absorb fluid, macromolecules, and cells in the ECS. After these constituents enter into the lumen of lymphatic capillaries, they are collectively referred to as lymph. Reflux of lymph in lymphatic capillaries is prevented by pseudo-valvular structures in the lymphatic endothelium, as lymphatic capillaries generally lack traditional valves (Trzewik et al., 2001). This pseudo-valve consists of gaps between endothelial cells, where high levels of lymphatic vessel hyaluronan receptor-1 (LYVE1) are expressed. Interactions between LYVE1 and hyaluronic acid in the ECS provide an anchor between lymphatic capillaries and the ECS (Leak and Burke, 1968). Upon increases in ISF pressure, these anchoring points facilitate a transient opening between lymphatic endothelial cells and movement of ISF into the lumen of the capillary. With reduction in ISF pressure, this opening is again minimized, preventing reflux of the newly-formed lymph (Galie and Spilker, 2009; Mendoza and Schmid-Schönbein, 2003). Lymphatic capillaries also lack smooth muscle cells in the vessel wall and therefore rely on other mechanisms to achieve directional conduction of lymph. Lymph is drained from lymphatic capillaries into downstream collecting lymphatic vessels, which are more anatomically robust. Unlike lymphatic capillaries collecting vessels are lined with smooth muscle cells and generally contain valvular structures. Because of this, individual regions of a collecting vessel bounded by valves are referred to as lymphangions. Lymphangions are considered the basic unit of the collecting lymphatic vessel and experiments focused on conduction of lymph often focus on the actions of smooth muscle

cells in individual lymphangions. Lymph in collecting vessels eventually drains back into the bloodstream at lymphatico-venous anastomoses, the largest of which is typically found at the left subclavian vein in the human body.

Conduction of lymph throughout the body relies on two major mechanisms: intrinsic and extrinsic pumping. Intrinsic pumping describes the contraction of smooth muscle cells in the lymphatic vessel wall. Contraction of the lymphangion is analogous to the contraction of the heart, with both changes in preload and afterload affecting lymph output from individual lymphangions. Experimentally, lymphangion contraction frequency and contractility can be increased by increasing preload, suggesting that transmural pressure is an important physiological mediator of intrinsic pumping (Gashev et al., 2004). Extrinsic pumping describes the cyclical compression and relaxation of lymphatic vessels due to changes in the volume of the ECS. Illustrative examples of this are in the heart and skeletal muscle, which elicit substantial volumetric changes in the ECS during contraction and relaxation. Thus, current estimates of the relative importance of intrinsic and extrinsic pumping depend of the tissue or organ, as the contribution of extrinsic pumping may change substantially across tissues.

The importance of the lymphatic system in the human body becomes immediately apparent in pathological contexts where lymphatic drainage is disrupted. For example, the Filarioidea roundworm develops parasitically in human lymphatic vessels and causing lymphatic inflammation that ultimately leads to sclerosis of large collecting vessels. The resulting lymphatic insufficiency causes catastrophic accumulation of edema upstream of the affect region and can lead to elephantiasis if untreated. Less severe examples include

iatrogenic lymphedema secondary to oncological surgery and genetic mutations resulting in abnormal lymphatic development.

Meningeal lymphatic structure and function

The disparate experimental findings that up to 50% of parenchymal solutes escape from the cranium via the cervical lymphatic trunk and the lack of traditional lymphatic vasculature in the brain have puzzled physiologists for decades. Furthermore, solutes of wide-ranging hydrodynamic radii drain into the DCLNs from the CSF and brain, suggesting that lymphatic solute clearance from the cranium is not size selective for macromolecular solutes up to ~27 nm (Figure 2). Recently, the several groups characterized lymphatic vessels in the meninges overlying the brain and proposed that these vessels may be the anatomical link between the brain and cervical lymphatic vasculature (Aspelund et al., 2015; Louveau et al., 2015). Meningeal lymphatic vessels are distributed anatomically in parallel with dural venous sinuses and arteries, reflecting anatomical patterns observed in peripheral tissues (Figure 3). In the initial characterization in the rodent, both groups demonstrated that lymphatic vessels in the meninges express hyaluronic acid receptor LYVE1, prospero homeobox 1 (PROX1), podoplanin (PDPN) and vascular endothelial growth factor receptor 3 (VEGFR3) which are common molecular markers of lymphatic endothelium. Both groups also assessed expression of CD31 these lymphatic vessels, but reported differing results. While Aspelund and colleagues found they were mostly CD31-negative, Louveau and colleagues reported that meningeal lymphatic vessels express CD31. Although mixed findings about CD31 expression in lymphatic endothelium exist in the literature, most studies report very low levels of CD31 expression (Lokmic et al., 2015; Podgrabinska et al., 2002). Louveau and colleagues went on to demonstrate that unlike the dural venous sinuses

and arteries, these lymphatic vessels do not contain smooth muscle cells in the vessel wall. Both groups examined meningeal lymphatic vessels for the presence of valvular structures, which were only found in the skull base by Aspelund and colleagues. Together, these findings led both groups to conclude that the meningeal lymphatic vessels under study were likely lymphatic capillaries and not collecting vessels.

Functionally, these vessels contain leukocytes organized in a linear fashion, the silhouettes of which can be visualized in vivo with 2-photon microscopy (Figure 4). These cells were shown to be $CD3^+$ T cells by immunofluorescence performed by Louveau et al. At the time of the report, it was unclear whether these leukocytes originated from the subarachnoid or dural compartments of the intracranial space. In addition to containing cells, both labs showed CSF or parenchymal tracers of different sizes including quantum dots or a 20 kDa polyethylene-glycol dye colocalized with meningeal lymphatic vessels in the calvarium and skull base. Importantly, this suggests that intracranial lymphatic vessels can access and participate in the clearance of solutes in the CSF. It was further shown that modest changes in vessel diameter or solute accumulation in the meningeal lymphatic vessels can be elicited by ligating the cervical lymphatic trunk inferior to the DCLNs. The morphological changes observed in meningeal lymphatic vessels after ligation of the cervical lymphatic trunk were interpreted as lymphatic insufficiency. A similar ligation experiment reported by Louveau and colleagues demonstrated increased T cell counts in the meninges, suggesting that the patency of cervical lymphatic trunk has effects on immune cell trafficking in addition to solute and fluid efflux.

These initial studies raised many questions about role of the meningeal lymphatic system in physiological and pathophysiological contexts. Although the functional data

described above was provided to argue that the meningeal lymphatic vessels can absorb solutes in the brain and CSF, it was unclear how these solutes might cross the arachnoid mater. Indeed, the arachnoid cell layer forms a significant biological barrier between the CSF and the lymphatic vessels associated with the dura mater. This ambiguity was partially due to the difficulty in sectioning the intact cranium to identify the exact meningeal layers that are invested by lymphatic capillaries. The mechanisms that underlie lymphatic solute absorption from the CSF are also unclear. For instance, although lymphatic capillaries can absorb solutes from the ISF via transient intercellular gaps as discussed above, cutaneous lymphatic endothelial cells express low density lipoprotein receptor-related protein 1 (LRP1). This receptor facilitates active transport of solutes via transcellular trafficking, therefore the lymphatic vasculature in the meninges may also feature potential mechanisms of active transport. This may be particularly important in the setting of Alzheimer's dementia (AD), because LRP1-mediated clearance of Aβ is a well-known mechanism of Aβ efflux at the BBB. This mechanism of Aβ clearance will be discussed in greater detail within the following section. Furthermore, despite evidence that these vessels were found near foramina in the base of the skull, the path that these lymphatic vessels take as they exit the cranium also remained unclear. The characterization of lymphatic vessels in the meninges also quickly drew attention from neurodegeneration and neuroinflammation research communities, with widespread speculation that meningeal lymphatic function may influence the development or progression of diseases such as multiple sclerosis and AD.

Alzheimer's Dementia

Clinical and neuropathological Alzheimer's dementia

Late onset AD is the most common form of dementia, and the risk of developing AD increases greatly with age. Clinical AD is characterized by progressive memory loss, difficulty completing familiar tasks, trouble understanding spatial relationships, and mood changes. The clinical progression of AD features marked brain atrophy (Fox, Freeborough, & Rossor, 1996) and the number of affected brain regions increases as cognitive impairment progresses. Typically, atrophy is first noted in the entorhinal cortex and hippocampus in cognitively intact patients and later involves the parietal and frontal cortex as cognitive impairment worsens (Scahill, Schott, Stevens, Rossor, & Fox, 2002). The diagnosis of AD requires the presence of neuritic plaques and neurofibrillary tangles in the brain, composed mostly of amyloid beta (Aβ) and tau proteins, respectively (Hyman et al., 2012; Selkoe, 2001a). The severity of cognitive impairment generally correlates with the burden of neurofibrillary tangles and neuritic plaques (Hyman et al., 2012), however these hallmarks of AD can be found in the aging human brain without clinical detection of cognitive impairment, suggesting that individual responses to Aβ and tau aggregation may vary substantially (Bennett et al., 2006; Rodrigue et al., 2012). Although both tau and Aβ aggregate in the ECS, Aβ received substantial attention for its potential role in the pathogenesis of AD. This is largely due to the formulation of the "amyloid cascade hypothesis," which postulates that deposition of Aβ occurs in the ECS upstream of the aggregation of tau in neurofibrillary tangles, synaptic loss, and cognitive impairment. The amyloid cascade hypothesis is founded upon the observation that Aβ is the principle protein found in neuritic plaques and that familial AD is generally caused by mutations in APP

which alter its proteolytic processing (Hardy and Higgins, 1992). Combining these findings with data demonstrating that Aβ has cytotoxic effects on neurons, this hypothesis dominated AD research since its development in 1992.

Mechanisms of Aβ formation and toxicity

The physiological role of amyloid precursor protein (APP) remains poorly understood. However, because of its association with AD, the molecular processing of the protein was also studied in great detail. Multiple cells express APP in the CNS, including neurons, oligodendrocytes, and endothelial cells. In the neuron, APP is translated in the soma and trafficked into nerve processes via anterograde axonal transport (Koo et al., 1990). APP is inserted into the cell membrane where it is subject to multiple enzymatic cleavage events. This includes cleavage by the α-secretase enzyme resulting in the production of sAPPα, followed by a second cleavage by γ-secretase enzyme (also referred to as presenilin). This processing sequence is considered to be a non-amyloidogenic pathway because the α-secretase cleavage site exists within the region of APP that contains Aβ (Lichtenthaler, 2012). Alternatively, APP may be reinternalized into an endosomal compartment and cleaved by the β-secretase enzyme (Koo and Squazzo, 1994; Vassar et al., 1999). Unlike α-secretase cleavage, cleavage by β-secretase occurs outside of the Aβ domain, producing the amyloidogenic precursor to Aβ, sAPPβ. Subsequent cleavage of sAPPβ by the γ-secretase enzyme in the endosome produces Aβ (Vassar et al., 1999). This Aβ peptide is then trafficked back to the membrane and is transferred to the extracellular compartment via exocytosis. It is important to note that several isoforms of Aβ can be produced from proteolytic processing of the APP protein. Most common and relevant to AD pathology are the $A\beta_{1\text{-}40}$ and $A\beta_{1\text{-}42}$ isoforms (Selkoe, 2001b). The thermodynamic stability varies between

isoforms, with significant biological consequence. Specifically, the $A\beta_{1-42}$ isoform contains more hydrophobic residues, conferring increased self-aggregation properties relative to the $A\beta_{1-40}$ isoform. Both $A\beta_{1-40}$ and $A\beta_{1-42}$ are found in diffuse and neuritic plaques.

In the ECS, Aβ enters into equilibrium between monomers, soluble oligomers, and insoluble fibrils. The hydrodynamic radius and free energy of the Aβ species in these pools varies widely. Indeed, the estimated hydrodynamic radius of monomeric is only ~0.9 nm (Nag et al., 2011), while Aβ oligomers may reach up to 50 nm (Garai et al., 2008) and insoluble fibrillary species may extend to greater than 200 nm. The diversity of radii, particularly between monomeric and oligomeric forms of Aβ reflects the fact that oligomers may contain up to 30-mers of Aβ peptides. As noted above, the thermodynamic stability also varies between these pools, increasing from monomeric to oligomeric and from oligomeric to fibrillary forms. Small oligomeric Aβ species have high free energy and generally quickly transition into larger oligomeric structures under physiological conditions, suggesting within-pool variability of structural stability as well (Nag et al., 2011). The structural differences in these pools give rise to different biological properties that affect toxicity and clearance mechanisms. Several studies reported that the neurotoxicity of Aβ increases disproportionately with increasing orders of the oligomeric forms. Although the magnitude of the estimated toxicity varies from study to study, up to a threefold increase in cytotoxicity from monomeric to dimeric Aβ forms was reported in in vitro studies, further increasing with trimer and tetrameric Aβ (Ono et al., 2009). Many mechanisms of Aβ toxicity are proposed, including neuronal excitotoxicity, inhibition of long term potentiation, formation of ion channels in the cell membrane, and (Bode et al., 2017; Li et al., 2011; Serra-Batiste et al., 2016; Walsh et al., 2002). Almost all of these mechanisms are attributed to oligomeric

species of Aβ, which generated significant interest in converting Aβ species in the oligomeric pool back into the monomeric pool to reduce its toxicity and increase its clearance from the CNS.

Aβ trafficking in the CNS

Histological evidence of Aβ in the AD brain raised questions about whether pathological changes in endogenous Aβ production or clearance underlie its accumulation in the CNS. There is clear evidence that increased production of APP and subsequent Aβ in the CNS is sufficient to induce the development of AD. Perhaps the best example of this phenomenon in humans is the overexpression of APP after chromosomal nondisjunction giving rise to trisomy of chromosome 21, which contains the gene encoding APP. This extra copy of chromosome 21 results in the relative overexpression of APP and results in early-onset AD, which is observed in up to 28% of Down's syndrome patients by the age of thirty (Lai and Williams, 1989; Wisniewski et al., 1985). Although the overproduction of Aβ is sufficient to induce AD, it is often not a feature of late-onset AD. Indeed, recent evidence demonstrated that Aβ production is unchanged in AD, but the clearance of Aβ is reduced (Mawuenyega et al., 2010). This key finding suggests that disruption of Aβ efflux is responsible for the loss of Aβ homeostasis observed in late-onset AD. Therefore, in most patients with AD, the impairment of Aβ efflux appears to cause Aβ aggregation in the CNS.

Several endogenous pathways exist for Aβ clearance in the CNS, including cellular degradation, efflux across the BBB directly into the bloodstream, and via trafficking from the ISF into the CSF. For cell-mediated degradation of Aβ, several studies indicated that LRP1 expressed by multiple cell lineages plays an important role of Aβ degradation. This includes the facilitation of efflux across endothelial cells into the bloodstream across the

BBB, and astrocytic and neuronal cellular degradation (Kanekiyo et al., 2013; Liu et al., 2017; Storck et al., 2015). Microglial behavior also appears to influence Aβ dynamics in the ISF, however there are conflicting reports about whether the dominant behavior of microglia is to degrade or propagate Aβ in normal conditions (Iaccarino et al., 2016; Venegas et al., 2017). In terms of CSF-ISF exchange, several findings support the notion that Aβ is removed from the brain via efflux into the CSF. Multiple species of Aβ are detectable in the CSF of humans at steady state (Bateman et al., 2006) and the concentration of Aβ in the CSF varies reliably with the progression of clinical AD. In rodent models, disruption of CSF-ISF exchange via genetic deletion of the AQP4 water channel reduces the clearance rate of radiolabeled Aβ (Iliff et al., 2012).Together, these findings suggest that CSF-ISF exchange contributes to parenchymal clearance of Aβ. The relative contributions of these Aβ clearance pathways were not empirically determined, though experimental disruption of each acutely is sufficient to induce Aβ accumulation in rodent models of AD.

The physiological effectors of Aβ exchange into the CSF are still incompletely understood, however many studies suggest a link between sleep and Aβ clearance via efflux into the CSF. Perhaps the earliest evidence supporting this notion is a report describing variations in the concentration of CSF and ISF Aβ associated with circadian rhythm and sleep-wake states. A study in 2009 by Kang and colleagues demonstrated a diurnal pattern in ISF and CSF Aβ, where Aβ in both compartments increased with wakefulness and decreased with sleep in human subjects and a mouse model of AD (Kang et al., 2009). This study demonstrated that ISF Aβ levels could be reduced with an orexin antagonist, suggesting a causative link between wakefulness and the concentration of ISF Aβ. Similar diurnal ISF Aβ

patterns were reported in the APPswe/PS1δE9 mouse line, as well as CSF Aβ in human subjects with presenilin mutations (Roh et al., 2012). Importantly, these findings were corroborated in the human by Huang and colleagues (Huang et al., 2012) found that CSF Aβ displays a diurnal variation in 20 young (35.5± 10 year old) healthy subjects, with maximum and minimum CSF Aβ near 2100 and 0900 hours, respectively. This study also found that the amplitude of this rhythm was reduced in aged subjects with CNS amyloidosis compared to age-matched controls. Together, these findings suggest that Aβ production, clearance, and/or CSF-ISF solute exchange may be entrained to the sleep cycle. It is important to note that subsequent studies in other patient populations did not observe diurnal variation in Aβ, however these differences were attributed to differences in patient populations and sampling techniques (Cicognola et al., 2016; Moghekar, Goh, Li, Albert, & O'Brien, 2012; Slats et al., 2012). Furthering the hypothesis that Aβ trafficking in the CNS is dependent on the sleep cycle, an elegant study by Shokri-Kojori et al. (Shokri-Kojori et al., 2018) recently demonstrated that one night of sleep deprivation increases parenchymal Aβ burden by 5% in 20 healthy control subjects (39.8±10.4 years old). This study provides direct evidence that parenchymal Aβ is acutely affected by the sleep wake cycle. In patients with AD, complaints of sleep and circadian disruption are common and include insomnia and fragmentation of sleep architecture (Weldemichael & Grossberg, 2010). However, the relationship between sleep disruption and accumulation of Aβ in the brain is complicated by the association of AD with aging and brain atrophy, both of which are also linked to sleep disruption (Landry, Best, & Liu-Ambrose, 2015; Myers & Badia, 1995; Sexton, Storsve, Walhovd, Johansen-Berg, & Fjell, 2014).

Notwithstanding the complex and likely bidirectional relationship between AD and sleep disruption, there is also evidence that aging impairs clearance of parenchymal Aβ as well as CSF-ISF exchange. In 2014, Kress and colleagues reported that parenchymal clearance of radiolabeled Aβ is reduced by up to 40% in aged mice compared to young mice (Kress et al., 2014). In the same study, they demonstrated that CSF-ISF exchange of 3 kDa and 45 kDa molecules is reduced by approximately 40% and 70%, respectively. Although the variety of Aβ clearance mechanisms outlined above were not controlled in this study, the association between attenuated CSF-ISF exchange and reduced Aβ clearance suggests that reduced CSF-ISF exchange may partially contribute to the impairment of Aβ clearance in aged mice. Shortly after this study was published, other age-related effects on Aβ efflux from the CSF were described by Patterson and colleagues, who demonstrated that CSF Aβ clearance is reduced in non-demented aging patients (Patterson et al., 2015). In this study, they found that $A\beta_{40}$ and $A\beta_{42}$ turnover rates were slowed in the CSF of aged human subjects (73.3 ± 6.6 years old) in comparison to younger controls (48.0 ±14.6 years old). Moreover, a remarkable 2.5 fold difference in Aβ half-life was reported between 30 year old and 80 year old participants, suggesting that Aβ has a markedly increased residence time in the aged human CSF. Together, the evidence that Aβ clearance from the ISF and CSF is reduced with aging and in AD patients strengthened the hypothesis that age-related impairment in Aβ clearance pathways underlies the accumulation of Aβ in the CNS of AD subjects.

The question of which Aβ efflux pathway dominates under physiological conditions is an interesting and important one. Though this is difficult to assess experimentally, Aβ clearance kinetics provide insight into this process. One study that employed a microimmunoelectrode to measure the rate of Aβ clearance in the mouse brain reported a

fast and slow phase of Aβ efflux (Yuede et al., 2016). Overall, the contribution of the fast phase to Aβ clearance was smaller than that of the slow phase, suggesting that multiple clearance mechanisms act on ISF Aβ simultaneously. In a clever experimental manipulation they inhibited p-glycoprotein, a BBB transport protein, and found that this increased the half-life of exogenous Aβ, but only during a slow clearance phase. The authors concluded that p-glycoprotein-dependent Aβ efflux across the BBB accounts for a relatively large contribution to Aβ clearance on a local level. The fast phase of Aβ clearance remains unknown and may be made up by several processes including advection, proteolytic degradation and/or cellular uptake.

Therapies for AD

As noted above, investigations throughout the last two decades drove major advances in the scientific understanding of AD pathogenesis. Despite these advances, patients suffering from AD still lack any FDA-approved options for disease modifying therapies and must rely on drugs that manage symptoms associated with AD instead. This includes acetylcholinesterase inhibitors and NMDA receptor blockers to help with progressive memory loss and confusion. To test the amyloid cascade hypothesis, multiple therapies were developed to modify the production, aggregation, or clearance of Aβ in the human brain. These include small molecule inhibitors of β-secretase (Egan et al., 2018; Kennedy et al., 2016) and γ-secretase (Doody et al., 2013; Dovey et al., 2001), and anti-Aβ antibodies that facilitate immune-mediated clearance of parenchymal Aβ (Honig et al., 2018; Salloway et al., 2014). Despite their ability to slow the production or increase the clearance of Aβ, every clinical trial examining these drugs in AD patients failed to show efficacy in slowing the progression of cognitive impairment compared to placebo. This led some to

question the validity of the amyloid cascade hypothesis and focus on other histological elements such as tau. Others have speculated that by the time patients are experiencing clinical symptoms of AD, the disease may function in an Aβ-independent fashion. In this case, successful clearance of plaques containing Aβ in the human brain would not be sufficient to prevent the neuroinflammatory processes responsible for progressive synaptic loss and atrophy in the cognitively-impaired brain. Thus, as in biomedical research focused on other human diseases, efforts toward early identification and treatment of patients with increased risk of developing AD have already begun. There is hope that ongoing clinical trials that enroll subjects with mild cognitive impairment will help to define the therapeutic window of therapies targeting Aβ, if such a window exists.

The Meningeal Lymphatic System, CSF Physiology, and Alzheimer's dementia

With the strong clinical evidence in human subjects demonstrating that exchange between the CSF and ISF compartments is conserved in humans and further preclinical evidence in rodents suggesting that impairment of CSF-ISF exchange can slow clearance of Aβ and tau proteins, the question of whether glymphatic function is impaired in the setting of neurodegenerative disease has become more intriguing (Iliff et al., 2014; Xu et al., 2015). Still, for solute exchange between these compartments to facilitate reduction of waste in the brain, there must be irreversible loss of Aβ from the CSF to prevent reflux into the brain. Unlike in the ISF compartment, the mechanisms responsible for Aβ clearance from the CSF have received almost no scientific attention in the past. The characterization of the meningeal lymphatic system raised important questions about the possibility of lymphatic

clearance of soluble Aβ produced in the brain parenchyma. Indeed, since these reports emerged in 2015 there were widespread speculations about a putative role for the meningeal lymphatic system in AD (Iliff et al., 2015; Louveau et al., 2016; Tarasoff-Conway et al., 2015).

My global hypothesis is that impairment of lymphatic drainage from the brain underlies the age-related accumulation of Aβ in the AD brain. Before performing experimental manipulations to test this hypothesis, however, there are fundamental questions that should be answered. These include (1) whether this meningeal lymphatic system, which was characterized in the rodent, also exists in the human, (2) if soluble Aβ can be trafficked out of the cranium and whether this process is impaired with increasing age, and (3) if there are identifiable physiological mediators of this process. To answer these fundamental questions, the specific aims of this dissertation are described below.

Specific aims

Determine if the human meninges contains lymphatic vasculature

The translational significance of any findings of meningeal lymphatic vessels in rodent models would be vastly reduced if an analogous system does not exist within the human meninges. To test this prediction, we examined the human meninges using a combination of immunofluorescence and spectral unmixing to reduce the widespread autofluorescence encountered in meningeal tissue. As a step toward understanding the potential role for meningeal lymphatic vessels in AD, we compared the structure of meningeal lymphatic vessels in AD and control subjects. We also considered deposition of Aβ in association with these vessels between AD and control subjects.

Determine the role of the meningeal lymphatic system in the efflux of Aβ

To assess the role of lymphatic Aβ clearance, we first evaluated whether exogenous soluble Aβ is cleared from the brain and CSF via the cervical lymphatic vasculature. Due to the reported reduction in Aβ clearance from the CSF in aging humans, we next evaluated the clearance of solutes, including Aβ, from the CSF in young and aged mice. Structural changes in lymphatic vessels associated with aging were also assessed by measuring the diameter and distribution of lymphatic vessels in meningeal whole mounts of young and aged mice.

Determine physiological controls on lymphatic solute efflux

To evaluate some of the physiological mediators of lymphatic solute absorption from the brain and CSF, we measured the efflux of two dextrans in co-injected into the motor cortex of mice that were subsequently kept under anesthesia or awakened and allowed to freely behave. We further identified differences in the physiological state in anesthetized mice, including the tension of O_2 and $PaCO_2$ in the arterial blood. Next, we evaluated the correction of these parameters to determine their effect on lymphatic drainage from the brain and CSF.

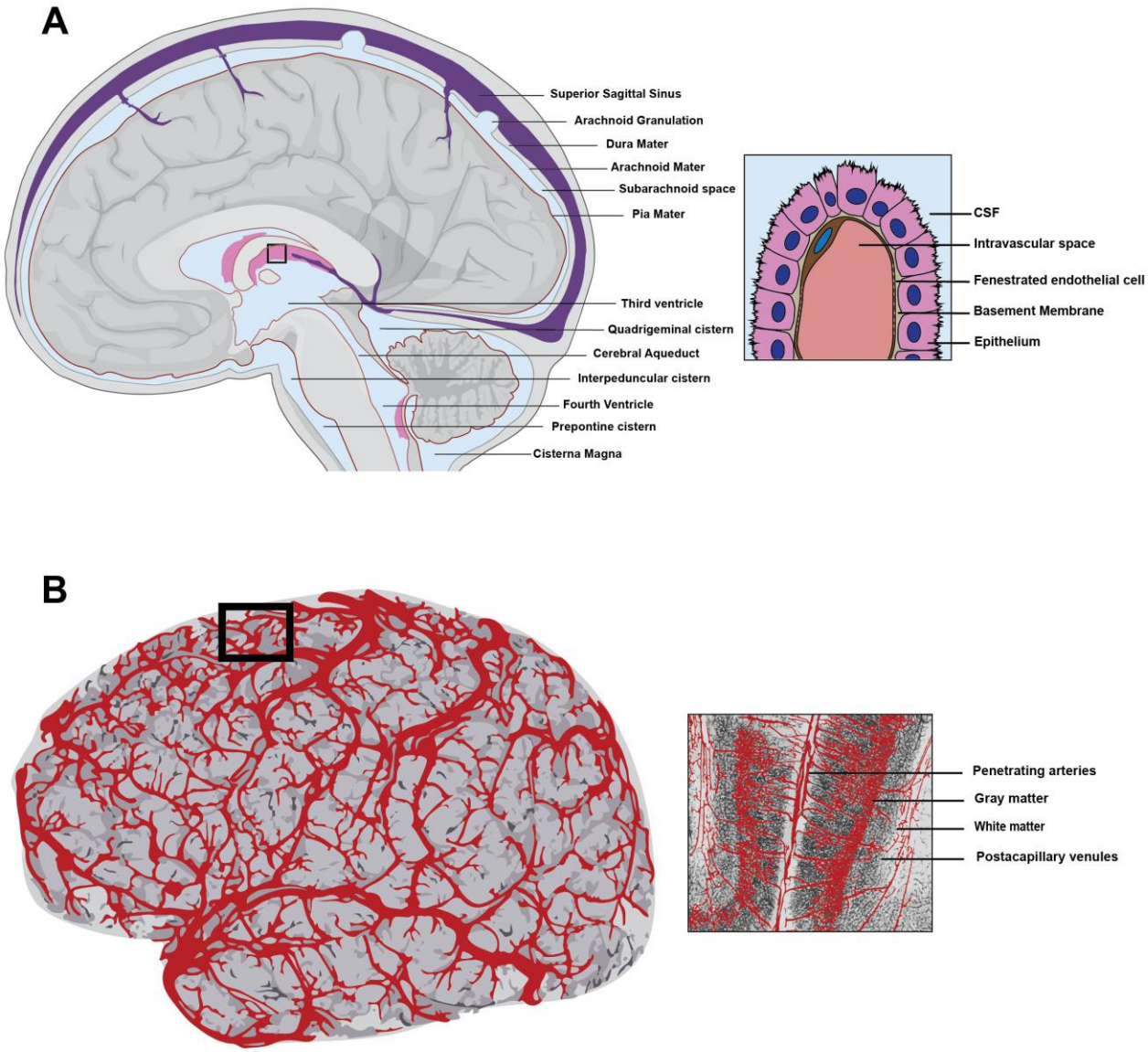

Figure 1. Topography of the intracranial space.

A. Illustration of a sagittal section of the human brain. Inset demonstrates the blood-CSF interface found at the choroid plexus. B. Illustration of the cortical blood supply to the human brain. Inset shows a coronal section demonstrating the distribution of penetrating arteries in the cortical gray matter. Panel A was adapted from the Textbook OpenStax Anatomy and Physiology under Creative Commons licensing Attribution 4.0.

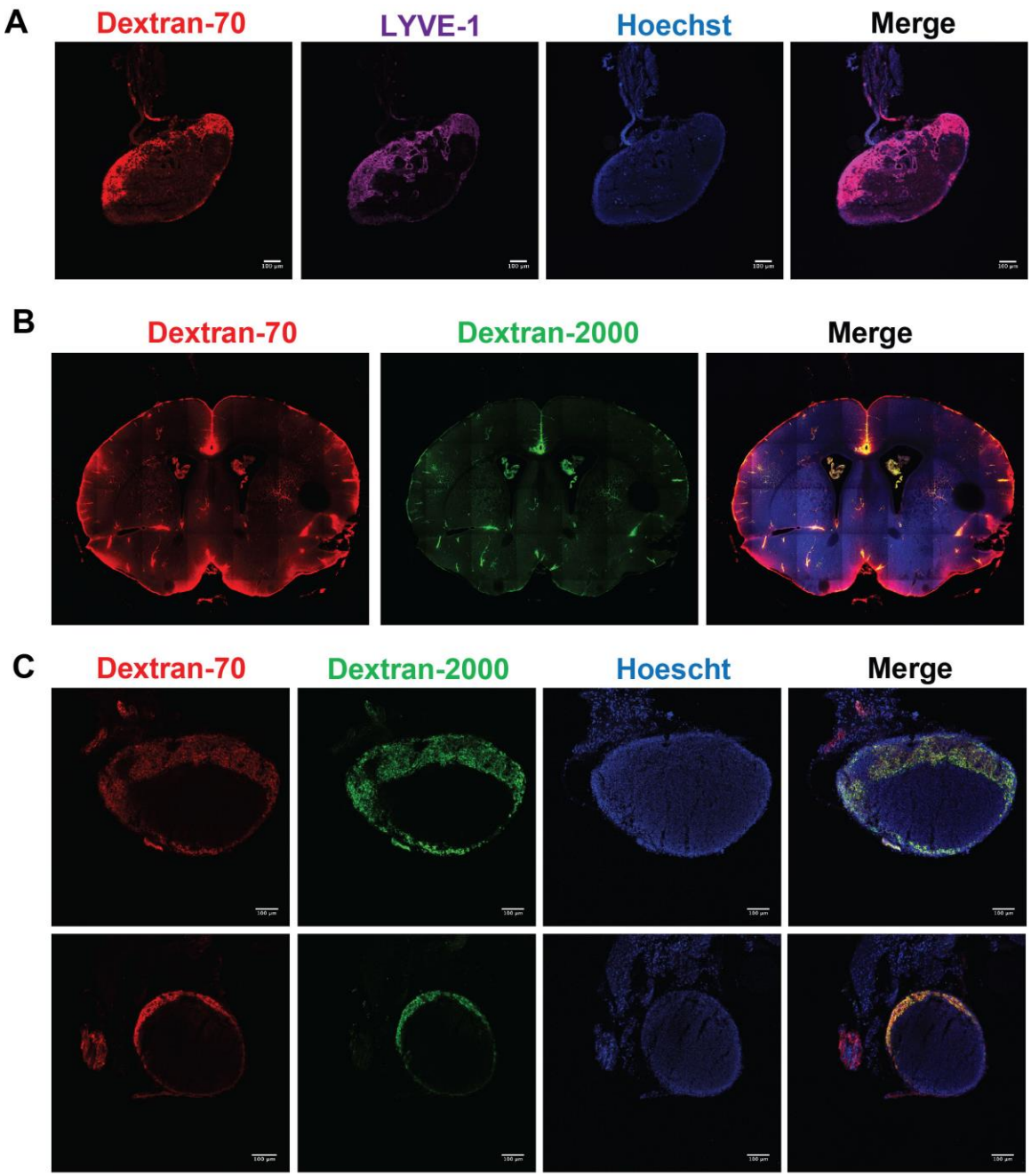

Figure 2. Molecular exchange between the CSF and ISF is size dependent, but lymphatic drainage is not.

A. Tracers infused into the CSF are trafficked into the DCLNs. B. Coronal brain sections demonstrating size-dependent penetration of CSF tracer into the brain. C. 70 kDa and 2000 kDa tracers are both drained into the DCLNs.

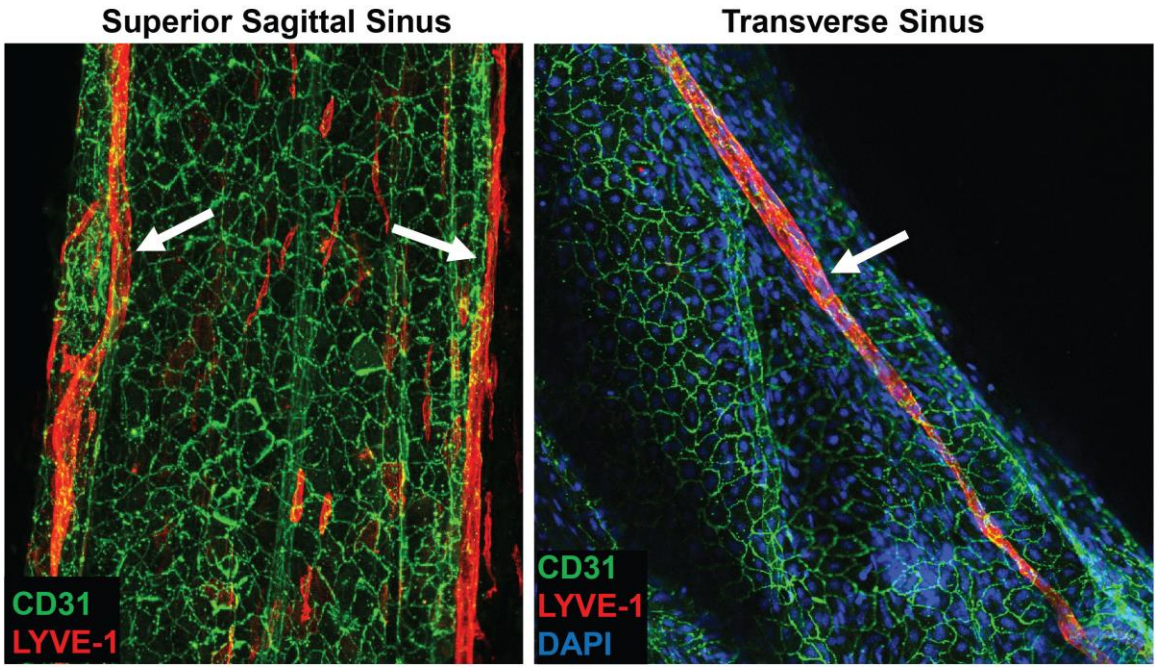

Figure 3. Lymphatic vessels in the rodent meninges.

LYVE1+ lymphatic vessels are distributed throughout the rodent meninges in close association with venous sinuses and cranial nerves. Representative images on left and right show LYVE1+ lymphatic vessels (arrows) associated with the superior sagittal sinus and transverse sinus in the calvarium.

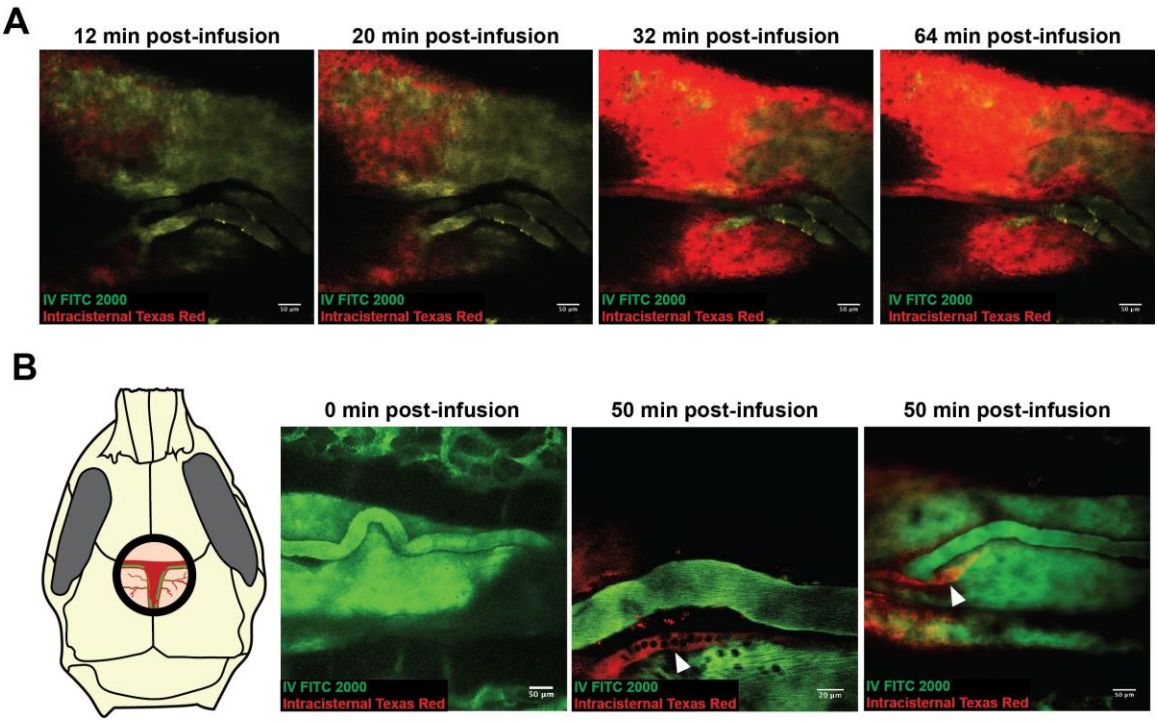

Figure 4. Time course of intracisternal tracer distribution around the superior sagittal sinus and visualization of meningeal lymphatic-like vessels.

A. In vivo time course of perivascular flow around the superior sagittal sinus. B. Left, illustration of thin skull preparation for multiphoton imaging. Right, In vivo perivascular tracer reveals lymphatic-like vessels associated with the superior sagittal sinus. Arrows represent lymphatic-like vessels lined with leukocyte-sized silhouettes.

Chapter Two: Characterizing the Human Meningeal Lymphatic System

Elements of this chapter were published in *Brain, Behavior, and Immunity:*

Goodman JR, Adham ZO, Lund AW, Woltjer RJ, Iliff JJ. "Characterization of dural sinus-associated lymphatic vasculature in human Alzheimer's disease subjects." *Brain, Behavior, and Immunity*. 2018 Jul 25. doi: 10.1016/j.bbi.2018.07.020.

Introduction

Alzheimer's dementia (AD) is the leading cause of dementia worldwide and is diagnosed histopathologically by the presence of intracellular neurofibrillary tangles and extracellular amyloid beta (Aβ) plaques (Glabe, 2005; Selkoe, 2001a). In sporadic AD, production of Aβ remains relatively stable during the aging process, yet the slowing of Aβ clearance observed among aging and AD subjects suggests that impairment of endogenous Aβ clearance may underlie Aβ deposition in the human brain (Mawuenyega et al., 2010; Patterson et al., 2015). Aβ is removed from the brain interstitium through several mechanisms, including local cellular degradation, receptor-mediated efflux across the blood-brain barrier, and perivascular exchange into the cerebrospinal fluid (CSF) compartment via the glymphatic system (Iliff et al., 2012; Ramanathan et al., 2015; Tarasoff-Conway et al., 2015).

The characterization of a meningeal lymphatic vascular system in mice has important implications for our understanding of interstitial homeostasis in the brain and central nervous system (CNS), CSF physiology, and CNS immune surveillance (Aspelund et al., 2015; Iliff et al., 2015; Louveau et al., 2015). These findings were recently confirmed in three human subjects and in nonhuman primates by Absinta et al.(Absinta et al., 2017) who visualized the meningeal lymphatic network by contrast-enhanced magnetic resonance imaging and immunohistochemical detection of meningeal lymphatic vessels with molecular markers of lymphatic endothelial cells. In both mice and humans, meningeal lymphatic vessels are distributed along large blood vessels and cranial nerves in the dura mater, reflecting patterns observed in the peripheral lymphatic vasculature. In mice, meningeal lymphatic vessels absorb macromolecules from the brain and CSF and transport these solutes to the deep cervical lymph nodes (DCLNs). This efflux route provides an anatomical

basis for the experimental observation that molecules introduced into the CNS accumulate in the DCLNs (Boulton et al., 1999; Bradbury and Cole, 1980; Cserr et al., 1992). Although meningeal lymphatic function remains largely unexplored, this pathway is speculated to play an important role in the clearance of pathological waste products such as Aβ from the brain interstitium and CSF (Louveau et al., 2015; Tarasoff-Conway et al., 2015). However, to our knowledge, no studies have evaluated whether changes in meningeal lymphatic vessel structure or function are observed in the setting of AD. It also remains unclear if Aβ is deposited in the walls of meningeal lymphatic vessels as is observed along leptomeningeal and intraparenchymal arteries in the cerebral amyloid angiopathy (CAA) that is present in more than 90% of AD brains (Kalaria and Ballard, 1999).

Methods

Human Tissue Samples

Samples were collected after obtaining consent from subjects or legal next of kin as part of donation to the Oregon Brain Bank. During the autopsy, human dural tissue containing the superior sagittal sinus was collected by pathologists at Oregon Health & Science University. Samples were fixed in 10% formalin for variable time periods before being processed and embedded in paraffin. This manuscript does not contain any identifiable personal patient information. Braak neurofibrillary tangle and CERAD amyloid plaque scores of AD-related pathologies were determined by standard procedures (Braak and Braak, 1995; Mirra et al., 1991). Non-AD diagnoses were established via comprehensive gross and histopathologic exam as described elsewhere (Erten-Lyons et al., 2013).

Throughout tissue preparation and image acquisition, researchers were blinded to the subjects' demographic information and diagnosis.

Tissue Preparation

7 μm coronal sections of paraffin-embedded human dura and superior sagittal sinus were cut and mounted on glass slides (Star Frost). Slides were baked at 50C overnight, deparaffinized using citrus clearing solvent, rehydrated using graded steps of ethanol, and rinsed in distilled water.

Immunofluoresence

Tissues were incubated in 10% formic acid for 10 minutes, steamed in citrate buffer (pH 6.0) for 30 minutes, and incubated overnight at 4C in 0.3% PBS triton with 2% donkey serum, 2.5% bovine serum albumin blocking buffer. Tissues were then incubated in primary antibodies diluted in blocking buffer overnight at 4C (1:40 D240 Podoplanin mouse monoclonal antibody, 1:800 4G8 pan-Aβ mouse monoclonal antibody, 1:300 6E10 pan-Aβ mouse monoclonal antibody BioLegend 803001, 1:100 LYVE1 rabbit polyclonal antibody Abcam 36993, 1:500 α-smooth muscle actin polyclonal antibody Abcam ab5694, 1:300 rabbit CD31 antibody Abcam ab28364). Corresponding fluorescent secondary antibodies were diluted 1:500 in blocking buffer and were incubated overnight at 4C. Tissues stained with Hoechst 33342 were incubated in 1:50,000 working solution for 10 minutes. Tissues stained with X-34 (Sigma) were incubated in 500 μM X-34 for 10 minutes, rinsed in DI water, incubated in 0.2% NaOH/80% EtOH for 2 minutes, and rehydrated in DI water for 10 minutes (Styren, et al., 2000). Slides were mounted using mowiol 4-88 mounting media (Sigma, cat. 81381). Because the podoplanin and Aβ (6E10 and 4G8) antibodies were

generated in the mouse, sequential sections were stained and compared to identify co-localized immunoreactivity.

Confocal Microscopy and Spectral Unmixing

Images were acquired in single frames or z-stacks using the Zeiss LSM 880 with a 20x objective. Due to abundance of autofluorescent material in the aged human meninges, a spectral unmixing strategy was implemented to separate nonspecific background signal from signal due to antibody binding. Specifically, the spectral profile of signal emitted during excitation in lambda mode was measured in unstained, Hoechst only, and Hoechst + secondary antibody treated meningeal tissue samples. After identifying the spectral signature of nonspecific signals in these reference tissues, spectrally separated images were acquired in real time using Emission Fingerprinting. Post image processing (including image thresholding, noise reduction, and maximum intensity z-stack projections) was carried out using ImageJ software.

Results

We first considered human meningeal tissue samples with conventional confocal microscopy, however we quickly identified that the abundant autofluorescence between 405 and 594 nm strongly confounded any subsequent interpretation of the data (Figure 5A). Therefore, we developed a spectral unmixing approach to excluding autofluorescent signal from specific fluorescent signal from secondary antibodies (Figure 5B). To define the presence and distribution of lymphatic vessels in human meningeal tissue, we used immunofluorescence in post mortem coronal sections of superior sagittal sinus (SSS, Figure

6A-B) derived from control subjects (n=5), AD subjects (n=6), and subjects diagnosed with mixed dementia or other neurological diseases (n=10). Demographic information including age at death, gender, clinical-pathological diagnosis, Braak stage, and Consortium to Establish a Registry for Alzheimer's Disease (CERAD) score (neuritic Aβ plaque burden) for each subject are reported in Table 1. To visualize podoplanin (PDPN, a lymphatic endothelial cell marker) immunofluorescence across the large SSS histological sample, we employed whole-slide fluorescence microscopy. Individual PDPN+ lymphatic vessels were visualized by high resolution microscopy with spectral unmixing to segment out tissue autofluorescence. We observed PDPN+ vessels in 19/21 subject samples, including 6/6 AD subjects, 4/5 control subjects, and 9/10 subjects with mixed dementia or other neurological diseases (Table 1).

PDPN+ lymphatic vessels with two distinct morphologies were observed in human postmortem SSS samples. One vessel type reflected traditional initial lymphatic morphology, with a single layer of endothelium, no smooth muscle or red blood cells, unoccupied lumen, and irregular morphology (Figure 6C). For simplicity, these PDPN+ vessels were termed "Type 1" lymphatic vessels. A second vessel type, termed "Type 2", was observed that exhibited an irregular endothelial border and material within the lumen, resembling the lymphatic vessels described in human autopsy samples by Louveau and colleagues (Louveau et al., 2015) (Figure 6C). In contrast to meningeal arteries and veins (Figure 6D), both vessel types were negative for the blood endothelial cell marker CD31 (Figure 6E), indicating that PDPN+ Type 1 and Type 2 vessels are not meningeal blood vessels. Like other peripheral lymphatic vessels, Type 1 vessels also labeled with the LYVE-1, however Type 2 vessels did not (Figure 6F). Type 1 and 2 lymphatic vessels exhibited specific distributions within the

dural tissue, with Type 1 vessels distributing within the periosteal and meningeal layers of the dura mater, and Type 2 vessels distributed between the SSS and periosteal layer of the dura (Figure 6B). As reported in the rodent, lymphatic vessels of both types were negative for the vascular smooth muscle cell marker smooth muscle actin (Figure 6E).

Both Type 1 and 2 lymphatic vessels were readily detectable in both control and AD subjects (Figure 7A, Table 1). To determine if there were structural differences in the lymphatic vessels of AD and control subjects, we measured the circumference of 5 lymphatic vessels per subject. We found no difference in lymphatic vessel circumference between AD and control subjects, with an average circumference of 350 ± 60 μm and 380 ± 80 μm, respectively (Figure 7B).

The deposition of Aβ in leptomeningeal and intraparenchymal cerebral arterial walls is a common feature among AD subjects that is thought to reflect the role of perivascular spaces as routes for efflux of Aβ from the brain parenchyma (Carare et al., 2008; Kalaria and Ballard, 1999; Weller et al., 2007). We hypothesized that if the meningeal lymphatic vasculature participates in clearance of Aβ, then Aβ deposition may also occur along the meningeal lymphatic vessels of AD subjects. To evaluate this hypothesis, we labeled sequential cortical and SSS sections with the 6E10 and 4G8 Aβ antibody clones, which display differential detection of prefibrillar oligomeric Aβ. Specifically, the 4G8 antibody binds to both fibrillar and prefibrillar oligomeric Aβ, while the 6E10 antibody only binds fibrillar Aβ (Kayed et al., 2007). As expected, Aβ immunoreactivity was largely absent from frontal cortical sections from control subjects while AD subjects exhibited dense frontal cortical Aβ immunoreactivity (Figure 8A). In the dura mater, we observed that Aβ reactivity was clone-specific in both AD and control subjects, with widespread, diffuse

immunoreactivity detected in the meninges by the anti-Aβ 6E10 clone, but scant reactivity with the anti-Aβ 4G8 clone (Figure 8A, Table 2). Several dural blood vessels also exhibited Aβ immunoreactivity, though more were found in sections labeled with the 6E10 clone than the 4G8 clone (Figure 8). Interestingly, when staining with the 6E10 clone, we observed Aβ immunofluorescence in the walls of dural lymphatic vessels, with 3/6 AD and 0/5 control subjects exhibiting Aβ6E10+PDPN+ lymphatic vessels (Figure 3B, Table 2). However, labeling with the 4G8 antibody did not result in PDPN+ lymphatic vessel-associated immunoreactivity (Figure 8B, Table 2). As noted above, the 4G8 antibody readily labeled cortical Aβ plaques, leptomeningeal Aβ, and Aβ associated with dural arteries (Figure 8A).

Because the 6E10 antibody only detects fibrillary species of Aβ, we surmised that if the immunoreactivity we observed with the 6E10 antibody was specific to Aβ, then similar patterns would be observed when staining with a congophilic dye such as Congo red or X-34. Importantly, there was no observable positive Congo red or X-34 labeling in meningeal sections of both control and AD subjects using this approach (Figure 8A-B). The lack of positive staining with both the 4G8 antibody and congophilic dyes argue that the anti-Aβ 6E10-immunoreactivity seen in dural tissue from control and AD subjects and in association with meningeal lymphatic vessels reflects non-specific antibody binding rather than the specific localization of Aβ to these structures.

Discussion

Confirmation of a lymphatic vessel network in the human meninges

Our observation of lymphatic vessels in the dura mater of 19/21 human subjects corroborates the recent report of lymphatic vessels in three human subjects by Absinta and

colleagues(Absinta et al., 2017). Together, these reports confirm that the meningeal lymphatic system is conserved among rodents, non-human primates, and humans.

While the PDPN+LYVE1+CD31- (Type 1) lymphatic vessels identified in the present study are consistent with peripheral tissue lymphatic capillaries and those described in the murine SSS (Louveau et al., 2015), we also identify PDPN+LYVE1-CD31- (Type 2) dural vessels. In mice, LYVE1 is heterogeneously expressed along the lymphatic hierarchy with progressive loss of expression in precollectors and collecting vessels. Thus, the Type 2 vessels we observe may represent a precollector (PDPN+LYVE1-SMA-) rather than capillary phenotype. Alternatively, inflammation can induce internalization and degradation of LYVE1, which may contribute to the discrepancy observed between naïve murine and post mortem human tissue (Johnson et al., 2007). As inflammatory cells are inconspicuous in both AD and control dura, this possibility seems less likely. Finally, though our data reveals that these structures lack staining for CD31 and are therefore not meningeal blood vessels, it is possible that these Type 2 structures lined with PDPN+ cells are also non-lymphatic. Future studies in non-human primate or human dura mater should consider orthogonal approaches such as flow sorting coupled with quantitative PCR to provide greater insight into the identity of these putative lymphatic vessels.

Our findings also highlight other differences between the human and rodent meningeal lymphatic system. In the murine meninges, the superior sagittal sinus is typically flanked by two lymphatic capillaries, whereas in the human subjects within our study, we noted >5 vessels in subjects that had identifiable lymphatic vessels associated with this considerably larger structure. Furthermore, murine meningeal lymphatic vessels typically display a measured diameter of 20-30 μm (Aspelund et al., 2015; Louveau et al., 2015)

whereas the calculated diameter range of human meningeal lymphatic vessels in our study varied widely from 19-470 μm. These findings corroborate the wide diameter range reported by Absinta and colleagues (Absinta et al., 2017). These differences, as well as the anatomical distribution of Type 1 and Type 2 vessels may have functional significance; dural Type 1 vessels may absorb the interstitial fluid within the dura itself while Type 2 vessels, although apparently lacking contractile mural cells, may conduct CNS- and dura-derived lymph towards the cervical lymphatic drainage. These possibilities are clearly speculative, and further functional studies will be necessary to evaluate them.

Absence of Aβ deposition in the meninges, meningeal blood vessels, and meningeal lymphatic vessels

The dura mater and several identified dural lymphatic vessels displayed diffuse immunoreactivity when stained with the 6E10 clone, but this pattern was not observed when staining with the 4G8 antibody clone. This was unexpected because the 4G8 antibody identifies a broader range of Aβ species, binding both prefibrillar Aβ oligomers and fibrillary Aβ, whereas the 6E10 antibody only binds fibrillary Aβ (Kayed et al., 2007). Despite the fact that these antibodies bind to different epitopes on the extracellular domain of the Aβ protein (Aho et al., 2010), the staining patterns of dense-core Aβ plaques that contain fibrillary Aβ are relatively similar (Liu et al., 2015; Rak et al., 2007). To determine if the 6E10 immunoreactivity was fibrillary Aβ or nonspecific, we stained dural samples both Congo Red and X-34, which detect fibrillary Aβ in an antibody-independent manner, were also negative. Taken with our observation that the dura mater of 4/5 control subjects displayed diffuse immunoreactivity with the 6E10 antibody, these findings suggest that Aβ is not deposited in the dura and that the 6E10-positive labeling was likely non-specific.

These findings suggest that although interstitial Aβ exchanges into the CSF compartment, it does not appear to appreciably deposit within or along meningeal lymphatic vessels associated with the SSS. This does not necessarily indicate that these lymphatic vessels do not participate in the clearance of soluble Aβ from brain tissue, but rather may simply reflect the fact that Aβ does not specifically deposit along these structures. The relative absence of mural cells investing the meningeal lymphatic vasculature or differences in the physical (such as pulsation) or chemical environment (such as vessel wall matrix composition) of the lymphatic versus arterial wall may prevent Aβ associated with these vessels from aggregating as it does in the wall of leptomeningeal or intraparenchymal arteries. Indeed, it was recently suggested that the unique chemical and shear environment within the cerebral arterial wall may underlie the Aβ deposition that is characteristic of cerebral amyloid angiopathy (Trumbore, 2016). Furthermore, tracer studies carried out in experimental animals and human subjects suggest that solutes in the CSF are transported along perineural routes through the basal cisterns and through the cribriform plate (Bedussi et al., 2017; Johnston et al., 2004). Thus meningeal lymphatic vessels in the calvarium may play only a minor role in Aβ clearance from the CSF, compared to those at the base of the skull.

Study Limitations

The use of the spectral unmixing approach was critical to defining small PDPN+ lymphatic vessels in the highly autofluorescent human meninges. Despite this, we still observed some nonspecific staining, which was attributable to secondary antibody binding. This issue is common to immunofluorescence in post mortem human tissue, highlighting the importance of using strategies to overcome endogenous tissue autofluorescence, and for the

use of approaches to evaluate meningeal lymphatic function that are orthogonal to microscopy.

Although this is the largest human cohort evaluated for meningeal lymphatic vessels, another limitation of this study is the relatively small sample size and narrow anatomical focus, including SSS tissue from 21 subjects, 6 of which were diagnosed with AD and 5 of which were control subjects. Since the concentration of Aβ in the CSF and brain vary with the stage of AD, this may affect the detection of Aβ in the dura mater. Future studies will benefit from including a larger number of subjects with a wide range of CERAD scores, allowing subjects to be stratified by stage of AD. Additionally, the use of ELISA-based assessment of Aβ from fresh-frozen meningeal tissues may provide a more sensitive readout for Aβ burden in this compartment in aging or AD. In this way, potential AD stage-associated changes in lymphatic vessel-Aβ association could be more comprehensively defined.

This study was further limited by the general scarcity of post mortem meningeal tissue and the time-intensive use of spectral unmixing in large tissue sections in order to detect small vessels within an intensely autofluorescent tissue. It is possible that changes in lymphatic vessel abundance, structure, and association with Aβ may vary in different meningeal compartments, thus the findings that we report may not generalizable to the wider meningeal lymphatic vasculature. In future studies, it will be important to characterize meningeal lymphatic vessels from other dural sinus structures (such as the transverse and straight sinuses) and meninges in the skull base, including those associated with cranial nerves.

Conclusions

Together, these findings confirm the presence of meningeal lymphatic vasculature in humans and provide insight into two possible populations of lymphatic vessels in the meninges: one with traditional characteristics of lymphatic vessel morphology and another with atypical morphology. We also report the absence of Aβ deposition in the wall of dural lymphatic vessels and that the use of multiple approaches is critical for accurate detection of Aβ in meningeal tissue. These findings suggest that although the meningeal lymphatic vessels in the calvarium may contribute to the clearance of interstitial solutes including Aβ from the brain parenchyma, Aβ does not appear to deposit in these potential efflux pathways in the same manner that it does along peri-arterial pathways in the setting of cerebral amyloid angiopathy.

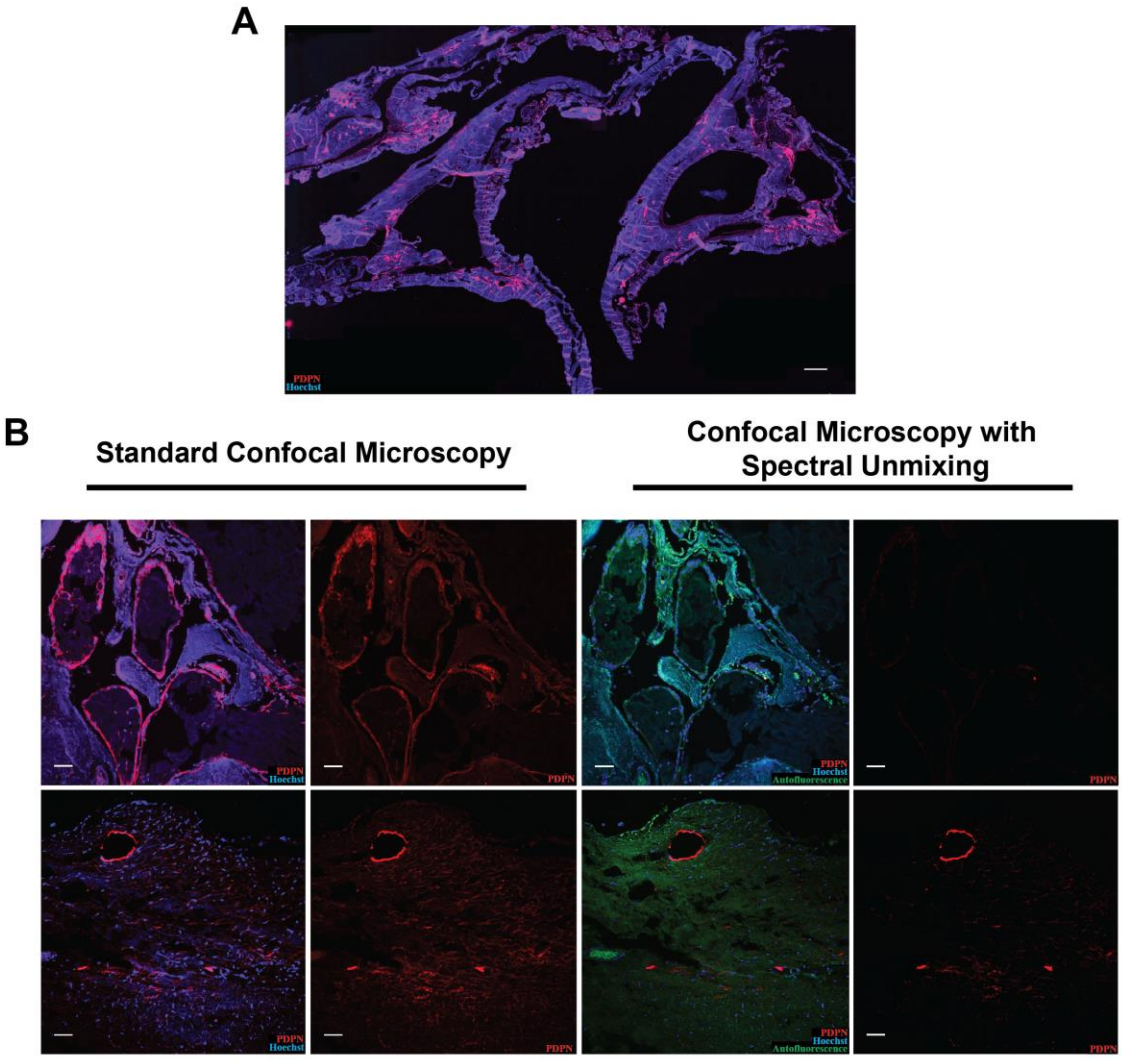

Figure 5. Spectral unmixing differentiates lymphatic vessels from autofluorescence in the human meninges.

A. Coronal sections of the human meninges acquired with conventional confocal microscopy display widespread autofluorescent signal. B. Comparison of conventional confocal microscopy and confocal microscopy with spectral unmixing in paraffin-embedded human meningeal tissue.

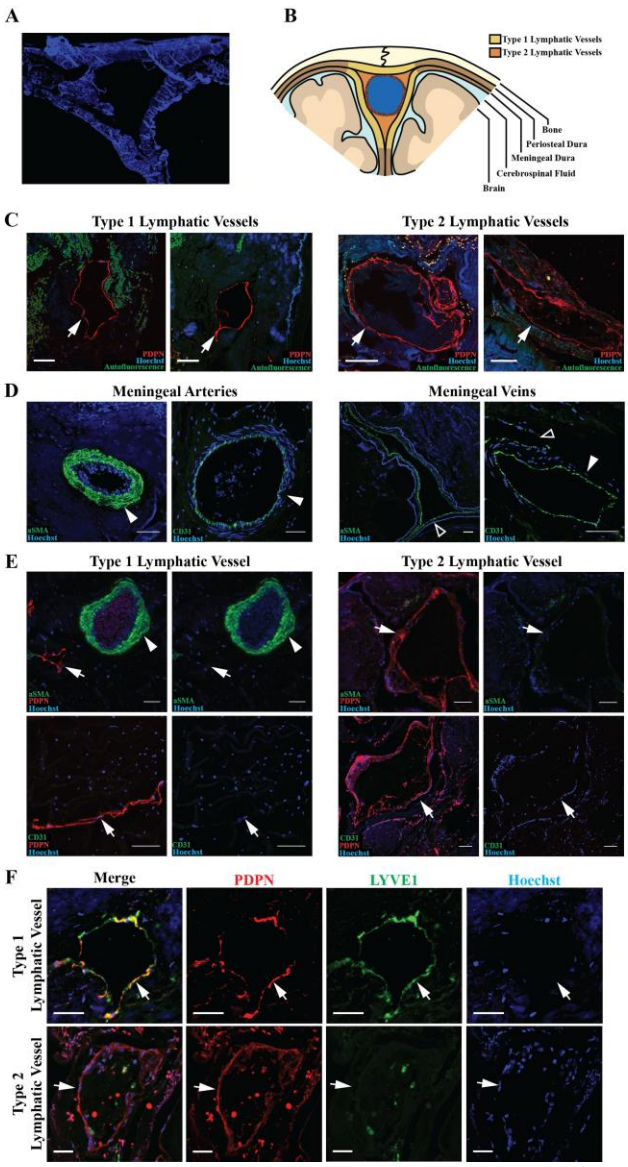

Figure 6. Lymphatic vessels with variable morphology invest the human meninges.
A. Representative image of coronal section of human superior sagittal sinus and meninges. B. Schematic demonstrating regions of the meninges where lymphatic vessels were found. Yellow regions represent the general distribution of Type 1 vessels and orange regions represent Type 2 vessels. C. Representative images of Type 1 and 2 lymphatic vessels (arrows). D. Dural blood vessels, including arteries (solid arrowhead) and veins (hollow arrowhead), labeled with vascular smooth muscle cell marker alpha-smooth muscle actin (aSMA) and the blood endothelial cell marker CD31. E. Dural lymphatic vessels do not co-label with aSMA or CD31. F. Type 1 vessels are PDPN+LYVE1+ and Type 2 vessels are PDPN+LYVE1-. Scale bars in C and D represent 100 μm and bars in E and F represent 50 μm.

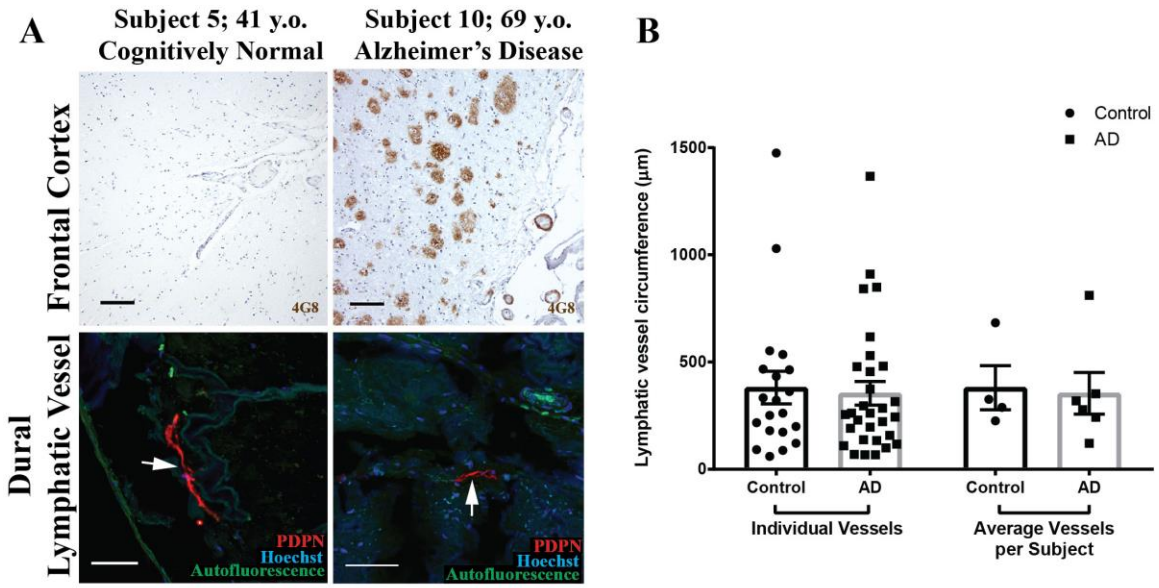

Figure 7. Meningeal lymphatic vessels in AD and control subjects.

A. Frontal cortical Aβ plaques and leptomeningeal vascular Aβ deposition in control and AD subjects. Type 1 and Type 2 meningeal lymphatic vessels (arrows) are readily detected among both groups. B. Quantification of lymphatic vessel circumference (14 Type 1 and 6 Type 2 vessels in control subjects; 22 Type 1 and 8 Type 2 in AD subjects). Columns on left reflect all vessels from all subjects (n = 20 and 30 from control and AD subjects, respectively). Columns on right reflect subject-wise averages of lymphatic vessel circumferences (n = 4 and 6 control and AD subjects, respectively). No group-wise differences in lymphatic vessel circumference were observed (unpaired two-tailed T-test with Welch's correction, p= 0.78 and 0.85 for individual vessels and average vessels per subject, respectively).

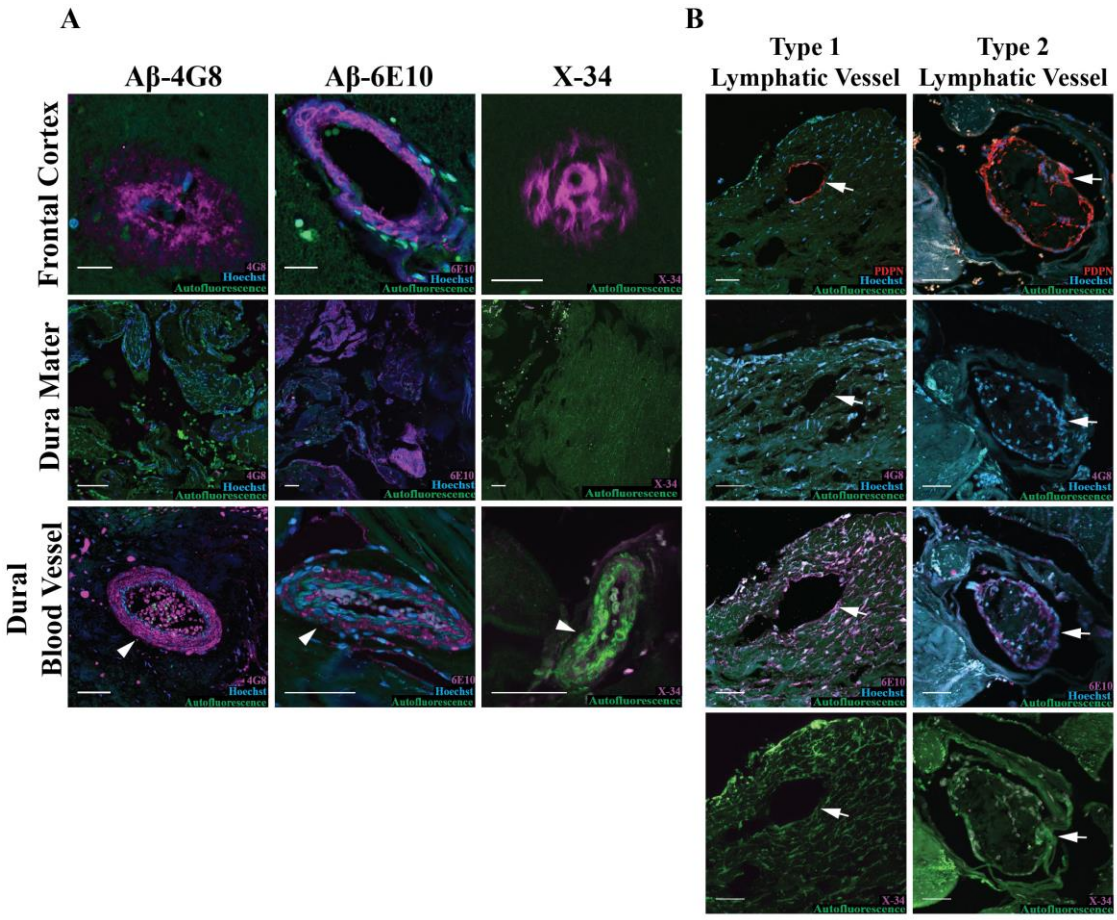

Figure 8. Dural lymphatic vasculature and meningeal Aβ immunoreactivity in AD subjects. A. Detection of Aβ immunoreactivity with 6E10 and 4G8 clones, and Aβ aggregates with the congophilic X-34 dye in frontal cortex (top), within dural tissue (middle), and in meningeal blood vessels (bottom, arrowhead). B. Representative Type 1 (left) and Type 2 (right) lymphatic vessel (arrows). Sequential slices stained with PDPN, 6E10, 4G8 and X-34 shows that co-localization between PDPN and the 6E10 in some vessels. PDPN co-localization with 4G8 immunoreactivity or with X-34 labeling was not observed. Scale bars in frontal cortex micrographs represent 20 um and scale bars in other micrographs represent 50 μm. Figure 2. Meningeal lymphatic vessels in AD and control subjects.

Subject	Age	Sex	Diagnosis	Braak Stage	CERAD Score	Type 1 Lymphatic Vessels	Type 2 Lymphatic Vessels
1	35	F	Control	NA	0	+	+
2	73	M	Control	NA	0	+	+
3	11	M	Control	NA	0	-	-
4	75	M	Control	NA	0	+	+
5	41	M	Control	NA	0	+	+
6	57	M	AD	6	3	-	+
7	70	M	AD	6	3	+	+
8	85	F	AD	6	2	+	+
9	86	F	AD	6	2	+	+
10	69	F	AD	6	3	+	+
11	79	M	AD	6	2	+	+
12	75	F	AD and LBD	6	1	-	+
13	89	F	LBD	4	1	+	+
14	85	M	LBD	3	0	+	-
15	74	M	LBD, HPC Sclerosis	4	0	-	+
16	>89	F	HPC Sclerosis	4	1	-	-
17	73	F	FTD/Tau	3	0	-	+
18	79	M	MS	2	0	+	+
19	71	M	PD	0	0	-	+
20	70	F	Psychosis	0	0	-	+
21	66	F	Leuko-encephalopathy	1	0	+	+

Table 1. Description of pathology observed in meninges and brain of individual subjects included in the study.

M, Male, F Female. AD, Alzheimer's disease; LBD, Lewy Body Dementia; HPC, hippocampal; FTD, frontal temporal dementia; MS, multiple sclerosis; PD, Parkinson's disease; NA, not applicable (Braak staging in control subjects were not evaluated).

Subject	4G8+ Meningeal Blood Vessel (5 vessels per subject)	6E10+ Meningeal Blood Vessel (5 vessels per subject)	4G8+ Meningeal Lymphatic Vessel (2 vessels per subject)	6E10+ Meningeal Lymphatic Vessel (2 vessels per subject)
1	0	3	0	0
2	0	3	0	0
3	0	0	N/A	N/A
4	0	1	0	0
5	0	3	0	0
6	1	2	0	1
7	0	2	0	0
8	0	4	0	2
9	0	0	0	1
10	0	3	0	0
11	0	4	0	0

Table 2. Detailed results of amyloid beta reactivity and distribution in AD and control subjects.

αSMA, Smooth muscle actin; N/A, Not applicable (no meningeal lymphatic vessels observed).

Chapter Three: Evaluating Meningeal Lymphatic Function in the Context of Alzheimer's Dementia

Introduction

Recent evidence in the human and mouse suggest that diurnal rhythms exist in the concentrations of interstitial fluid (ISF) and cerebrospinal fluid (CSF) amyloid beta (Aβ), and that loss of these diurnal rhythms is a feature of aging and the Alzheimer's dementia (AD, Huang et al., 2012; Roh et al., 2012). Evidence from studies in human subjects also suggests that clearance of Aβ from the CSF is impaired in AD and aging human subjects (Mawuenyega et al., 2010; Patterson et al., 2015). In human subjects without a presenilin mutation or trisomy 21, these changes in Aβ clearance appear to occur in the absence of altered Aβ production. Though there are very few studies considering solute clearance from the CSF in AD, two recent studies implemented dynamic positron emission tomography to measure this parameter in subjects with AD and healthy control subjects. Interestingly, both studies found that the rate of solute efflux from the CSF is impaired in subjects with AD compared to age-matched controls (de Leon et al., 2017; Schubert et al., 2019). Moreover, in the same study Shubert and colleagues demonstrated that the rate of CSF efflux is impaired in subjects with mild cognitive impairment. Collectively, these findings suggest that after entering into the CSF compartment, the reabsorption of Aβ in the CSF is impaired in both aging and AD.

One critically understudied pathway for solute efflux in the CSF is the lymphatic pathway. Recent evidence demonstrated the presence of lymphatic vessels in the meninges of rodents (Aspelund et al., 2015; Louveau et al., 2015). This reinvigorated interest in the role of lymphatic vessels in draining solutes from the brain and CSF, and prompted widespread interest in possible connections between meningeal lymphatic function and the development of progressive neurodegenerative diseases like AD. Preclinical studies in the

rodent and human suggest that lymphatic function also declines with age (Chevalier et al., 1996; Gashev and Chatterjee, 2013; Unno et al., 2011). Therefore, one possibility is that age-related decline in lymphatic function underlies the age-related reduction in Aβ clearance observed in humans. To begin to address this, however, foundational experiments characterizing lymphatic Aβ trafficking are necessary to determine if this is a pathway for Aβ clearance from the CSF. In this study, we characterized the trafficking of exogenous fluorescently-tagged Aβ into the CSF and brain of mice and measured the accumulation of the Aβ in the deep cervical lymph nodes (DCLNs) which are functionally downstream of lymphatic pathways that drain the central nervous system (CNS). To measure lymphatic drainage of Aβ in a more physiological context, we also measured anti-Aβ immunoreactivity in the DCLNs of aged Tg2576 mice, which overexpress a mutant isoform of amyloid precursor protein under the prion-related protein promoter.

Together, the findings presented in this study demonstrate that Aβ is trafficked out of the brain and CSF via the lymphatic pathway, and confirm that lymphatic efflux is impaired in the aged animal. We believe these findings will inform future investigations of meningeal lymphatic biology in the context of AD.

Methods

Animals

Male and female 8-10 week old C57BL/6J mice from Jackson Laboratories were used for all experiments except those featuring the use of the Tg2576 mouse. The Tg2576 mouse expresses a mutant form of amyloid precursor protein (isoform 695) with the Swedish mutation (KM670/671NL) under the hamster prion protein promoter. These mice were

purchased from Taconic and bred and aged in house. All mice were acclimated to their housing for several days before experiments were performed. For studies comparing young and aged mice, mice were aged in house for 14 months before performing experiments. All experiments were approved by the Institutional Animal Care and Use Committee of Oregon Health & Science University.

Intraparenchymal and intracisternal tracer injections

Anesthesia was induced in mice via an intraperitoneal dose of ketamine/xylazine ((1.75 mg ketamine/0.25 mg xylazine per 20 gram mouse) and animals were placed in 3-point stereotaxic apparatus. A surgical plane of anesthesia was ensured throughout the procedure by regular pedal reflex checks. During all surgical procedures, mice were placed on a heating pad or under a heating lamp to maintain body temperature.

For intraparenchymal injections, a 2 cm midline scalp incision was made over the sagittal suture and skin was reflected to locate bregma. A burr hole was introduced in the right parietal bone (0.4 mm caudal, 1 mm lateral to bregma) using a Microtorque II drill. A 26 Ga needle (Hamilton) was inserted to a depth of 1 mm and rested for 10 minutes before injecting 1 μL of Aβ1-40 HiLyte-555 (Anaspec) at a rate of 100 nL/minute. After completion of the injection, the needle was removed from the brain and the incision was closed with cyanoacrylate glue. Animals were removed from stereotaxic apparatus and placed on a heating pad at 37C for the duration of the experiment. Animals were sacrificed 30minutes after the initiation of the injection via intracardiac infusion of saline unless otherwise noted. In the event that tracer was injected into the lateral ventricle, evidenced by widespread perivascular but not parenchymal fluorescent signal, animals were excluded from the study.

For intracisternal infusions, animals received the same intraperitoneal dose of a ketamine/xylazine. A 2 cm midline incision was made caudally from lambda. Skin was reflected laterally and blunt dissected to expose muscle. The most superficial muscle layer was sectioned and reflected laterally and the deeper layers were kept intact and reflected laterally using 6-0 braided suture. The atlanto-occipital membrane was visualized via blunt dissection through ligamentous tissue and the bevel of a 30.5-gauge needle attached to PE-10 tubing was inserted into the cisterna magna. Needle placement was secured using cyanoacrylate glue. 2 μL 1:1 solution of 10 kDa dextran (Thermofisher) and Aβ1-40 HiLyte-555 (Anaspec) was infused into the cisterna magna at a rate of 1 μL/minute.

For experiments utilizing intraparenchymal and intracisternal tracer infusion, calvaria, skull bases, and DCLNs were imaged using fluorescence dissection microscopy (Zeiss AxioZoom V16).

In vivo dynamic measurement of lymphatic drainage

Preceding intracisternal infusion, anesthetized mice were placed on heating pad in a supine position. Fur on anterior cervical region was removed using the chemical depilatory agent Nair. A 3 cm midline incision was made from the superior aspect of the sternum to the inferior aspect of the mandible. Submandibular gland was blunt dissected and reflected laterally to expose the sternocleidomastoid and trachea. 6-0 suture was passed beneath the muscle belly of the sternocleidomastoid and the muscle was reflected laterally to expose the DCLN. After insuring a high quality surgical field, mice were placed in stereotaxic apparatus and underwent intracisternal infusion. Immediately after completion of intracisternal co-infusion, mice were placed under fluorescence dissection microscope (Zeiss AxioZoom V16) and imaged every minute for 1 hour.

Immunofluorescence

Mice were fixation-perfused with fresh 4% paraformaldehyde stored at 4c. The calvarium, brain, skull base, and DCLNs were harvested and post-fixed in 4% paraformaldehyde overnight at 4c.

Whole mount calvaria were decalcified in 0.5M EDTA for 72 hours, blocked overnight in blocking buffer (5% donkey serum, 2% bovine serum albumin in 0.3% triton-X 100 phosphate buffered saline) stained with primary antibodies overnight, washed 3x in PBS, stained with secondary antibodies, and washed 3x in PBS. All steps were performed at 4c. Calvaria were mounted using mowiol 4-88 with clothespins securing the coverslip in place while drying.

Brains and DCLNs were dehydrated by submersion in 30% sucrose overnight at 4c, frozen in OCT by submersion in 2-methylbutane on dry ice, and stored at -80c. 100 μm brain sections were collected as floating sections in PBS and 20 μm deep cervical lymph node sections were collected directly onto glass slides. Brain sections were washed 3x with PBS and mounted using mowiol 4-88. Lymph node sections were washed 3x PBS, stained overnight with primary antibody, washed 3x in PBS, stained with secondary antibody for 4 hours at room temperature, washed 3x in PBS, and mounted with mowiol 4-88.

All sections were imaged using either the LSM880 (Zeiss) or AxioScan (Zeiss) within 48 hours of mounting using the same laser power, photomultiplier voltage, and gain across groups. Post-image processing was performed using ImageJ. This includes image thresholding, fluorescence intensity measurements, and maximum intensity z-stack projections.

Antibodies

Primary antibodies were used as follows: Rat LYVE1 (1:1000), Mouse Aβ 4G8 clone (1:300, biotinylated), Rabbit CD31(1:300). Donkey secondary antibodies (1:500, ThermoFisher) against rat, mouse, and rabbit were used for secondary detection in brain calvarium tissue. To avoid detection of mouse IgG in lymph nodes, streptavidin-Cy5 secondary antibody (2 μg/mL, Jackson ImmunoResearch Laboratories) was used to detect Aβ in lymph nodes of Tg2576 mice.

Statistics

All statistical analyses were performed using GraphPad Prism 7. Data are presented as the mean ± standard error and individual values are represented as black circles overlying graphs. 2-way ANOVA with and without repeated measures and Sidak's post hoc correction for multiple comparisons was implemented for groupwise comparisons. An unpaired t-test with Welch's correction was used for pairwise comparisons. Results with a p-value less than or equal to 0.05 are considered significant.

Results

Efflux of Aβ via the meningeal lymphatic pathway

To test the prediction that the meningeal lymphatic pathway participates in the clearance of Aβ, we injected exogenous $A\beta_{1\text{-}40}$ HiLyte-555 into the CSF and motor cortex, and harvested the brain and DCLNs 30 minutes after the injection. Indeed, we found that $A\beta_{1\text{-}40}$ injected into either compartment was drained into the DCLNs, suggesting that lymphatic uptake is a pathway by which $A\beta_{1\text{-}40}$ is removed from the cranium (Figure 9A).

Although exogenous Aβ is cleared via the lymphatic system, it may not be an important physiological pathway relative to other known mechanisms of Aβ clearance. Therefore, we examined the meningeal lymphatic vessels and DCLNs of Tg2576 mice aged 8-12 months. After confirming the presence of parenchymal senile plaques and vascular amyloidosis (Figure 9B), we co-labeled whole mount meningeal preparations and DCLN sections for LYVE1, a marker of lymphatic endothelium, and the pan-Aβ 4G8 antibody. Interestingly, we noted Aβ immunoreactivity around the dural sinuses which co-localized with immunoreactivity for LYVE1, suggesting that meningeal lymphatic vessels may absorb Aβ produced in the brain. We further observed Aβ immunoreactivity in the DCLNs, but not in the inguinal lymph nodes of the Tg2576 mice, which are unlikely to have physiological access to Aβ in the CSF (Figure 9C).

Aging and lymphatic solute efflux

Historically, studies of AD have focused on mechanisms of parenchymal Aβ clearance (Tarasoff-Conway et al., 2015). However, the inverse association between aging and clearance of Aβ from the CSF raises questions about mechanisms of Aβ clearance from the CSF (Patterson et al., 2015). Indeed, in studies of lymphatic function in peripheral organs, aging reduces uptake of interstitial solutes (Chevalier et al., 1996; Nagai et al., 2011; Proulx et al., 2017). To test the hypothesis that the elevated concentration of Aβ in the CSF is due to age-related reduction in lymphatic function, we co-infused a 1:1 solution of $A\beta_{1\text{-}40}$ HiLyte-555 and a 10 kDa dextran conjugated to Cascade Blue into the CSF of young and old mice (Figure 10A). Similar to the findings reported by Kress and colleagues (Kress et al., 2014), we observed an age-related reduction in parenchymal tracer penetration with both $A\beta_{1\text{-}40}$ and 10 kDa dextran (Figure 10B, 2-way ANOVA $P<0.01$ and <0.0001, respectively).

To measure lymphatic clearance of these tracers, we used fluorescence dissection microscopy to acquire images of the DCLN in the blue channel (10 kDa dextran) over the course of 60 minutes. We noted a severe reduction in the rate of solute efflux into the DCLNs of aged animals in comparison to young animals (Figure 10C, two-way ANOVA with repeated measures, $p<0.05$). In fact, impairment of lymphatic outflow in aged animals was so great that both the $A\beta_{1-40}$ and 10 kDa dextran were largely undetectable using fluorescence dissection microscopy after 60 minutes. To compare tracer efflux into the DCLNs of old and young mice, we used confocal microscopy on sections of the DCLNs (Figure 10D). Interestingly, we did not find a statistically significant reduction in lymphatic efflux of the 10 kDa dextran (Unpaired t test with Welch's correction, $p=0.07$) or $A\beta_{1-40}$ in the DCLNs of young and aged mice (Unpaired t test with Welch's correction, $p=0.75$).

Structural analysis of the meningeal lymphatic vasculature in young and aged mice

Given the robust effect of aging on impairment of lymphatic CSF drainage, we next examined the structural features of the meningeal lymphatic vasculature in old and young mice. We hypothesized that if the meningeal lymphatic vessels in the calvarium play an important role in lymphatic drainage, then lymphatic capillaries in aged animals would display distended morphology due to reduction in lymphatic flow to the DCLNs. To accomplish this, we used immunofluorescence and confocal microscopy to measure the diameter and branching morphology of $LYVE1^+$ lymphatic vessels in the calvarium of the old and young mice that underwent intracisternal infusion of $A\beta_{1-40}$ and 10 kDa dextran (Figure 10A). We did not observe any statistical difference between the vessel width in lymphatic vessels associated with the superior sagittal sinus (Unpaired t test with Welch's correction, $p=0.99$) or the transverse sinus (Unpaired t test with Welch's correction,

p=0.09). This was surprising because it was previously shown that acute surgical ligation of the cervical lymphatic trunk resulted in increased meningeal lymphatic diameter (Louveau et al., 2015). Similarly, we found no difference in the number of vessels, nor in the branching number (Figure 11A).

Because of the discrepancy between the marked reduction in lymphatic CSF drainage in aged mice and the lack of morphological change in lymphatic capillaries in the calvarium, we further investigated the colocalization between the fluorescence intensity of $A\beta_{1\text{-}40}$ and 10 kDa dextran and $LYVE1^{+}$ lymphatic endothelium (Figure 11B). Specifically, we surmised that if these lymphatic capillaries absorb solutes from the CSF, then the signal intensity from these fluorescent solutes will be increased in regions associated with lymphatic endothelium. The rationale behind this assertion is that initial lymphatic capillaries concentrate solutes relative to the interstitial fluid (Brace et al., 1977; Casley-Smith and Sims, 1976; Zawieja and Barber, 1987). We acquired micrographs along the superior sagittal sinus and the transverse sinus, and compared $A\beta_{1\text{-}40}$ and 10 kDa dextran fluorescence intensity within the lymphatic endothelium in young and old mice. Using this approach, we did not observe increased uptake of either $A\beta_{1\text{-}40}$ or 10 kDa dextran in lymphatic vessels associated with the superior sagittal sinus or the transverse sinus compared to signal more generally associated with venous sinuses (Figure 11B).

Discussion

In this study, we demonstrate that both exogenous and endogenous Aβ escapes out of the cranium via the cervical lymphatic pathway. To our knowledge, this is the first study to describe Aβ trafficking along the lymphatic pathway, though one previous report

considered Aβ in the lymph nodes of Tg2576 mice (Pappolla et al., 2014). This confirms the widespread speculation that the lymphatic system participates in the clearance of Aβ from the CSF.

Having observed that the lymphatic system participates in the clearance of Aβ, we surmised that age-related changes in the meningeal lymphatic system would lead to reduction of solute clearance, including Aβ, from the CSF as was described in human subjects (Patterson et al., 2015). As we predicted, we found that lymphatic function is reduced in aged mice compared to young mice. The magnitude of this effect was surprising, as very little observable tracer efflux was noted in any of the aged mice. Because this is a major path for solute efflux in the rodent, this suggests that solute trafficking is dramatically altered in the aged animal. In the same mice, we found that CSF-ISF exchange was reduced in the aged group compared to the young group. Interestingly, we found a significant effect of aging on parenchymal penetration of both $A\beta_{1\text{-}40}$ and 10 kDa dextrans. This suggests that in aging, both lymphatic efflux and CSF-ISF exchange are impaired. Whether the residence time of these solutes in the CSF is increased or their distribution into the spinal cord is altered is not yet clear. This may be resolved in future experiments by using in vivo magnetic resonance imaging to simultaneously measure tracer distribution in multiple compartments (See Appendix A). Importantly, we found that analysis of tracer distribution across lymph node sections was unable to detect any difference between old and young animals, despite the obvious difference between these groups shown by fluorescence dissection microscopy, which suggests that this approach is inappropriate for measuring lymphatic drainage of solutes from the brain and CSF.

In previous studies, age-related reduction in lymphatic function was associated with decreased contractility in collecting vessels, which slows uptake at the lymphatic capillary bed (Chevalier et al., 1996; Nagai et al., 2011). It was also demonstrated that the meningeal lymphatic vessels in the calvarium and skull base appear to dilate with acute ligation of the cervical lymphatic trunk (Aspelund et al., 2015; Louveau et al., 2015). We anticipated that the profound reduction in meningeal lymphatic drainage in aged mice would be accompanied by signs of lymphatic pathology, including distension or atrophy of lymphatic capillaries. Yet, when we considered these parameters in lymphatic vessels in the calvarium, we did not detect any statistical difference in vessel number or morphology between young and old mice. It is important to note, however, that lymphatic vessels associated with the transverse sinus may be larger than those in younger animals and this study may be underpowered to detect this difference. For instance, a post-hoc power analysis conducted on these results suggested that 10, not 7, animals would be needed per group to detect a statistically significant difference between these groups. This finding suggests that lymphatic vessels in the calvarium either do not display any morphological changes associated with pathology in aged animals with profound impairment of lymphatic drainage from the cranium or that the lymphatic vessels we considered do not participate in a significant portion of CSF drainage. In a previous study, it was demonstrated that obstruction of the cribriform plate with cyanoacrylate glue reduces lymphatic drainage of radiolabeled tracers in the CSF (Bradbury and Westrop, 1983). Thus, one possibility is that the major component of solute efflux observed in the cervical lymphatic trunk occurs across the cribriform plate or in lymphatic vessels within skull base, not in the lymphatic vessels in the calvarium. Another possibility is that pathological changes in the endothelial cells of meningeal lymphatic capillaries of the

calvarium may not be reflected by morphological changes, but may still result in reduced function. For instance, changes in the junctions between lymphatic endothelial cells in capillaries from "button-like" to "zipper-like" junctions can alter the fluid and solute absorption substantially (Lund et al., 2016). Although these changes can be measured by VE-Cadherin expression patterns, they were not assessed in our study. Still, because lymph formation and flow is possible through capillaries with both junction types, we find it unlikely that junctional differences between young and old mice would account for the magnitude of the difference observed in our in vivo lymphatic drainage experiment.

One of the key assumptions in previous studies considering meningeal lymphatic biology is that increased colocalization between fluorescent tracer injected into the brain or CSF and meningeal lymphatic vessels demonstrates functional uptake of that tracer into lymphatic vessels (Aspelund et al., 2015; Louveau et al., 2015). In line with this rationale, multiple studies have demonstrated that solutes are more concentrated in initial lymphatic vessels than in the ISF, suggesting that functional lymphatic capillaries should demonstrate increased solute concentration (Brace et al., 1977; Casley-Smith and Sims, 1976). Interestingly, we found that meningeal lymphatic vessels in the calvarium did not display enhanced $A\beta_{1\text{-}40}$ or 10 kDa dextran fluorescence intensity in either young or aged animals. Although our findings initially seemed at odds with previous reports, there are several important details of the aforementioned studies that may explain this seeming disparity. For instance, Aspelund and colleagues reported colocalization between meningeal lymphatic vessels in the skull base and a parenchymal infrared dye, but did not report similar measurements in the calvarium (Aspelund et al., 2015). In contrast, Louveau and colleagues focused on the meningeal lymphatic vessels in the calvarium. In this study, they reported

that lymphatic vessels in the calvarium absorb Evans Blue infused into the CSF as measured by colocalization between fluorescence intensity in the superior sagittal sinus and lymphatic vessels. Unfortunately, it is unclear if a statistical test was performed to assess a difference between tracer intensity in lymphatic vessels and the superior sagittal sinus. If a greater mean fluorescence intensity were found in regions associated with the lymphatic vessels, this would suggest specific uptake into the lymphatic vessels, rather than simple colocalization with the superior sagittal sinus. Although Louveau et al. also provided visualization of lymphatic uptake of quantum dots using in vivo two-photon microscopy, no additional comparison was made between signal intensity observed in the lymphatic vessel and the adjacent superior sagittal sinus. Therefore, our finding that tracer intensity does not increase in meningeal lymphatic vessels in the calvarium is consistent with the findings of Louveau et al., however our interpretation of the data is divergent. Our observation that lymphatic vessels in the calvarium do not concentrate $A\beta_{1\text{-}40}$ or 10 kDa dextran raises important questions about the relative importance of the lymphatic capillaries in the calvarium with respect to efflux of soluble waste products in the central nervous system.

Together, these findings suggest that lymphatic uptake of solutes from the CSF is significantly impaired; similar to what is reported in peripheral lymphatic vessels. They also demonstrate that that soluble Aβ is trafficked out of the CSF along this pathway and that there may be differences in CSF efflux along anatomically-distinct subpopulations of lymphatic vessels in the meninges. Further examination of lymphatic function in the base of the skull is necessary to determine the relative importance of the meningeal lymphatic system in Aβ clearance from the CSF.

In conclusion, these findings have important implications for the study of AD. Clearance of solutes in the CSF, including Aβ, is reduced in both the aging human and mouse, indicating that one or more clearance mechanisms acting on the CSF is impaired with aging. In the current study, we identify that one efflux pathway for Aβ is dramatically impaired in aging mice. Although it is tempting to conclude that the impairment of lymphatic drainage underlies the age-related reduction in Aβ clearance rate, several important mechanistic experiments are still needed. Specifically, a study considering the temporal relationship between lymphatic function, CSF Aβ levels, and parenchymal Aβ deposition is needed to determine if lymphatic impairment precedes the reduction in Aβ clearance from the CSF. Furthermore, manipulation of lymphatic function in a mouse model of AD would provide mechanistic insight into the relationship between parenchymal Aβ deposition and lymphatic function. Future studies in our lab will focus on genetic and surgical modulation of lymphatic function to elucidate the relative contribution of the lymphatic system in Aβ clearance from the brain.

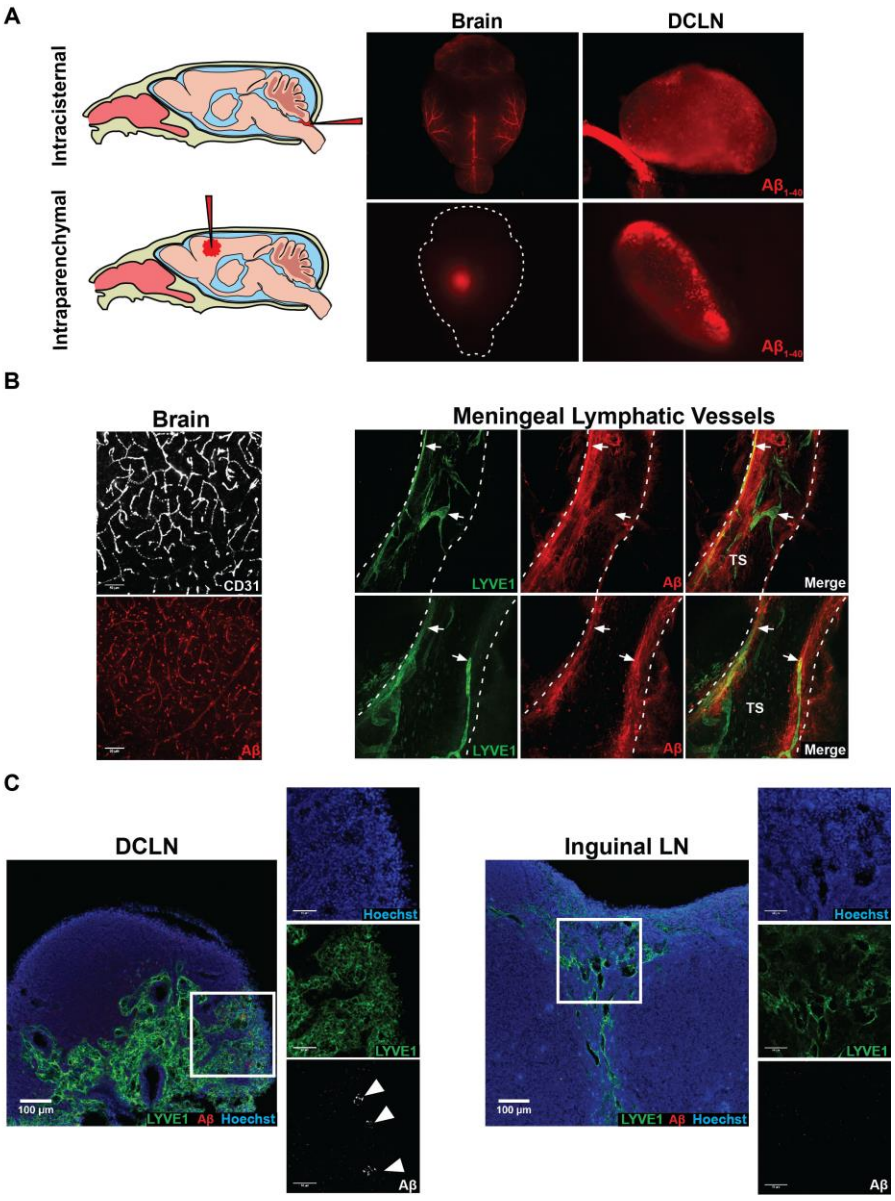

Figure 9. Exogenous and endogenous Aβ are cleared via the meningeal lymphatic vasculature.

A. Exogenous Aβ1-40 injected into either the cerebrospinal fluid (top) or the brain parenchyma (bottom) is cleared from the cranium via the deep cervical lymph nodes (n=3/group). B. Aβ in the Tg2576 mouse meninges colocalizes with meningeal lymphatic vessels in the mouse calvarium (n=4). Lines approximate the transverse sinus and arrows represent lymphatic vessels. C. Aβ (arrowheads) is trafficked into the deep cervical lymph nodes (left, n=4), but not the inguinal lymph nodes (right, n=4). TS, Transverse Sinus.

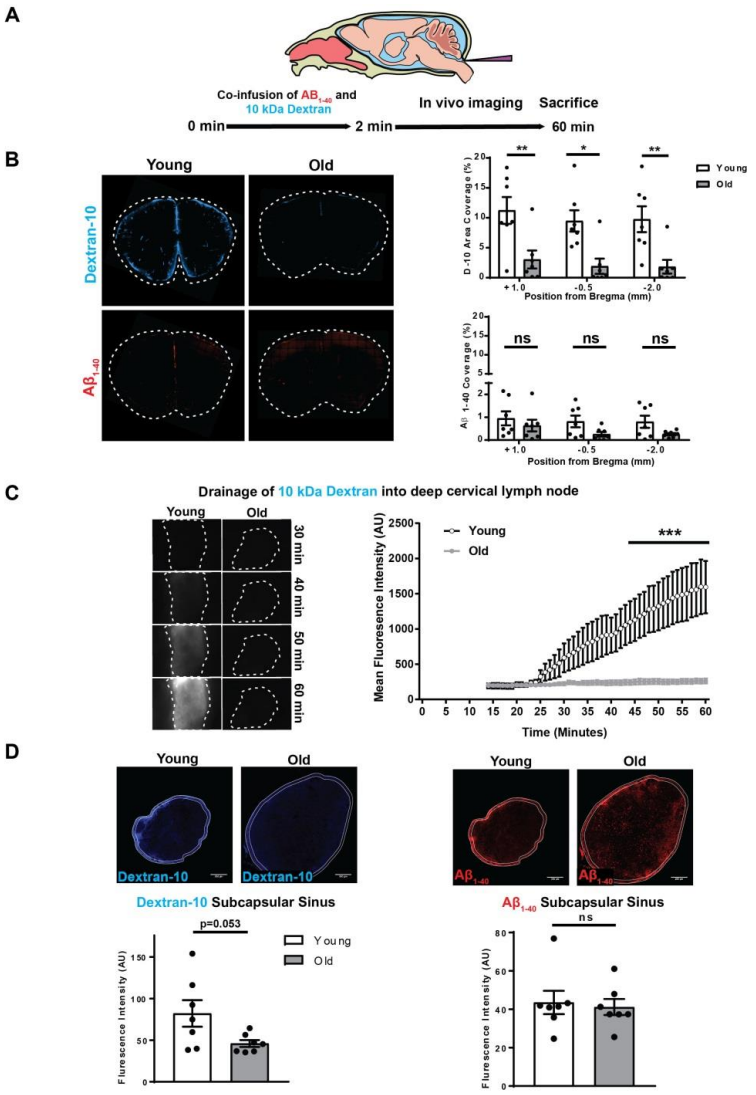

Figure 10. Aging slows meningeal lymphatic clearance of 10 kDa dextran in the CSF. A. Cartoon and experimental schematic (n=7/group). B. Left, representative brain sections from young and old mice 60 minutes after infusion. Right, parenchymal distribution of 10 kDa dextran and Aβ1-40 in old and young mice. C. Left, representative images of deep cervical lymph nodes in young and old mice with respect to time. Right, average 10kDa dextran fluorescence intensity in the deep cervical lymph node of young and old animals with respect to time. D. Top, measurement of fluorescent tracer in the subcapsular sinus of deep cervical lymph nodes in young and old mice. Bottom, representative images of deep cervical lymph node sections in young and old mice. Groupwise differences were assessed using two-way ANOVA and Sidak's correction for multiple comparisons. Pairwise differences were assessed using an Unpaired t test with Welch's correction. *p<0.05, **p<0.01, ns, not significant.

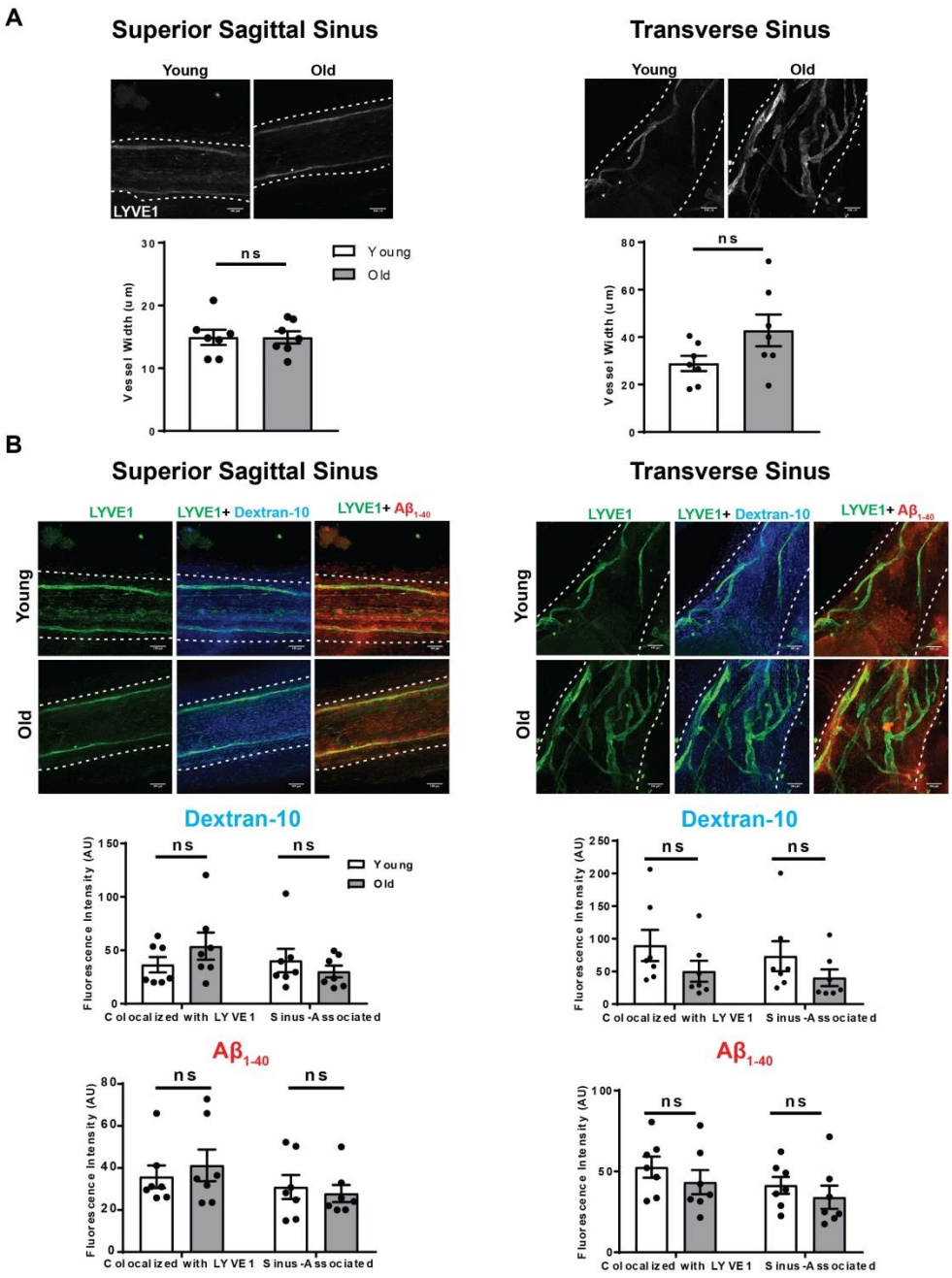

Figure 11. Aging does not alter the morphology of meningeal lymphatic vessels in the calvarium.

A. Top, Structural analysis of meningeal lymphatic vessels associated with the superior sagittal sinus and transverse sinus in young and old mice. Bottom, Representative images of lymphatic vessels near the superior sagittal sinus and the transverse sinus in old and young animals. B. Colocalization between 10 kDa dextran or Aβ1-40 and LYVE1+ and sinus-associated regions in lymphatic vessels in young and old mice.

Chapter Four: Elucidating Physiological Controls on Lymphatic Drainage from the Brain and Cerebrospinal Fluid

Introduction

Throughout the last several decades, reports emerged that challenge the notion that CSF reabsorption occurs predominantly through direct efflux from the subarachnoid space into the dural venous sinuses at the arachnoid granulations. Indeed, work from the Westrop, Cserr, and Johnston laboratories provided a critical foundation of studies supporting that CSF efflux also occurs via lymphatic reabsorption (Boulton et al., 1999, 1998; Bradbury et al., 1981; Bradbury and Cole, 1980; Bradbury and Westrop, 1983; Cserr and Knopf, 1992; Johnston et al., 2004). In addition to measuring lymphatic efflux of CSF, Bradbury and colleagues showed that the major component of lymphatic CSF efflux occurs at the cribriform plate in the base of the skull by demonstrating a dramatic reduction in efflux when the cribriform plate was sealed with cyanoacrylate glue (Bradbury and Westrop, 1983). More recently, interest in this pathway was reinvigorated by the description of a lymphatic capillary network in the meninges of rodents (Aspelund et al., 2015; Louveau et al., 2015) and humans (Absinta et al., 2017; Goodman et al., 2018). The characterization of these lymphatic capillaries led several groups to argue that lymphatic CSF efflux from the cranium occurs predominantly via these lymphatic vessels, which were most robustly characterized in the calvarium rather than in the skull base (Louveau et al., 2015; Raper et al., 2016). However, little evidence of direct solute uptake by meningeal lymphatic capillaries exists (Aspelund et al., 2015), with most groups relying on measuring tracers infused into the CSF at the deep cervical lymph nodes (DCLNs). Because of this, others maintain that the majority of lymphatic CSF efflux occurs in the base of the skull (Ma et al., 2019, 2017). While the relative importance of these sites in lymphatic solute uptake remains to be determined, even less is known about physiological mediators of this CSF efflux pathway.

In peripheral organs, lymphatic reabsorption of solutes in the interstitial fluid (ISF) is mediated by cyclical changes in the extracellular volume, termed extrinsic pumping, and contractions of smooth muscle cells lining lymphatic collecting vessels, termed intrinsic pumping. Previous work showed the importance of extrinsic pumping in lymphatic clearance of ISF solutes by demonstrating reduced lymphatic function under anesthesia, which can be rescued by physical compression of the tissue the lymphatic vessels reside in (Proulx et al., 2017). However, the unique homeostatic maintenance of pressure and volume in the intracranial space may confer properties to lymphatic drainage from the brain in awake and anesthetized states that are distinct from peripheral organs. Recently, a study found that lymphatic drainage from the CNS is markedly reduced in anesthetized mice compared to awake mice, suggesting a possible difference in lymphatic solute drainage in different states of arousal (Ma et al., 2019). The authors concluded that, like in peripheral tissues, anesthesia impairs lymphatic uptake of tracers in the CSF and furthermore that CSF efflux is inversely proportional to perivascular fluid movement. This raises very interesting questions about the relationship between CSF-ISF exchange via the perivascular space and CSF efflux. However, anesthesia can dramatically alter an animal's physiological state by reducing its respiratory drive and causing subsequent derangements in the arterial blood gas (Massey and Richerson, 2017). Therefore, we sought to determine the effect of ventilation and arterial tension of O_2, and CO_2 on lymphatic reabsorption of solutes in the CSF. To accomplish this, we measured lymphatic efflux into the DCLNs in nonventilated and ventilated mice after intraparenchymal and intracisternal coinjections of fluorescent dextrans (70 and 2000 kDa). In addition to measuring tracer distribution in the DCLNs, we also measured the parenchymal and intracranial distribution of solutes injected into these compartments to

determine if arterial blood gases or ventilation altered tracer distribution throughout the cranium.

Materials and Methods

Animals

Male and female 8-10 week old C57BL/6J mice from Jackson Laboratories were used for experiments. Mice were acclimated to their housing for several days before experiments were performed. For all surgical experiments, the core body temperature was monitored via rectal thermometer and maintained using either a heating pad or heating lamp. All experiments were approved by the Institutional Animal Care and Use Committee of Oregon Health & Science University.

Intraparenchymal tracer injections

Anesthesia was induced using 3% isoflurane and animals were placed in 3-point stereotaxic apparatus. Isoflurane was reduced to 2% and a surgical plane of anesthesia was ensured throughout the procedure by regular pedal reflex checks. A 2 cm midline incision was made in the scalp over the sagittal suture and the skin was reflected to locate bregma. After allowing the skull to dry, a burr hole was introduced in the right parietal bone (0.4 mm caudal, 1 mm lateral to bregma) using a Microtorque II drill. A 26 Ga needle (Hamilton) was inserted to a depth of 1 mm and rested for 10 minutes before injecting 1 μL of 1:1 solution of 70 and 2000 kDa dextran (25 mg/mL and 10 mg/mL, respectively; ThermoFisher) at a rate of 100 nL/minute. During the injection, for animals that were to remain under anesthesia, isoflurane was tapered off and mice received an intraperitoneal dose of

ketamine/xylazine (1.75 mg ketamine/0.25 mg xylazine per 20 gram mouse). The needle was removed from the brain following the injection and incision was closed with cyanoacrylate glue. Animals were removed from stereotaxic apparatus and either placed on a heating pad for the duration of the experiment (anesthetized group) or placed in their housing box after righting response was observed (awake group). Animals were sacrificed at 30, 60, and 120 minutes via intracardiac infusion of saline. In the event that tracer was injected into the lateral ventricle, animals were excluded from the study.

Intracisternal tracer injections

For intracisternal injections, anesthesia was induced using 3% isoflurane and animals were placed in 3-point stereotaxic apparatus. Isoflurane was reduced to 2% and a 2 cm midline incision was made caudally from lambda. Skin was reflected laterally and blunt dissected to expose muscle. The most superficial muscle layer was sectioned and reflected laterally and the deeper layers were kept intact and reflected laterally using 6-0 braided suture. The atlanto-occipital membrane was visualized via blunt dissection through ligamentous tissue and the bevel of a 30.5-gauge needle attached to PE-10 tubing was inserted into the cisterna magna. 2 μL 1:1 solution of 70 and 2000 kDa dextran (25 mg/mL and 10 mg/mL, respectively; ThermoFisher) was infused into the cisterna magna at a rate of 1 μL/minute. During the injection, for animals that were to remain under anesthesia, isoflurane was tapered off and mice received an intraperitoneal dose of ketamine/xylazine (1.75 mg ketamine/0.25 mg xylazine per 20 gram mouse). To minimize tracer leakage, cyanoacrylate glue was placed over the atlanto-occipital membrane and the incision was reapproximated. All mice that were awakened displayed the righting reflex within 8 minutes

of the injection start time. 30 minutes after initiation of the injection, animals were fixation perfused.

Mechanical ventilation

For experiments featuring ventilation of the mice, mice were anesthetized via intraperitoneal ketamine/xylazine and endotracheally intubated with a Becton Dickinson intravenous 22 ga catheter after Spoelstra et al., 2005.(Rivera et al., 2005) Mice were ventilated immediately on 100% inspired O_2 after intubation using a mechanical ventilator designed specifically for mice (Hugo Sachs Elektronik MiniVent type 845). In experiments featuring hypercapnic challenge, the inspired gas was switched to a mixture of 5% CO_2 and 95% O_2 throughout the duration of hypercapnic challenge. In all experiments, the end expiratory pressure was set to +3 cm H_2O, the inspiratory pressure was set to +10 cm H_2O, and tidal volume was set to 250 μL. Symmetrical chest rise and consistent effluent gas in the positive end expiratory column during expiration were used as criteria for accurate placement of the endotracheal tube. After insuring successful intubation, mice were paralyzed with an intraperitoneal dose of succinylcholine (25 mg/kg) to prevent the animals from challenging the ventilator. Heart rate and muscle tone readings were monitored using electrocardiogram and electromyography to insure depth of anesthesia but not recorded for experimental purposes.

Monitoring of physiological parameters

Arterial blood for blood gas measurements was either collected at the end of experiments or repeated sampling from the femoral artery. After termination of the experiment, blood was collected directly from the left ventricle via cardiac puncture. For

repeated blood gas measurement, the superficial femoral artery was isolated and ligated with 5-0 braided suture. Immediately proximal to the ligature, a small incision in the arterial wall was made with microvascular scissors, with temporary compression applied proximally to prevent bleeding. Blood was collected directly from the femoral artery at relevant time points. All arterial blood samples were analyzed immediately using a handheld blood gas analyzer (iStat, CG8+ cartridge). Cerebral blood flow and intracranial pressure were monitored simultaneously during experiments. To accomplish this, the mouse was placed in a 3-point stereotactic apparatus during mechanical ventilation and the scalp was visualized using a chemical depilatory agent. A 2 cm midline incision was made and the scalp was reflected laterally to visualize the cranium. A Laser Doppler Flometry probe (Moor Instruments DRT4) was placed over the left parietal bone to measure cerebral blood flow. For intracranial pressure (ICP) monitoring, a small burr hole was made in the right parietal bone using a Microtorque II drill. The burr hole was carefully made to avoid damaging the dura mater, and after visualizing the brain, a pressure transducer (SPR-1000, Millar Instruments) was lowered through the dura mater into the parietal cortex for intraparenchymal monitoring. To insure accurate probe placement and monitoring at the beginning and end of every experiment, transient compression of the abdomen was used to approximate a Valsalva maneuver, which transiently increased ICP by 25-35 mmHg before returning to baseline.

Microscopy

Mice were fixation-perfused with fresh 4% paraformaldehyde stored at 4°c. The calvarium, brain, skull base, and DCLNs were harvested and post-fixed in 4% paraformaldehyde overnight at 4°c. Calvaria, skull bases, and DCLNs were imaged

immediately using fluorescence dissection microscopy (Zeiss AxioZoom V16). Brains were dehydrated by submersion in 30% sucrose overnight at 4°c, frozen in OCT by submersion in 2-methylbutane on dry ice, and stored at -80°c. 100 μm brain sections were collected as floating sections in PBS. Brain sections were washed 3x with PBS and mounted using mowiol 4-88. All sections were imaged using either the LSM880 (Zeiss) or AxioScan (Zeiss) within 48 hours of mounting using the same laser power, photomultiplier voltage, and gain across groups. Post-image processing was performed using ImageJ. This includes image thresholding, fluorescence intensity measurements, and maximum intensity z-stack projections. All post-image processing was performed blinded to experimental groups.

Statistics

All statistical analyses were performed using GraphPad Prism 7. Data are presented as the mean ± standard error and individual values are represented as black circles overlying graphs. 2-way ANOVA with and without repeated measures and Sidak's post hoc correction for multiple comparisons was implemented for groupwise comparisons. An unpaired t-test with Welch's correction was used for pairwise comparisons. Results with a p-value less than or equal to 0.05 are considered significant.

Results

Parenchymal distribution and drainage of solutes in freely-breathing mice

To test the effect of anesthesia on parenchymal solute distribution and meningeal lymphatic drainage, we co-injected 70 and 2000 kDa dextrans into the motor cortex of adult mice. Upon completion of the injection, mice were either awakened and behaved freely in

either their home cage or remained under anesthesia for 30, 60, or 120 minutes (Figure 12A and Figure 19A). In mice survived for 120 minutes, we measured fluorescence intensity in subregions from three representative coronal sections to map tracer distribution in the brain parenchyma (Figure 12B and Figure 19B). We observed a state-dependent effect on tracer distribution in cortical regions, with greater 70 kDa dextran fluorescence intensity observed in cortices of awake mice compared to anesthetized mice (Figure 12B, two-way ANOVA with repeated measures, $p= 0.03$ and 0.05 for ipsi- and contralateral, respectively). This effect was not observed in the subcortical white matter of the corpus callosum (Figure 12B, two-way ANOVA with repeated measures, $p=0.6$ and 0.4 for ipsi- and contralateral, respectively). To exclude the possibility that this finding was an artifact of variation in tracer injection, we compared tracer distribution in brain section of mice at 30 minutes and found no difference in cortical tracer intensity of awake or anesthetized mice (Figure 20, two-way ANOVA, $p= 0.44$ and 0.99 for ipsi- and contralateral, respectively). Interestingly, this effect was also dependent on the tracer size, as we found no difference in the distribution of the 2000 kDa tracer in any brain section or subregion (Figure 19B).

To determine the cranial distribution of solutes after they exit the brain, we considered the calvarium and the skull base of mice 30 minutes after cortical injection. In the calvarium, we measured fluorescence intensity of around the SSS and meninges adjacent to the SSS (Figure 12C and Figure 19C). In the base of the skull, we measured fluorescence intensity near the trigeminal nerve (CN V) and in the meninges overlying the rostral aspect of the basiphenoid bone (Figure 12C and 19C). Though we did not observe an effect of anesthesia on the cranial distribution of tracer, we found that the majority of tracer was

distributed along the base of the skull, rather than in the calvarium (two-way ANOVA, $p<0.0001$).

To determine the effect of anesthesia on lymphatic clearance of parenchymal solutes, we harvested and measured fluorescence intensity of tracer in the DCLNs from mice at 30, 60, and 120 minutes (Figure 12D and Figure 19D). Interestingly, we observed a significant reduction in the rate of lymphatic tracer clearance in anesthetized animals compared to awake animals (two-way ANOVA, $p<0.01$). We also observed that, although the dextrans were delivered into the right motor cortex, the tracer distribution occurred bilaterally in the DCLNs, suggesting that lymphatic drainage of solutes is not lateralized (Figure 21).

Arterial blood gases in anesthetized mice

Several types of anesthesia, including ketamine/xylazine are known to depress the hypercapnic ventilatory response, which is responsible for modulating respiratory rate in response to changes in the blood pH (Massey and Richerson, 2017). This results in the development of an acute respiratory acidosis, characterized by reduced respiratory rate, lowered blood pH, increased arterial tension of CO_2, and normal $HCO3^-$. To determine the effect of ketamine/xylazine anesthesia on the arterial blood gases (ABGs) of wild type mice, we anesthetized mice and sampled blood from the superficial femoral artery after thirty minutes of anesthesia. We observed a significant respiratory acidosis in non-intubated mice, with a blood pH of 7.22 ± 0.03, and paCO2 of 64 ±4 mmHg (Figure 13). Mice were also hypoxemic and oxygen desaturated, with an average paO_2 and oxygen saturation of 50 ± 4 mmHg and 74 ± 5%, respectively (Figure 13). To correct these derangements in blood gases, we endotracheally intubated mice and empirically determined ventilation settings that corrected the ABGs (Figure 13). We found that mice ventilated at a rate of 300 breaths min^{-1}

(BPM) on 100% O_2 corrected the $paCO_2$, paO_2, O_2 saturation, and pH (Figure 13). Furthermore, to control for the effect of respiratory rate, we also characterized the ABGs of mice before and after hypercapnic challenge with 5% CO_2 for 30 minutes (Figure 13).

Intracranial distribution and drainage of parenchymal solutes in mechanically-ventilated mice

We surmised that the severe derangement in ABGs in freely breathing anesthetized mice may contribute to the arousal state differences reported in previous studies due to changes in cerebral blood flow (CBF) or ICP. Indeed, a well characterized direct relationship between arterial CO_2 and CBF exists in humans and rodents, wherein dilation of the cerebral blood vessels is directly mediated by elevations in $paCO_2$. This cerebrovascular response to $paCO_2$ results in increased flow velocity in cerebral blood vessels and causing a global increase in CBF across the brain (Beasley et al., 1979; Kety and Schmidt, 1948; Markwalder et al., 1984). This response may subsequently increase ICP depending on the magnitude of change in CBF. Furthermore, vascular pulsatility was proposed as one of the motive forces for CSF-ISF exchange, which is also altered by hypercapnia (Czosnyka et al., 1996; Iliff et al., 2013). Therefore, to test the effect of hypercapnia on lymphatic parenchymal solute drainage, we repeated the analysis of parenchymal tracer drainage in mice that were ventilated at a high respiratory rate (300 BPM), high respiratory rate with 5% CO_2 inspired gas (300 BPM + 5% CO_2), or mice that were awake and freely behaving in their home cage. Mice in all groups were sacrificed via fixation perfusion 30 minutes after the injection was initiated, and the calvaria, brains, skull bases, and DCLNs of these mice and measured tracer distribution in each compartment.

Similar to the parenchymal distribution of tracers in awake and nonintubated anesthetized mice at 30 minutes, we did not observe any difference in the parenchymal distribution of tracers among ventilation states. In these animals, we again noted greater tracer distribution in the base of the skull compared to the calvarium (Figure 14A and Figure 22A). Considering lymphatic drainage, we observed that parenchymal tracer absorption was rescued in mice ventilated at 300 BPM, and this rescue of lymphatic drainage was blocked by inducing hypercapnia via adding 5% CO_2 into the inspired gas (Figure 14B and Figure 22B).

Intracranial distribution and drainage of CSF solutes in mechanically-ventilated mice

Recent studies focused on the exchange between the CSF and ISF compartments, comparing anesthetized and freely behaving awake mice. Specifically, several groups showed that the rate of solute exchange is altered in the anesthetized mouse, though conflicting reports claimed that ketamine/xylazine either increases or decreases CSF-ISF exchange (Gakuba et al., 2018; Ma et al., 2019; Xie et al., 2013). An inverse relationship between lymphatic CSF drainage and CSF-ISF exchange was proposed on the basis of similar comparisons between anesthetized and awake mice (Ma et al., 2019). Therefore, we sought to determine if hypercapnia alters solute exchange between the CSF and ISF and to confirm that lymphatic drainage of solutes in the CSF is directly impaired in the hypercapnic state. To test this, we co-infused 70 and 2000 kDa dextrans directly into the CSF at the cisterna magna of mice that were ventilated at 300 BPM, 300 BPM + 5% CO_2, or 300 BPM and subsequently awakened. Mice were intubated and anesthetized with isoflurane during the infusion, after which the incision was reapproximated, and the mice were either extubated and allowed to awaken and freely behave in their home cage or tapered isoflurane off and maintained anesthesia with intraperitoneal ketamine/xylazine for 30 minutes. In all groups,

the duratomy was sealed with cyanoacrylate glue before removing the needle to prevent reflux of the tracer. We harvested the calvaria, brains, skull bases, and DCLNs of these mice and measured tracer distribution in each compartment.

For both tracer sizes, we observed a significant groupwise effect on CSF-ISF exchange considering the total area coverage (Figure 15 and Figure 23, $p<0.001$ and $p<0.01$, respectively). We performed multiple post-hoc comparisons and observed an increase in CSF-ISF exchange in mice ventilated at 300 BPM compared to the awake and hypercapnic challenge groups (Figure 15 and Figure 23). Similar to the intraparenchymal injections, we observed greater mean fluorescence intensity in the skull base meninges and perineural region of the trigeminal nerve than in the SSS and meninges in the calvarium in all groups (Figure 16A and Figure 24A). Unlike parenchymal tracer drainage, we did not observe statistically-significant differences in tracer distribution across the DCLNs in different ventilation states (Figure 16B and Figure 24B).

Monitoring cerebral blood flow and intracranial pressure during hypercapnic challenge

To examine possible mechanisms underlying the observation that hypercapnia reduces the rate of lymphatic absorption of parenchymal solutes, we monitored the changes in cerebral blood flow and intracranial pressure in an independent experiment. We monitored these parameters simultaneously at baseline (300 BPM) and for 15 minutes after initiation of hypercapnic challenge (300 BPM + 5% CO_2). At the end of each experiment, we confirmed hypercapnia in mice via arterial blood gas measurements of blood collected from the left cardiac ventricle. Although we observed a modest increase in cerebral blood flow

after induction of hypercapnia, this was not sufficient to increase intracranial pressure (Figure 17).

Discussion

Historically, conflicting findings were reported in many studies focused on solute trafficking in the brain and CSF. The underlying cause behind these discrepancies remains unclear. Recently, some groups indicated that one source of variability may be different anesthetic regimens. Anesthesia is used ubiquitously throughout biomedical research to perform animal surgery and accomplish various interventions in animal models of human disease. Although intubation and mechanical ventilation is regularly used in humans, these practices are inconsistently implemented in mice. Given that most studies focused on solute trafficking in the CNS do not use ventilation to control arterial blood gases, the type of anesthesia used and the depth of anesthesia achieved may have an important bearing on experimental outcomes. In the current study, we found that hypercapnia affects several parameters of solute trafficking in the CNS, including lymphatic drainage and CSF-ISF exchange. Thus, differences in the arterial CO_2 tension may contribute to the discrepancies in the literature. We also observed several fundamental aspects of solute trafficking in the brain and CSF that may inform future studies focused on lymphatic drainage from the brain.

Solute trafficking in awake and nonintubated anesthetized mice

Our observation that tracer distribution after intracortical injection is reduced in non-intubated anesthetized mice compared to awake mice is consistent with previous reports of increased parenchymal solute clearance in mice anesthetized with ketamine/xylazine

anesthesia (Groothuis et al., 2007; Xie et al., 2013). Moreover, our observation that gray matter distribution of the 70 kDa, but not 2000 kDa dextran was altered by anesthesia suggests a size-based effect on interstitial solute distribution. Given the large difference in approximate hydrodynamic radii of the 70 kDa and 2000 kDa dextrans (6.49 and 26.89 nm, respectively (Armstrong et al., 2004), it is possible that the distribution of the 2000 kDa dextran was unchanged in anesthetized mice due to its inability to traffic within the gray matter. However, this tracer was selected with respect to current estimates of the parenchymal extracellular space, which Thorne and colleagues report accommodates the movement of solutes with hydrodynamic radii of up to 35 nm (Thorne and Nicholson, 2006). Unlike the size-dependent effect on tracer distribution in the gray matter, we did not observe any effect of anesthesia on either tracer's distribution in the subcortical white matter, suggesting that once a solute enters into the white matter it travels in a state and size-independent manner.

Interestingly, despite the fact that interstitial tracer distribution was affected by anesthesia, we found that after tracer exchanged into the CSF compartment, it was equally distributed in awake and anesthetized mice, concentrating in the meninges and perineural space in the anterior skull base. This finding suggests that the extraparenchymal behavior of solutes in CSF is unlikely to be governed by the same physiological mechanisms that determine interstitial solutes distribution. Moreover, we observed that once tracer enters into the CSF, it is distributed bilaterally in the skull base, which is reflected by our observation that both DCLNs display similar tracer distribution after injection into the right cortex (Figure 21).

Notwithstanding the similar tracer signal distribution in the calvarium and skull base, the rate of tracer accumulation in the DCLNs was markedly reduced in non-ventilated anesthetized mice. Together, these findings suggest that lymphatic absorption of solutes from the brain may be dependent on at least two functions: (1) the rate of solute exchange between the ISF and CSF, (2) the rate of lymphatic solute absorption from the CSF (Figure 18). Without considering the physiological status of the mouse, the finding that anesthesia impairs lymphatic drainage from the brain is in accordance with previous work assessing lymphatic function in peripheral tissues and the CNS by Proulx and colleagues (Ma et al., 2019; Proulx et al., 2017). In their 2017 study, the authors reported rescue of lymphatic tracer uptake in the mouse footpad via massage, indicating that anesthesia-mediated impairment of lymphatic function is due to extrinsic lymphatic pumping. However, in the current study we observed significant pathological changes in the arterial blood gas of nonintubated mice after 30 minutes of ketamine/xylazine anesthesia.

Pathological changes in arterial blood gas alter solute distribution in the CNS

Consistent with previous findings reported in the literature, we observed that ketamine/xylazine causes free-breathing mice to develop a respiratory acidosis, hypercapnia, and hypoxemia. Correction of these pathological changes in the mouse with endotracheal intubation and mechanical ventilation at a respiratory rate of 300 BPM rescued lymphatic drainage of solutes injected into brain parenchyma, while 300 BPM + 5% CO_2 corrected the O_2 desaturation and hypoxemia but did not rescue lymphatic drainage. Because we found that hypercapnic challenge alone was sufficient to reduce lymphatic uptake of solutes in cortex, we concluded that hypercapnia has a strong effect on lymphatic drainage from the brain.

As suggested above, lymphatic solute clearance from the brain may also be dependent on the rate of CSF-ISF exchange. If hypercapnia affects CSF-ISF exchange, this may explain the reduction of lymphatic drainage in hypercapnic mice. To evaluate this possibility, we measured the effect of hypercapnia on CSF-ISF exchange. As a proxy for CSF-ISF exchange, we injected tracers into the cisterna magna and measured their penetration into the brain parenchyma. Interestingly, we found that tracer penetration into the brain was highest in anesthetized animals with normalized arterial blood gases and that hypercapnia reduced tracer penetration into the brain. Parenchymal tracer penetration was not solely determined by arterial CO_2 tension, however, because the awake group (which presumably has normal arterial blood gases) had the lowest tracer penetration. This finding is consistent with previous findings that suggest ketamine/xylazine anesthesia potentiates CSF-ISF exchange and clearance of solutes (Groothuis et al., 2007; Xie et al., 2013), and suggests that hypercapnia may reduce the magnitude of this effect. One key difference between the findings in this study and those reported by Xie and colleagues is that their anesthetized mice were not mechanically ventilated. Given our observations that hypercapnia develops in nonventilated mice and that hypercapnia reduces CSF-ISF exchange, we would anticipate that Xie and colleagues would not have observed an effect of anesthesia on CSF-ISF exchange. One possible explanation for this inconsistency is the difference in technical approaches to measuring CSF-ISF exchange. Xie and colleagues utilized a multiphoton microsopy approach to measuring cortical penetration in vivo, whereas we used confocal microscopy across multiple brain sections. Although multiphoton microscopy is spatially limited, it enables greater temporal resolution for measuring CSF-ISF exchanges in addition to repeated measures, which may increase the sensitivity of detecting differences in a

dynamic biological process like CSF-ISF exchange. Still, our findings suggest that the magnitude of this effect may be underestimated in the absence of mechanical ventilation.

One mechanism that may contribute to the impairment of CSF-ISF exchange in hypercapnic mice is the direct effect of hypercapnia on the cerebral vasculature. Iliff and colleagues previously demonstrated that the motive force for CSF-ISF exchange is due to arterial pulsatility by showing increased parenchymal tracer penetration after administering the inotropic agent dobutamine (Iliff et al., 2013). In the rabbit, hypercapnic challenge resulting in arterial tension of CO_2 similar to that in our study (67 mmHg) reduced cerebrovascular pulsatility index by 47±16% (Czosnyka et al., 1996). Therefore, reductions in vascular pulsatility due to hypercapnia may underlie the impairment of CSF-ISF exchange that we observed in hypercapnic mice.

In terms of lymphatic solute drainage from the CSF, we did not observe a difference in solute uptake from the CSF in different ventilation states at 30 minutes. We suspect that the rate of lymphatic solute uptake from the CSF is far more rapid from those in the brain and that the lymph nodes were saturated at 30 minutes in all groups. Although this experiment failed to demonstrate that hypercapnia reduces lymphatic absorption of solutes directly from the CSF, several other findings in this study suggest that the formation of lymph from the CSF is also subject to physiological control by hypercapnia or the waking state. First is the observation that although CSF-ISF exchange is lowest in the waking state, lymphatic drainage of parenchymal solutes is maximized. This indicates that despite the relatively low availability of tracer in the CSF, more of it is being absorbed by the lymphatic vasculature in a normocapnic, waking state. Second, while CSF-ISF exchange is also reduced in a hypercapnic state, lymphatic clearance of parenchymal tracer is minimized. Together,

these findings suggest that impairment of CSF-ISF exchange is not sufficient to reduce lymphatic drainage of solutes in the brain. Therefore, while hypercapnia alters solute exchange between the CSF and ISF, we think it likely that either hypercapnia or the waking state also acts on the lymphatic absorption of solutes (Figure 18). Future studies evaluating the effect of hypercapnia on lymphatic drainage directly from the CSF should consider earlier time points, or measure lymphatic drainage dynamically to directly demonstrate this relationship.

We hypothesized that changes in ICP secondary to increased CBF caused by hypercapnia may modulate lymphatic drainage. However, we were unable to detect substantial changes in ICP after hypercapnic challenge despite detecting a modest increase in CBF using transcranial laser Doppler flowmetry. Studies considering the direct effects of hypercapnia on lymphatic contractility and flow dynamics are uncommon in the literature, with only two studies identified by the authors of the current study. These studies reported transient and acute increases in lymphatic flow velocity during hypercapnia in lambs, dogs, and pups that were attributed to increased production of ISF related to increased hydrostatic pressure in the pulmonary capillary bed (Haberkern and Bland, 1981; Stinson et al., 1977). However, large hydrostatic pressure gradients exist at baseline between cerebral capillaries and the ISF, with little net water flux into the brain (Sweet et al., 1950). Thus, global cerebral edema secondary to respiratory acidosis is rarely reported in the humans, with reported cases describing $paCO_2$ >85 mmHg (Joyce and McGee, 2011; Roh et al., 2016).

Although ISF production may not be strongly dependent on CBF, one might surmise that CSF production is increased at the choroid plexus in hypercapnic states, thereby altering the hydrostatic pressure gradient between the CSF and lymph compartments. On

the contrary, studies in the literature report that CSF production is actually reduced in the setting of respiratory acidosis. Specifically, hypercapnia increases plasma-derived solutes in the CSF during hypercapnia in rodents, which was previously attributed to increased CSF production at the choroid plexus (Habgood, 1995). Furthermore, if hypercapnia-mediated impairment of CSF production underlies the reduction in lymphatic reabsorption, we would expect to observe reductions in intracranial solute distribution in hypercapnic mice compared to waking mice. Conversely, we found no statistical differences in the intracranial tracer distribution between hypercapnic and waking mice. Thus, lymphatic access to these solutes in different cranial regions does not appear to be impaired by hypercapnia.

Another possibility is that extrinsic pumping of lymph is affected by hypercapnia. One major candidate for extrinsic pumping mechanisms in the intracranial space is the intracranial pressure wave, which is propagated across both the brain and the CSF with distinct periodicity. Intracranial pulsatility, measured as the amplitude of ICP waves, is dependent on parenchymal compliance as well as several hemodynamic factors including cerebral perfusion pressure, heart rate, and vascular pulsatility (Czosnyka et al., 1996; Eide, 2016; Piper, 1997; Wagshul et al., 2011). If ICP waves contribute to conduction of lymph through capillaries, one would anticipate that their magnitude or periodicity would be reduced by hypercapnia. However, the periodicity of ICP waves, largely due to heart rate, is not changed with increasing $paCO_2$ (Rothe et al., 1990). To our knowledge, empirical tests of the potential relationship between ICP wave magnitude and hypercapnia are unreported in the literature. As described above, previous studies demonstrated that vascular pulsatility is reduced with hypercapnia (Czosnyka et al., 1996), which is a major component of the motive force for ICP waves. Therefore, one possibility is that although there was not a detectable

increase in ICP during hypercapnic challenge, reduced vascular pulsatility in hypercapnic mice may affect ICP waveforms. Future studies can employ Fourier transformation of continuous ICP monitoring data to assess the cardiac components of ICP waves in hypercapnic and normocapnic mice. Furthermore, vascular pulsatility can be pharmacologically manipulated with inotropic agents to directly test this hypothesis in future experiments.

In measuring solute behavior in the ISF and CSF, it is critical to establish and maintain physiologic control of experimental animals. In this study, we show that without intubation and adequate ventilation, mice develop significant derangements in oxygen saturation, paO_2, and $paCO_2$ that contribute to marked physiological effects on solute exchange between the brain and CSF and lymphatic absorption via the cervical lymphatic vasculature. We believe that labs should establish ventilation protocols empirically based on arterial blood gas measurements, since dead space volume and ventilator parameters may vary from lab to lab.

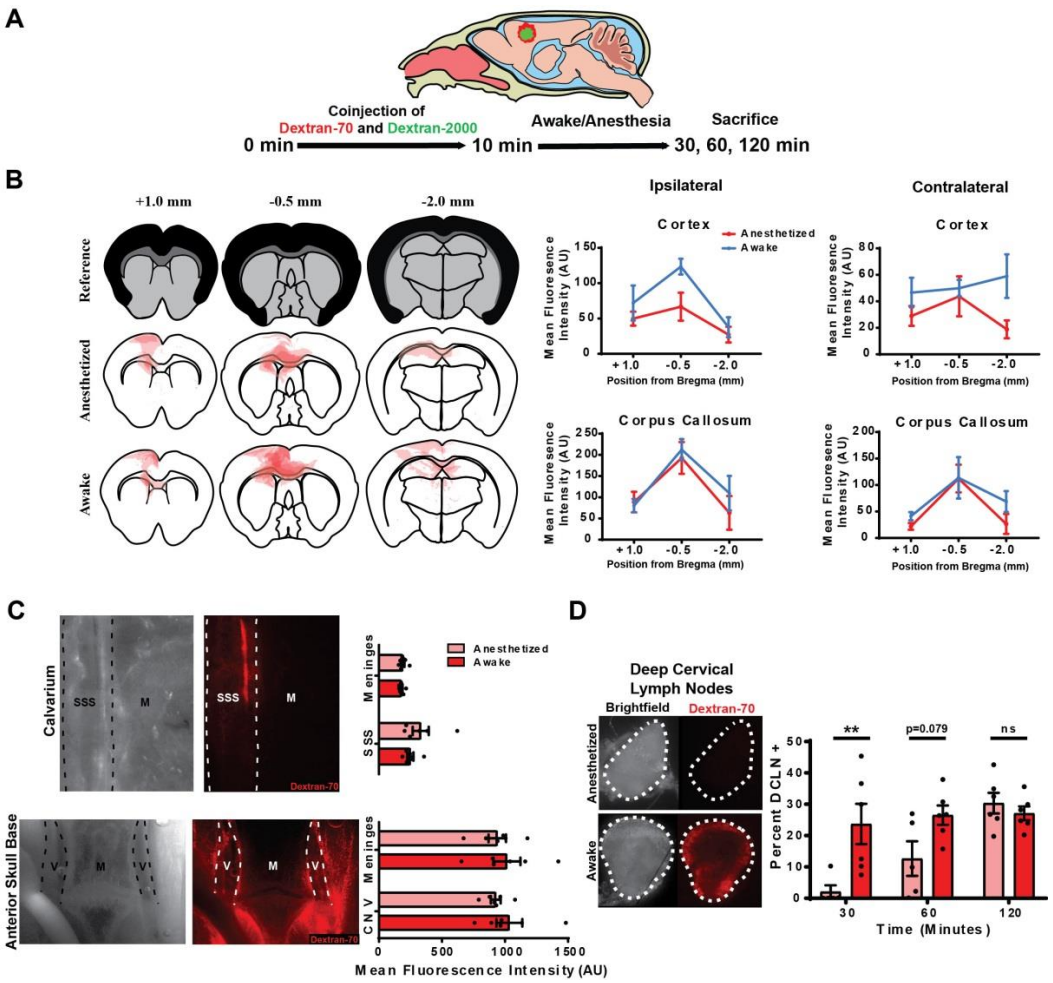

Figure 12. Anesthesia reduces interstitial distribution of macromolecules and slows lymphatic drainage of interstitial tracer.

A. Cartoon and experimental schematic (n=6/group). B. Left, Overlay of approximate dextran-70 (red) distribution in three brain regions 120 minutes following intracortical injection. Black and gray regions in the reference section represent cortical and corpus callosum regions of interest, respectively. Right, Corresponding subregion analysis of cortex and corpus callosum. C. Left, Representative images of 70 kDa tracer distribution in the calvarium and anterior skull base. Right, Quantification of fluorescence intensity in segmented regions. D. Left, Representative deep cervical lymph nodes 30 minutes after parenchymal injection of 70 kDa dextran. Right, Quantification of tracer distribution in the deep cervical lymph nodes of mice 30, 60, and 120 minutes after parenchymal tracer injection. Groupwise differences were assessed using two-way ANOVA and Sidak's correction for multiple comparisons. M, Meninges; SSS, Superior Sagittal Sinus; V and CN V, trigeminal nerve, **p<0.01; ns, not significant.

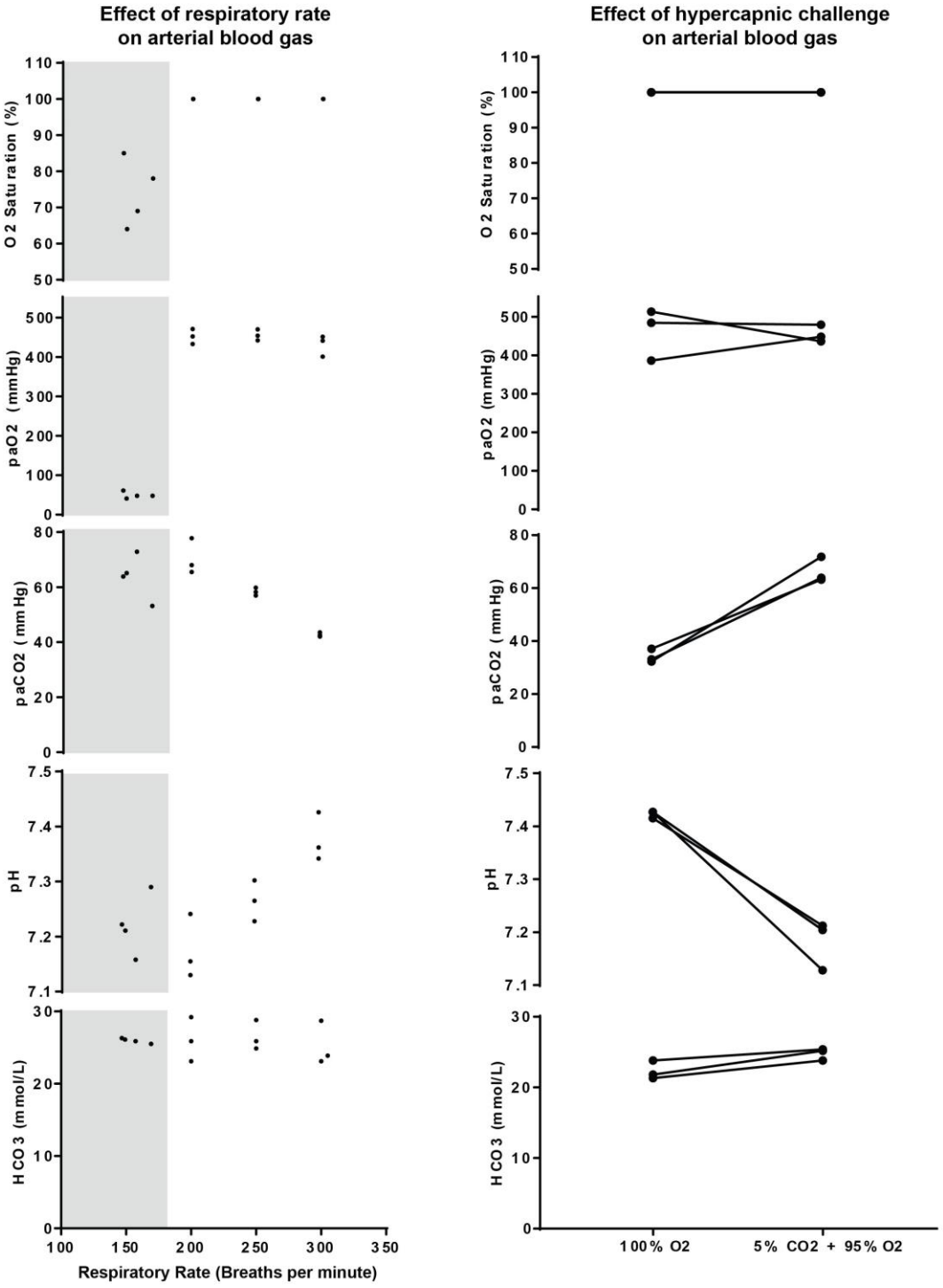

Figure 13. Characterization of arterial blood gases in nonintubated, intubated, and C02-challenged mice. Left, arterial blood gas in non-intubated mice (gray) and intubated mice mechanically ventilated at different respiratory rates.

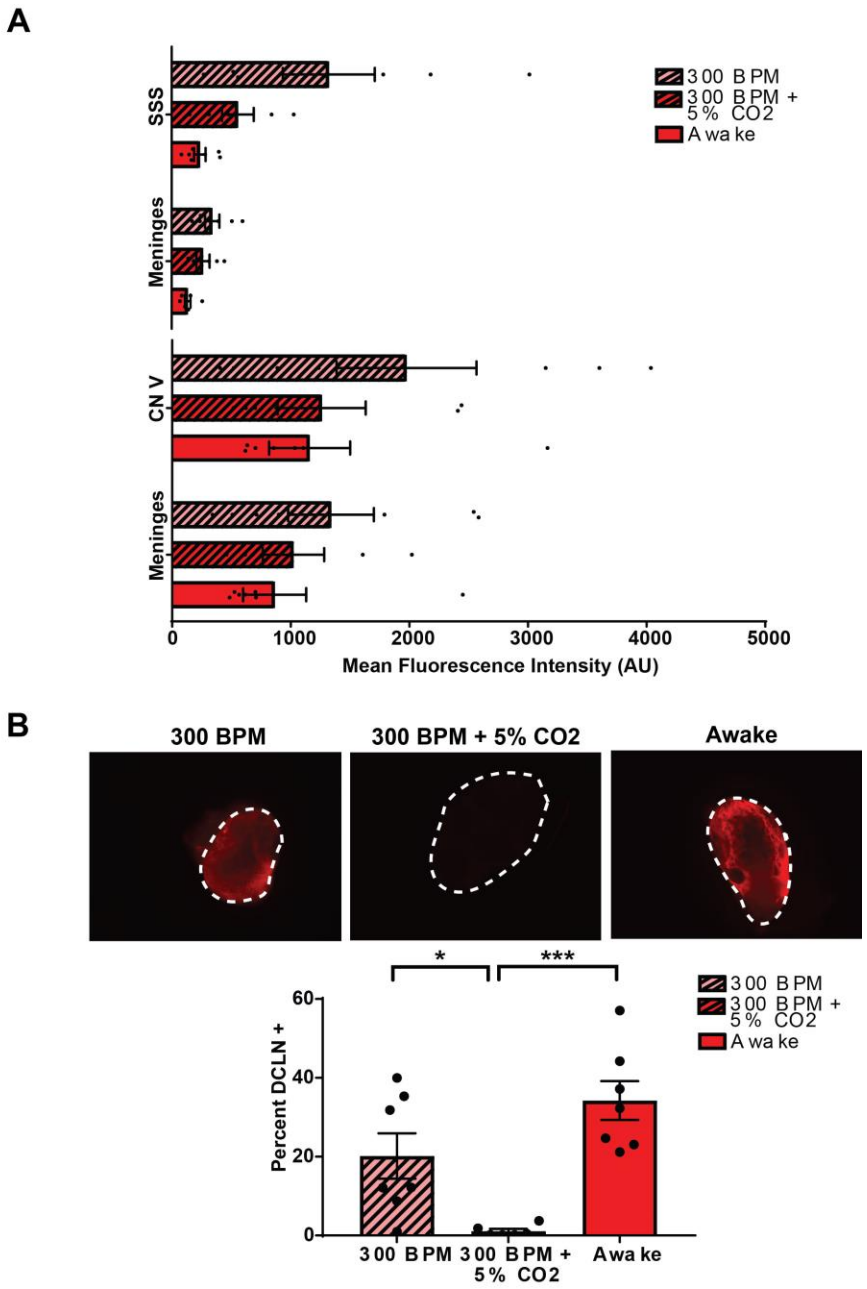

Figure 14. Intracranial tracer distribution and lymphatic drainage of parenchymal tracer in mechanically ventilated mice.

A. Intracranial distribution of 70 kDa dextran, including the superior sagittal sinus (SSS), and meninges in the calvarium and the trigeminal nerve (CN V) and meninges in the skull base.

B. Signal intensity in the deep cervical lymph nodes (DCLNs) after 30 minutes after injection.

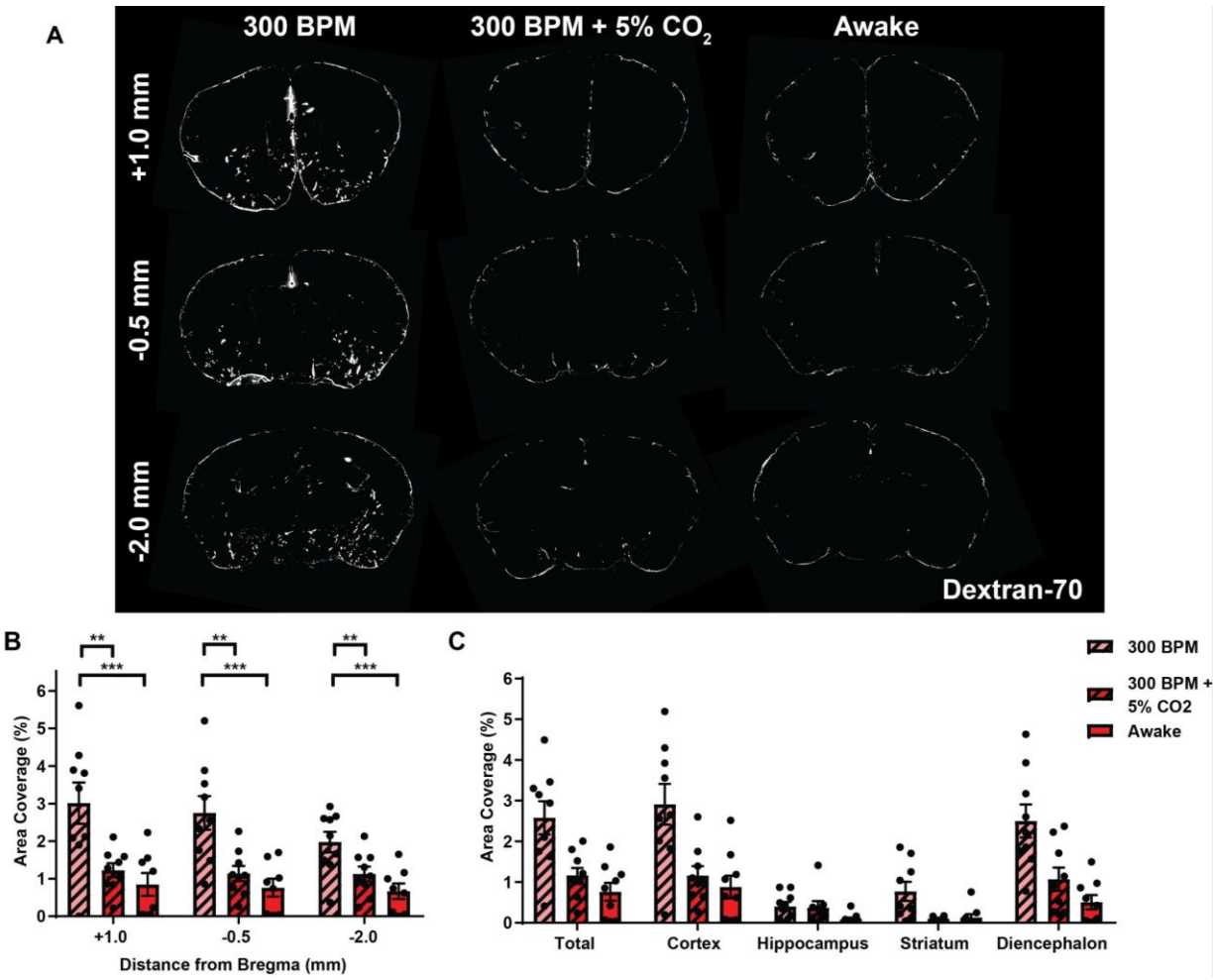

Figure 15. Hypercapnia reduces CSF-ISF exchange of 70 kDa tracer in mice.

A, Representative coronal brain sections taken from mice 30 minutes after intracisternal tracer infusion. B, Quantification of total area coverage by tracer at three brain regions. C, Average area coverage in brain subregions averaged across three brain sections. **p<0.01, ***p<0.001.

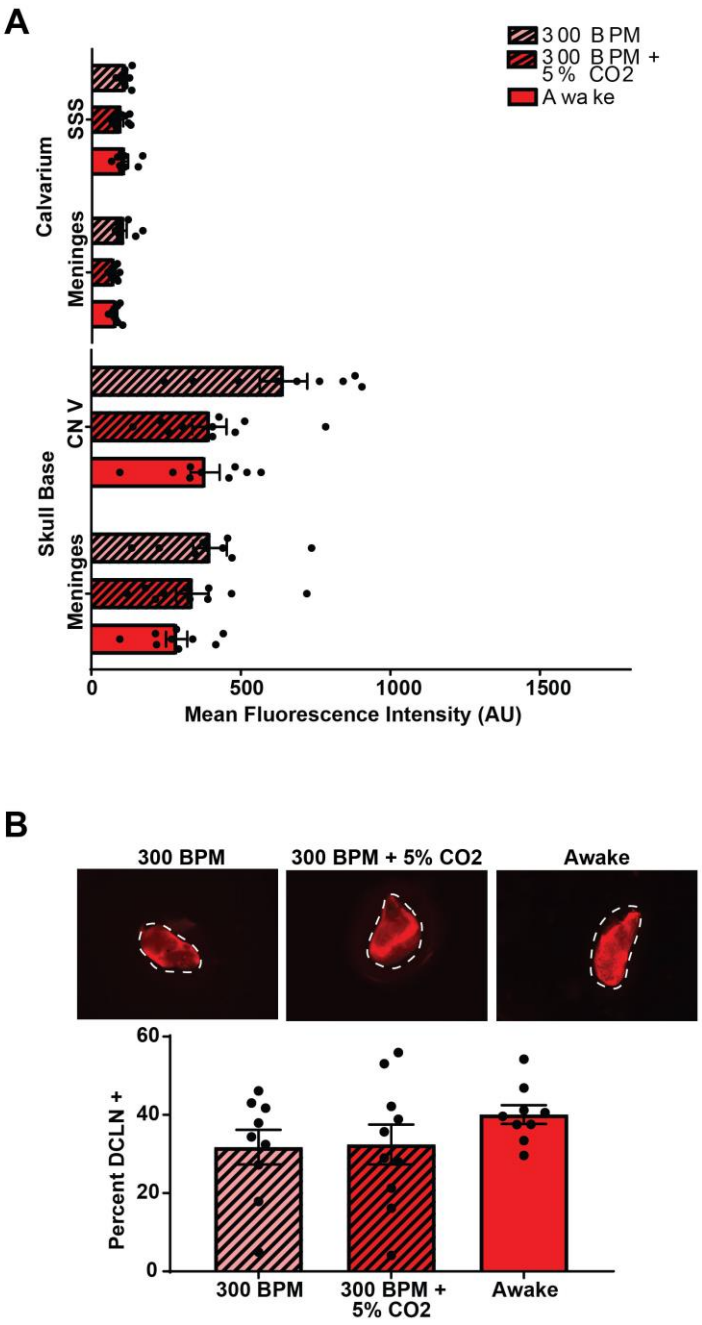

Figure 16. Intracranial tracer distribution and lymphatic drainage of 70 kDa dextran injected into the CSF of mechanically ventilated mice.

A. Intracranial distribution of 70 kDa dextran, including the superior sagittal sinus (SSS), and meninges in the calvarium and the trigeminal nerve (CN V) and meninges in the skull base.

B. Signal intensity in the deep cervical lymph nodes (DCLNs) after 30 minutes after injection and ventilation at different respiratory rates.

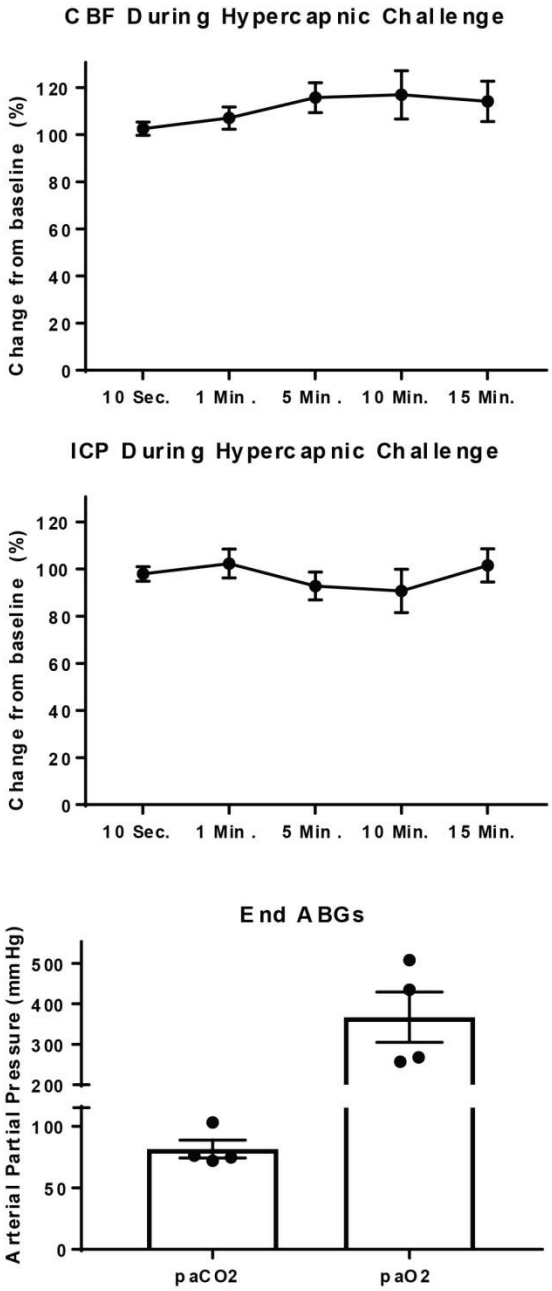

Figure 17. Cerebral blood flow and intracranial pressure during hypercapnic challenge.

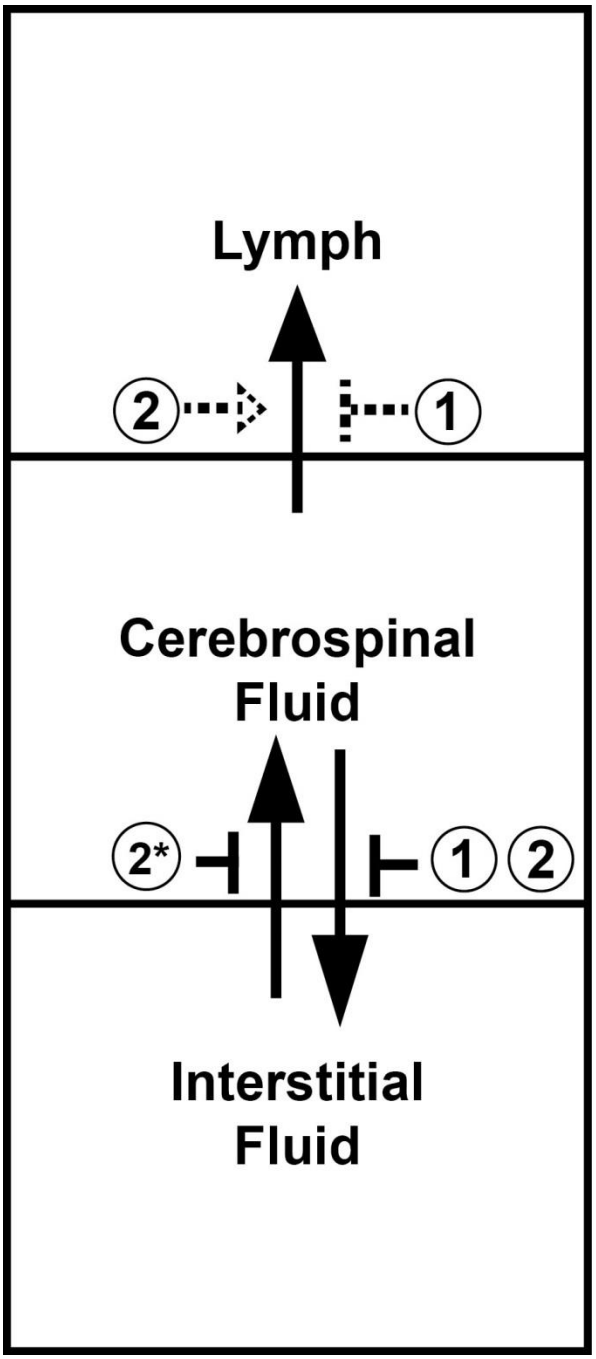

Figure 18. Model of physiological effectors on the interstitial fluid, cerebrospinal fluid, and lymphatic compartments.

Asterisk indicates findings described by Xie et al., 2013. Dotted lines indicate possible effects based on the data presented in this dissertation.

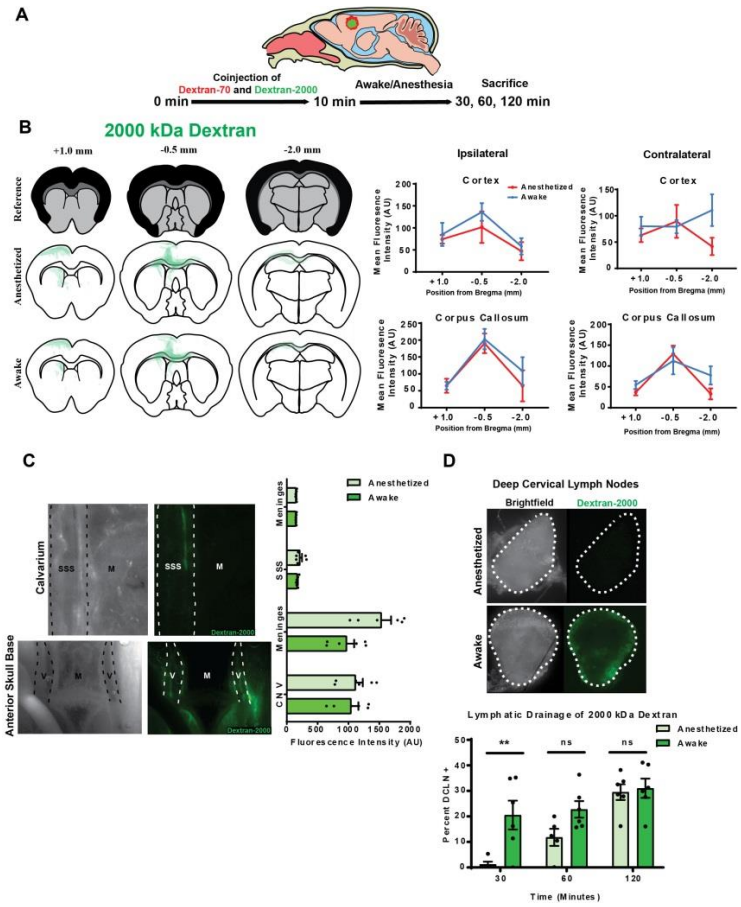

Figure 19. Anesthesia reduces interstitial distribution of macromolecules and slows lymphatic drainage of interstitial tracer.

A. Cartoon and experimental schematic. B. Left, Overlay of approximate 2000 kDa (green) distribution in three brain regions 120 minutes following intracortical injection. Black and gray regions in the reference section represent cortical and corpus callosum regions of interest, respectively. Right, Corresponding subregion analysis of cortex and corpus callosum. C. Left, Representative images of 2000 kDa tracer distribution in the calvarium and anterior skull base. Right, Quantification of fluorescence intensity in segmented regions. D. Top, Representative deep cervical lymph nodes 30 minutes after parenchymal injection of 2000 kDa dextran. Bottom, Quantification of tracer distribution in the deep cervical lymph nodes of mice 30, 60, and 120 minutes after parenchymal tracer injection. Graphs represent mean intensity and error bars represent SEM. Groupwise differences were assessed using two-way ANOVA with repeated measures and Sidak's correction for multiple comparisons. M, Meninges; SSS, Superior Sagittal Sinus; V and CN V, trigeminal nerve, **$p<0.01$; ns, not significant.

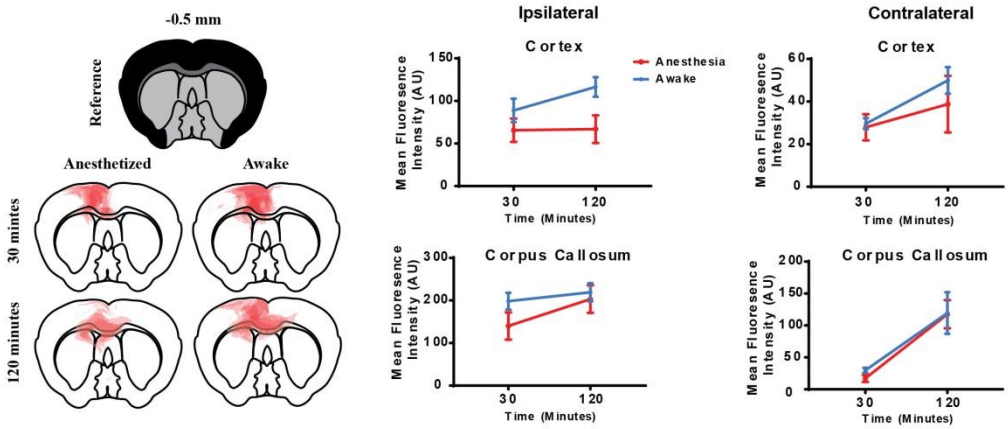

Figure 20. Effect of anesthesia on interstitial 70 kDa dextran over time.
Left, Overlay of approximate dextran-70 (red) distribution at injection site 30 and 120 minutes following intracortical injection. Black and gray regions in the reference section represent cortical and corpus callosum regions of interest, respectively. Right, Corresponding subregion analysis of cortex and corpus callosum showing no difference in distribution 30 minutes after injection.

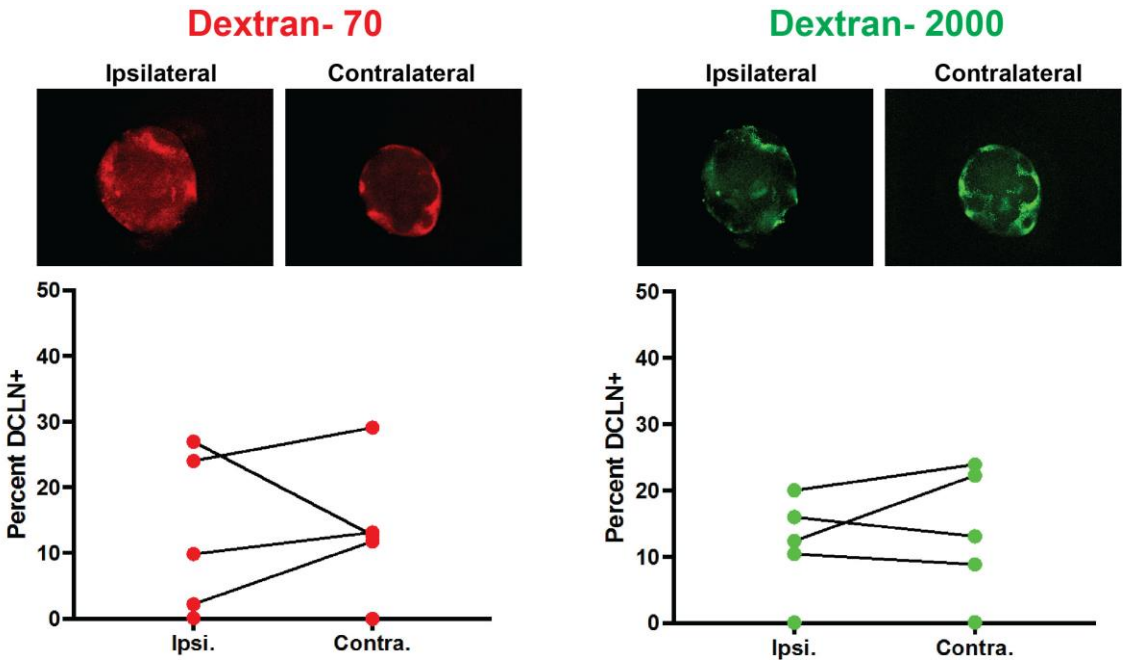

Figure 21. Tracers injected into the right motor cortex drain into deep cervical lymph nodes bilaterally.

Left, representative ipsilateral and contralateral lymph nodes 60 minutes after injection of 70 kDa dextran. Right, representative ipsilateral and contralateral lymph nodes 60 minutes after injection of 2000 kDa dextran. Points on graph represent pair-matched tracer distribution in deep cervical lymph nodes of individual animals.

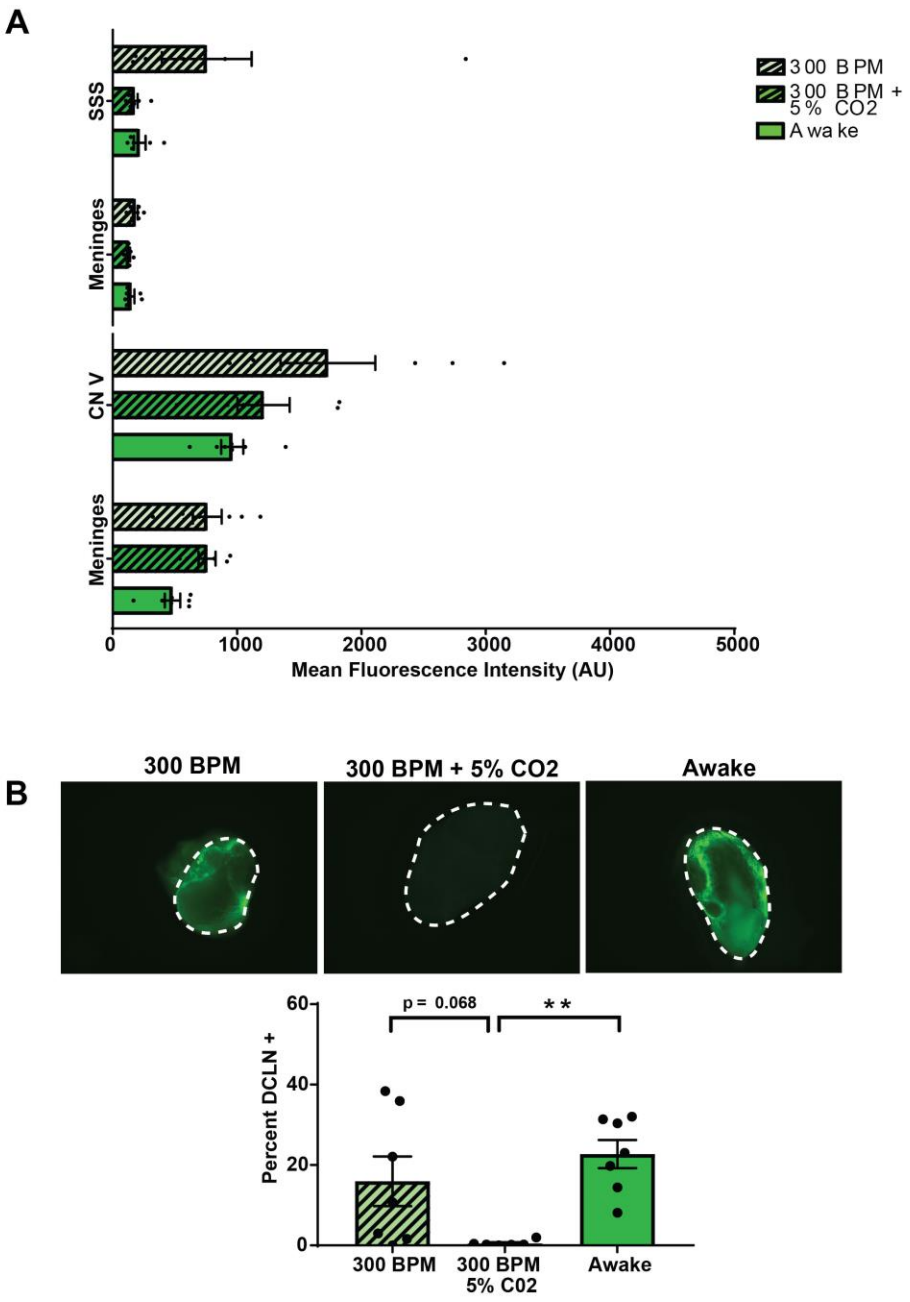

Figure 22. Intracranial tracer distribution and lymphatic drainage of 2000 kDa dextran injected into the motor cortex of mechanically ventilated mice.

A. Intracranial distribution of 2000 kDa dextran, including the superior sagittal sinus (SSS), and meninges in the calvarium and the trigeminal nerve (CN V) and meninges in the skull base. B. Signal intensity in the deep cervical lymph nodes (DCLNs) after 30 minutes after injection and ventilation at different respiratory rates.

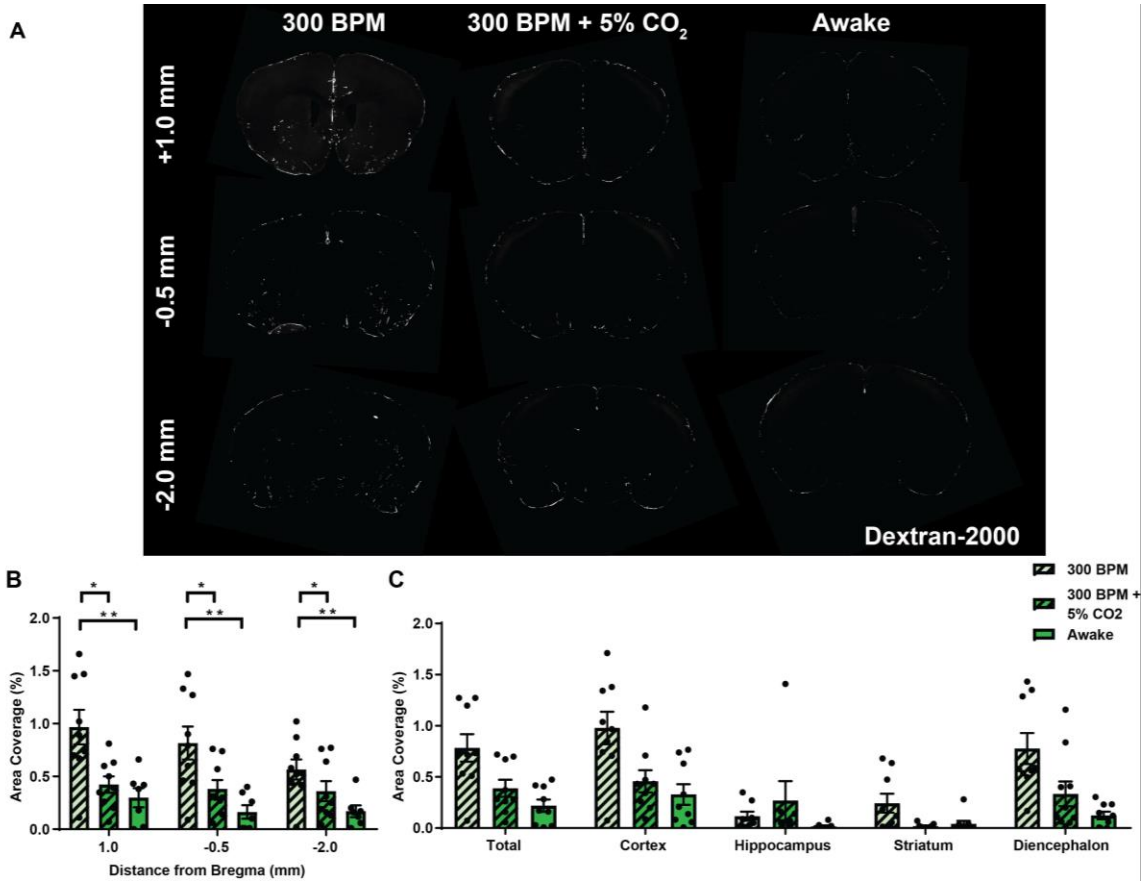

Figure 23. Hypercapnia reduces CSF-ISF exchange of 2000 kDa tracer in mice.
A, Representative coronal brain sections taken from mice 30 minutes after intracisternal tracer infusion. B, Quantification of total area coverage by tracer at three brain regions. C, Average area coverage in brain subregions averaged across three brain sections. *$p<0.05$, **$p<0.01$.

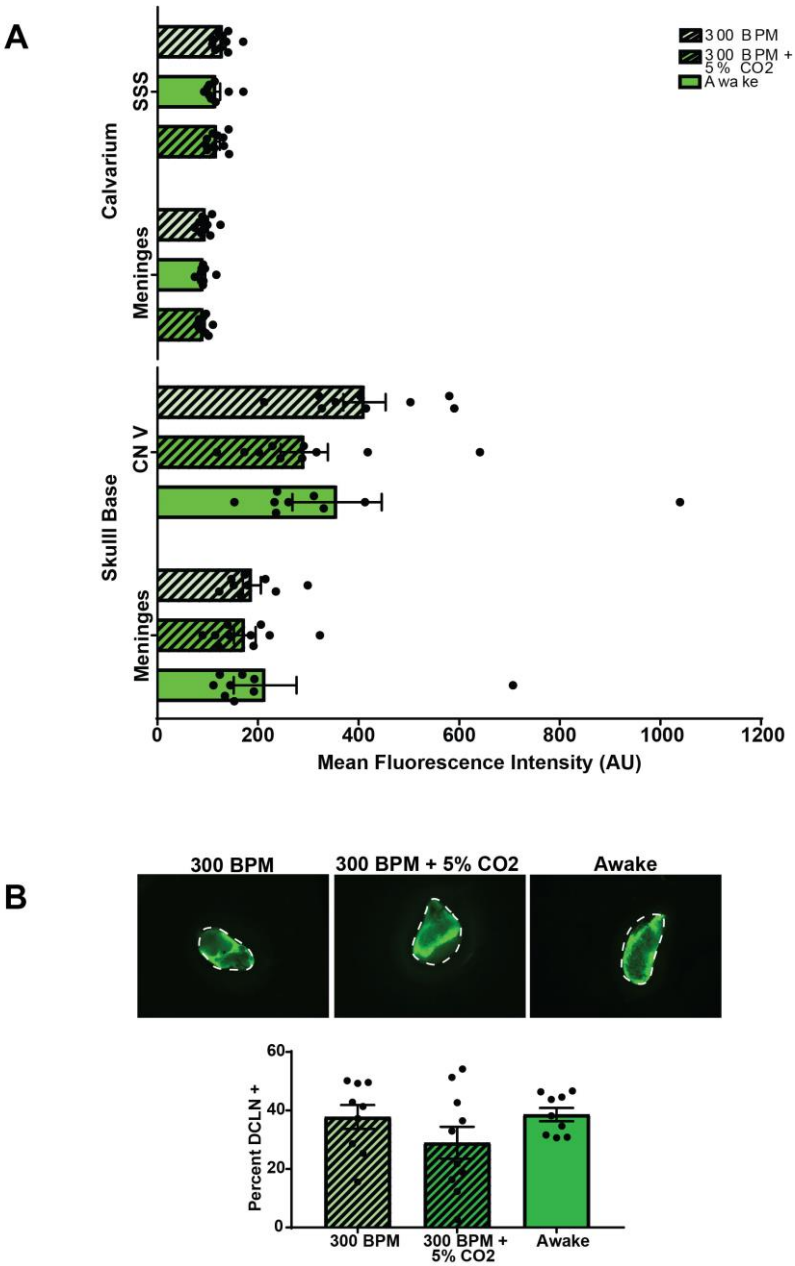

Figure 24. Intracranial tracer distribution and lymphatic drainage of 2000 kDa dextran injected into the CSF of mechanically ventilated mice.

A. Intracranial distribution of 2000 kDa dextran, including the superior sagittal sinus (SSS), and meninges in the calvarium and the trigeminal nerve (CN V) and meninges in the skull base. B. Signal intensity in the deep cervical lymph nodes (DCLNs) after 30 minutes after injection and ventilation at different respiratory rates.

Chapter Five: Discussion and Future Directions

Summary

The anatomy and physiology of the meningeal lymphatic system was intensely studied since its characterization in 2015. Independent discoveries from other labs dramatically expanded our understanding of this previously understudied system. As with many exciting new fields, conflicting reports about the form and function of the meningeal lymphatic vasculature in pathological settings now exist. In this chapter, these recent findings will be comprehensively discussed in the context of the data presented in this dissertation. Future directions of this research will also be discussed.

Identification of meningeal lymphatic vessels in the human dura mater

The characterization of the meningeal lymphatic system in the rodent raised many questions about its role in human pathology. After their initial characterization, there was also a question of what meningeal layer these lymphatic vessels are found in, since the rodent meningeal layer are difficult to separate surgically (Raper et al., 2016). As a first step toward determining if these findings in the rodent were also conserved in humans, we developed an approach to identifying meningeal lymphatic vessels in the human dura mater using confocal microscopy with spectral unmixing. We implemented this technique in examining the largest cohort of meninges published to date, with tissues collected from non-demented control subjects, subjects with AD pathology, and subjects with Lewy Body Disease pathology. We identified lymphatic vessels in the dura mater of almost all of the subjects, indicating that a network of lymphatic capillaries also exists in the human meninges. Meningeal lymphatic vessels were also detected in two subjects by Absinta and colleagues using conventional immunohistochemical methods (Absinta et al., 2017). As noted in Chapter 2, we found that two possible subpopulations of lymphatic vessels in the meninges, which appeared to have

different anatomical distributions. In addition to the different molecular signatures ($PDPN^{+}LYVE1^{+}$ and $PDPN^{+}LYVE1^{-}$), we also observed an increased density of lymphatic vessels in the human meninges compared to the rodent. The implications of these observations are not yet clear and will be informed by future studies in the human meninges.

Although these findings confirmed the presence of lymphatic vessels in the human meninges, they also raise questions about solute trafficking via these vessels in the dura mater. For instance, it is unclear how or if solutes in the brain and CSF are trafficked across the arachnoid membrane and across the endosteal layer of the dura mater in order to be accessible to the lymphatic vessels that we observed in the human dura mater. This fundamental question was not addressed in any published studies and is a significant assumption made by several groups that suggest lymphatic vessels in the calvarium contribute to the efflux of solutes from the brain and CSF. Because we only considered samples of dura mater associated with the superior sagittal sinus, one possibility is that lymphatic vessels are distributed in different layers in the meninges throughout the cranium. This may confer differential access to solutes and fluid in the subarachnoid space, and would be easily evaluated by sampling meninges throughout the cranium and determining the histological distribution of lymphatic vessels with the same imaging techniques described in Chapter 2. Another possibility is that these lymphatic vessels in the dura mater do not contribute to the absorption of solutes and CSF in the subarachnoid space.

The meningeal lymphatic system in Alzheimer's Dementia

After the initial characterization of the meningeal lymphatic system, there was widespread speculation regarding its involvement in the development of AD pathogenesis (Iliff et al., 2015; Louveau et al., 2017, 2016; Tarasoff-Conway et al., 2015). Until very

recently, however, no empirical evidence was available to support these claims. In 2018, the preclinical work of DaMesquita and colleagues provided significant progress in the study of the meningeal lymphatic system in aging and AD. In this study, several approaches were used to examine the role of the meningeal lymphatic system in aging and AD. Chief among them were the use of three approaches to modulate lymphatic drainage from the brain and CSF. To ablate the lymphatic capillaries in the meninges, DaMesquita and colleagues performed intracisternal injection of a photoactivatable small molecule called verteporfin. Upon exposure to light in the far-red spectrum, verteporfin generates highly-reactive oxygen free radicals that are cytotoxic to cells, which causes sclerosis of blood vessels when used clinically. Therefore, after intracisternal delivery of verteporfin, the authors exposed the calvarium of the mouse to transcranial phototherapy for 83 seconds. To augment lymphatic function in the meninges, the authors both delivered recombinant mutant vascular endothelial growth factor C C156S (VEGF-C^{C156S}) transcranially using a hydrogel elution technique and developed a vector driving expression of murine VEGF-C under the cytomegalovirus promoter. This vector was then packaged into the adeno-associated virus 1 serotype and 1 x 10^{13} vector genomes were injected into the CSF of mice. In an extensive series of experiments, the authors reported that impairment of the meningeal lymphatic system via verteporfin treatment reduces CSF-ISF exchange, impairs learning and memory, and exacerbates the progression of AD phenotypes in a mouse model of AD. These findings were later corroborated by Wang and colleagues in the APP/PS1 mouse model of AD (Wang et al., 2019). DaMesquita et al., also found that augmentation of meningeal lymphatic function via both approaches increased CSF-ISF exchange and improved learning and memory in aged mice, but did not slow the progression of AD pathology and cognitive

impairment in 5XFAD mice. Together, these findings suggest a major role for the meningeal lymphatic system in the steady state homeostasis of the CNS, as well as the development of AD.

Considering these findings in the context of the experiments described in this dissertation, there is one major congruency. Along with DaMesquita and colleagues, we have demonstrated that aging impairs lymphatic drainage from the CSF. This phenomenon was also observed by Ma and colleagues, with each group using tracers of different molecular weight and hydrodynamic radius (Ma et al., 2017). Although the magnitude of efflux varied between studies, this may be explained in part by the varying anesthetic regimens, sensitivity of fluorescent tracer detection, and age of mice used. These observations from three independent labs strongly suggests that, in the rodent, the rate of solute efflux from the CSF via the cervical lymphatic vasculature is reduced with increasing age. As discussed in Chapter 3, lymphatic function in peripheral tissues is also impaired as humans age, which indicates that lymphatic drainage of solutes in the brain and CSF are subject to the same age-related effects. Whether this is due to changes in extrinsic or intrinsic lymphatic pumping mechanisms is yet to be determined. If this phenomenon is conserved in humans, this may help to explain the reduction in Aβ clearance from the CSF observed in aging humans without parenchymal Aβ pathology (Patterson et al., 2015). Outside of AD, this may also have important implications for trafficking of immune cells in the SAS and meninges. In 2015, Louveau and colleagues demonstrated that acute obstruction of the cervical lymphatic trunk increased the number of meningeal T cells, therefore it would be very interesting to explore the effects of aging on meningeal immune cell populations (Louveau et al., 2015). This may also inform the pathophysiology of idiopathic normal pressure hydrocephalus,

which is a disease that features dementia, incontinence, and gait abnormalities secondary to the development of idiopathic communicating hydrocephalus. Idiopathic normal pressure hydrocephalus is strongly linked to aging, with prevalence in one epidemiological study increasing from 0.2% to 6% before and after 80 years of age (Jaraj et al., 2014). To test these age-related effects in humans directly, a quantitative and noninvasive means of measuring solute efflux into the DCLNs is needed. Lymphatic drainage of CSF in humans is now possible with contrast enhanced magnetic resonance imaging (Eide et al., 2018; Eide and Ringstad, 2018; Ringstad et al., 2017). However, because intrathecal contrast is necessary for measurement of solute efflux, this approach is unlikely to be used in healthy volunteers to study the effects of aging on lymphatic solute clearance from the CSF. One possibility to address this issue would be the development of an MRI sequence analogous to arterial spin labeling or phase contrast MRI, which allow for noninvasive monitoring of water movement in the intracranial space.

Several incongruencies also exist between the findings reported by DaMesquita et al. and those in this dissertation. The authors reported that, unlike their observations in the human meninges, they did not observe deposition of Aβ in the meninges of the 5XFAD mouse. Indeed, both their finding that the human meninges contains Aβ and that a mouse model of AD did not contain Aβ are in contrast to the findings reported in this dissertation. First considering the discrepancy between the findings of Aβ in the human meninges, one possible explanation is that the monoclonal antibody, 6E10, employed by DaMesquita and colleagues is binding nonspecifically in the meninges, resulting in a false positive result due to technical approach. Indeed, we reported that the 6E10 clone binds nonspecifically in the human meninges when monomeric, oligomeric, and fibrillar Aβ species are decidedly absent

(Goodman et al., 2018). Another simple approach for quantitative evaluation of Aβ burden in the human meninges would be to homogenize meningeal tissue samples and quantify Aβ using an enzyme-linked immunosorbent assay. Though antibody-dependent, this quantitative approach could be used to demonstrate burden of Aβ in the AD meninges without the confounding variables of autofluoresence or nonspecific staining observed in studies using immunofluorescence. An explanation for the discrepancy between findings in the mouse meninges is less straightforward. One possibility may be a difference in the kinetics of Aβ deposition between the 5XFAD mouse used by DaMesquita and colleagues and the Tg2576 mouse used in our studies. The fundamental differences between these mice are the number of mutations encoded in the APP and presenilin genes and the promoter driving expression of APP. Expression of APP and presenilin in the 5XFAD mouse is mediated by the Thy1 promoter and its APP contains the Florida (I716V), Swedish (K670N/M671L), and London (V717I) mutations), while its presenilin contains the M146L and L286V mutations. The Tg2576 mouse only contains the Swedish mutation (K670N/M671L) in APP, driven by the hamster prion-related protein promoter. The difference in number and type of mutations results in remarkable differences in the progression of cognitive impairment and neuropathology in the two mice. The 5XFAD mouse develops severe Aβ pathology at 2 months, whereas the Tg2576 mouse does not develop Aβ pathology until 11-12 months of age. With this major temporal difference in the parenchymal deposition of Aβ between models, it is perhaps not surprising that the meningeal burden of Aβ is also different. Another possibility is that the additional mutations in APP and presenilin in the 5XFAD mouse bias production of thermodynamically-stable isoforms of Aβ to the extent that

quantitatively less Aβ is exchanged into the CSF and subsequently deposited into the meninges. A third possible explanation is that deposition of Aβ in the meninges is actually due to expression of APP within the meninges itself, not due to Aβ trafficking from the brain. For instance, the promoters differ between mouse models, with Thy1 driving expression in the 5XFAD mouse and hamster prion-related protein driving expression in the Tg2576 mouse (Hsiao et al., 1996; Oakley et al., 2006). Although we are not aware of transcriptional profiling efforts in the meninges, if cells in the arachnoid or dura mater express the prion-related protein and do not express Thy1, this would also account for the difference in findings. Examination of Aβ deposition in the meninges of other mouse models of AD may shed light on this issue.

Another major inconsistency between the work of DaMesquita and colleagues and this dissertation is with respect to age-related changes in the meningeal lymphatic vasculature. In this dissertation, we found that although there was a dramatic reduction in lymphatic drainage from the CSF, there was no change in the diameter, branching, or number, of lymphatic vessels in the calvarium. This either indicates a divergence between the form and function of lymphatic vasculature in the meninges which may be explained by molecular changes that alter lymph formation or propagation, or it suggests that the lymphatic vessels in the meninges do not play a role in the clearance of solutes from the brain and CSF. In contrast, DaMesquita reported a reduction in the diameter and percent coverage of lymphatic vessels in the calvarium of aged mice. They further showed that recovery of lymphatic vessels in the calvarium of aged mice via overexpression of murine VEGFC was associated with increased lymphatic drainage. This draws a link between the presence of meningeal lymphatic vessels in the calvarium and lymphatic drainage to the

DCLNs. One possible explanation for this inconsistency is that "aged mice" used by DaMesquita were 20-24 months, whereas the "aged mice" used in this dissertation were 14 months old. If atrophy of lymphatic vessels in the calvarium was preceded by a marked reduction in their function at least 6 months prior to detectable structural changes, it is conceivable that these findings are compatible.

Notwithstanding the differences in these experimental outcomes, three important conclusions can be made from these data when taken together. First, we have definitively demonstrated that soluble forms of Aβ are drained from the brain and CSF via the cervical lymphatic vasculature. This confirms the widespread suspicion that lymphatic drainage participates in the clearance of Aβ. Second, three studies demonstrated that lymphatic drainage of these compartments is impaired in aging mice. Considering that lymphatic drainage is one mechanism of Aβ clearance from the CNS, this supports the notion that age-related reduction of Aβ clearance from the CSF is, in part, due to the attenuation of lymphatic drainage with increasing age. Third, two independent groups also demonstrated that impairment of lymphatic outflow from the cranium increases the rate of parenchymal Aβ accumulation in rodents. These findings strongly suggest a role for lymphatic drainage in the progression of AD and CNS amyloidosis.

Several knowledge gaps exist with regard to lymphatic function and the development of AD. It is currently unclear if these age-related effects on lymphatic function occur in humans which may be evaluated if a noninvasive means of measuring lymphatic outflow of CSF can be developed. When this assay becomes clinically feasible, the rate of lymphatic efflux can be measured in conjunction with positron emission tomography to quantify parenchymal Aβ burden to assess this relationship directly in humans (Cselényi et al., 2012;

Rinne et al., 2010). The relative importance of lymphatic Aβ clearance remains to be determined in the context of other Aβ clearance pathways, cellular degradation, efflux across the BBB, and other CSF efflux pathways. This question is very difficult to answer experimentally due to the complexity of Aβ trafficking in the CNS and high likelihood of inadvertently altering multiple efflux parameters with pharmacological, genetic, or surgical interventions. In addition to these critical unknowns, a rigorous evaluation of the rate of lymphatic impairment as animals age would provide valuable insight into the temporal nature of this relationship. As described above, evidence now exists that obstruction of the flow of lymph in the cervical lymphatic trunk increases the deposition of Aβ in the brain. Were this directly relevant to humans, one would expect to observe an increase in the incidence of AD in patients undergoing cervical lymphadenectomy and radical neck dissections secondary to malignancy. However, this relationship is not described in the literature, which may be due to compensatory lymphatic drainage on the contralateral side or limited long-term survival in this patient population. Although the lack of evidence for this relationship does not argue against it, it is possible that the mouse models used by Wang et al. and DaMesquita et al. may overestimate the importance of lymphatic drainage, given the rate and type of Aβ production in these mice. Indeed, compensatory Aβ clearance pathways may be upregulated in humans and less aggressive models that better recapitulate the pathogenesis of late-onset AD. These possibilities could be evaluated by measuring the progression of Aβ pathology in patients after cervical lymphadenectomy using radiolabeled positron emission tomography ligands. By answering these key questions, the therapeutic value of targeting lymphatic drainage in AD can be determined.

The physiology of CSF reabsorption

The study of the physiological mechanisms that control CSF-ISF exchange and lymphatic drainage of solutes is in its infancy, but several important studies made significant progress (J. Iliff et al., 2013; Lee et al., 2015; Xie et al., 2013). One early study demonstrated that exchange between the ISF and CSF compartments is maximized in the sleeping and anesthetized animal and that adrenergic tone in the CNS appears to mediate this effect by inducing changes in the volume of the ECS (Xie et al., 2013). A subsequent study of lymphatic drainage from the CSF demonstrated that ketamine/xylazine anesthesia reduced the rate of lymphatic clearance from this compartment, in stark contrast to robust lymphatic clearance observed in the waking animal (Ma et al., 2019). The authors interpreted these findings in the context of prior studies they had published along with the work of Xie and colleagues, leading them to speculate on a possible relationship between CSF-ISF exchange, lymphatic drainage, and arousal state (Ma et al., 2019; Proulx et al., 2017; Xie et al., 2013). In Chapter 4, we reported similar findings with respect to lymphatic clearance from the brain parenchyma. However, in pursuit of the underlying mechanism, we also discovered that hypercapnia can acutely reduce lymphatic drainage of solutes from the brain. Considering the relationship between CSF-ISF exchange and hypercapnia, we also observed that hypercapnia reduced exchange between the two compartments, while establishing normocapnia in anesthetized mice increased exchange relative to the awake mice.

Together, these findings serve two major purposes: they provide evidence of physiological derangements in arterial blood gas that rapidly develop in mice after induction of anesthesia and they provide valuable insight into the biology of solute trafficking in the CNS. Indeed, the hypercapnia, hypoxemia, and oxygen desaturation that was observed in

free-breathing animals likely represents the typical arterial blood gas status of most mice undergoing ketamine/xylazine anesthesia for as little as 30 minutes. This finding is likely generalizable to other anesthetic agents that depress the respiratory drive and hypercapnic ventilatory response, such as isoflurane and urethane (Massey and Richerson, 2017). Due to the strong relationship between cerebral blood flow and arterial tension of CO_2, this is particularly important in experiments related to neurophysiology and solute trafficking in the CNS.

The experiments described in Chapter 4 are the first to draw a link between the rate of parenchymal solute efflux via the lymphatic vasculature and arterial tension of CO_2. Though the underlying mechanism still remains unclear, we suspect that events downstream of CO_2-mediated elevations in cerebral blood flow likely play a significant role. Regardless of the mechanism, this effect of hypercapnia on lymphatic drainage may alter the interpretation of the experiments in Chapter 3 that described an age-related reduction in lymphatic function. For instance, because all of these experiments were conducted in free-breathing anesthetized mice, it is possible that aged mice are more sensitive to anesthetic agents or become more severely hypercapnic than young mice, but that lymphatic drainage is unaltered by age. Future experiments should confirm that lymphatic drainage is reduced in normocapnic aged mice. One would expect that if this physiology is conserved in humans, that chronic states of hypercapnia might be associated with hydrocephalus or AD pathology. Such states are complicated by coexisting pathologies that often involve the nervous system. However some of these conditions such as sleep apnea and chronic obstructive pulmonary disease are associated with increased risk of developing cognitive impairment and AD-like pathology (Daulatzai, 2015; Elias et al., 2018; Rusanen et al., 2013). Using the in vivo

techniques to measure lymphatic drainage from the CSF described in Chapter 3, the relationship between chronic hypercapnia and lymphatic CSF drainage can be directly tested in mouse models of chronic obstructive pulmonary disease (Ghorani et al., 2017). In an orthogonal approach, clearance of Aβ from the brain and CSF could be measured in mouse models of AD subjected to chronic hypercapnia compared to normocapnic mice. Moreover, associations between idiopathic normal pressure hydrocephalus and sleep apnea also exist in the literature (Román et al., 2018). Preclinical studies considering the effect of chronic hypercapnia on CSF reabsorption and cognitive decline would provide insight into a causal relationship between the two phenomena.

Several additional insights into solute trafficking were described in Chapter 4 of this dissertation, which highlight a number of assumptions in the literature. One major assumption that is widely pervasive in recently-published articles is that solute efflux into the cervical lymphatic trunk occurs by the meningeal lymphatic vasculature. This is likely because the newly-discovered lymphatic vasculature in the dura mater is seemingly upstream of the cervical lymphatic trunk. Several studies suggest that capillaries in the dura mater of the calvarium are major contributors to lymphatic drainage from the brain to the cervical lymph (Da Mesquita et al., 2018; Louveau et al., 2015). Other studies also make this assumption, with a similar association between lymphatic drainage and the presence of lymphatic vessels in the calvarium reported by Antila and colleagues in 2017 (Antila et al., 2017). This study featured an orthogonal approach to ablation of the meningeal lymphatic vasculature, wherein a VEGF-C-Ig chimeric protein trap was overexpressed in the rodent brain via CNS transduction with adeno-associated virus 9. Although these groups identified an inverse association between density of lymphatic vessels in the calvarium and lymphatic

drainage from the brain, this is not necessary for impairment of lymphatic drainage as we demonstrated in Chapter 4. At best, until the relative importance of lymphatic vessels distributed throughout the cranium, these vessels may serve as a proxy for the presence or absence of lymphatic vessels distributed throughout the cranium in regions that are more difficult to assess. Another assumption is widely made in the literature is that solutes in the SAS are equally accessible to lymphatic vessels in different intracranial regions. However, we consistently observed that tracer distribution was higher in the skull base than in the calvarium, regardless of whether the tracer was injected into the cortex or into the cisterna magna. A similar trend was reported by Ma and colleagues, who reported higher tracer intensity in the cisterns (Ma et al., 2019). When considering this in the context of our finding that there was no increase in tracer colocalized with $LYVE1^+$ vessels in the calvarium, and our finding that lymphatic capillaries are located within the human dura mater (not the SAS or arachnoid mater), this calls the biological relevance of the meningeal lymphatic vessels in the calvarium into question. To date, only one published study reported colocalization between intracranial lymphatic vessels and a fluorescent tracer injected into the brain, and this was in lymphatic vessels associated with the pterygopalatine artery in the anterior skull base (Aspelund et al., 2015).

Thus, future experiments may gain valuable insight from studying lymphatic vasculature in the skull base. Several techniques may facilitate evaluation of lymphatic vessels in the skull base. One such technique is in situ whole head sectioning with holocraniohistochemistry, which enables the cranial distribution of tracers to be visualized with the brain and cranial nerves intact (Tomlinson et al., 2017). This technique is compatible with immunofluorescence and intracisternal tracer infusion, which makes it a

strong candidate for pursuing similar questions evaluated in this dissertation. Another technique that would facilitate interrogation of this anatomical region features a combination of tissue clearing and light sheet microscopy. Recent advances in tissue clearing enable clearing of ossified structures like the cranium and whole-mouse imaging techniques were also successfully developed, which will facilitate the characterization of lymphatic vessels in this complex anatomical region (Cai et al., 2018; Greenbaum et al., 2017; Yang et al., 2014).

Conclusions and Future Directions

In conclusion, in this dissertation I have demonstrated that meningeal lymphatic vessels exist in the human dura mater, that soluble forms of Aβ are cleared from the brain and CSF via the lymphatic system, and that lymphatic drainage of solutes from the brain and CSF is a dynamic process that is regulated in part by hypercapnia. Future studies are likely to elucidate other physiological controls on this system and its relevance to other neurological diseases, such as multiple sclerosis and communicating hydrocephalus.

With respect to the role of the lymphatic system in solute trafficking from the brain and CSF, several critical unknowns still exist. First, it is of utmost importance to systematically identify the intracranial meningeal lymphatic vessels that have access to solutes in the CSF. Considering the findings in this dissertation in the context of previous work, it is clear that solutes are unequally distributed throughout the cranium, with preferential distribution to the base of the skull. This corresponds with the only region that has meningeal lymphatic vessels that colocalize with increased tracer intensity. This unknown could be addressed by infusing an electron-dense tracer, such as quantum dots, into the subarachnoid space and using transmission electron microscopy to map its distribution throughout the leptomeninges and dura mater, including its entry into the lumen of

meningeal lymphatic vessels. Second, the relationship between aging and impairment of cervical lymphatic drainage which has been shown by multiple groups must be more carefully characterized. Specifically, identifying the age-related mechanism responsible for hindering the efflux of solutes into the cervical lymphatic trunk, whether lymphatic or otherwise. This is important because there are strong temporal relationships between the accumulation of pathological proteins, such as Aβ, in the brain with increasing age. Therefore, expanding our understanding of the natural progression of lymphatic impairment in aging in addition to the molecular changes in aging lymphatic endothelial cells may provide critical insight into this process. This can be accomplished by developing an MRI-based in vivo drainage assay that can be performed repeatedly on rodents repeatedly to measure within-animal impairment of lymphatic function as animals age. Second, the transcriptional profile of meningeal lymphatic endothelial cells from different regions of the cranium in the young, middle aged, and old mice can be quantitatively assessed using fluorescence-activated cell sorting and subsequent RNAseq. This would expand on the work described in this dissertation and by DaMesquita and colleagues, and may provide insight into the molecular mechanisms that contribute to reduced lymphatic drainage in aging mice. Finally, because we found that hypercapnia impairs lymphatic drainage in part by reducing CSF-ISF exchange, further examination of the connection between CSF-ISF exchange and lymphatic drainage of solutes in the brain is critically important to the greater scientific understanding of this clearance pathway. As noted in previous sections, solute efflux from the brain via CSF-ISF exchange is at least a two-step process that requires irreversible escape from the CSF compartment. The further elucidation of physiological parameters that

influence one or both of these compartments will undoubtedly provide insight into translationally-relevant biology.

The continued investigation of the meningeal lymphatic system in health and disease is imperative because it is clear that lymphatic drainage from the brain and CSF is a relatively important contributor to CSF reabsorption and is impaired by aging, which is a significant risk factor for diseases like AD and communicating hydrocephalus. As noted in chapter one of this dissertation, multiple sites of CSF reabsorption exist, including efflux across the cribriform plate along olfactory nerve endings and along cranial nerves in the skull base (Johnston et al., 2004; Zakharov et al., 2004)., therefore understanding the importance of the meningeal lymphatic system relative to these other pathways will inform investigations that aim to treat diseases associated with CSF reabsorption. In seeking disease-modifying solutions, an understanding of the relevant pathophysiology is paramount, which must first arise from a firm understanding of the physiology of CSF reabsorption. Despite the early conflicting reports, the meningeal lymphatic system remains a promising and understudied path for solute efflux from the brain and CSF.

Appendix A: Pilot experiments

Ablation of the Meningeal Lymphatic Vasculature

There is widespread interest in studying the function of the meningeal lymphatic system in the context of neurodegenerative disease, multiple sclerosis, and hydrocephalus. However, there are currently no targeted approaches to ablating the meningeal lymphatic vasculature. Indeed, the only existing approach to obstructing the meningeal lymphatic vasculature in the literature features injection of verteporfin (Visudyne) and subsequent activation of verteporfins via light exposure over the calvarium (Da Mesquita et al., 2018). Although this approach reportedly ablates the meningeal lymphatic vessels, two major limitations will likely preclude its widespread usage. First, the mechanism of lymphatic ablation is through widespread generation of reactive oxygen species, which cause the sclerosis of blood and lymphatic vessels. Though it was not thoroughly characterized, widespread neuroinflammation likely results after light-induced activation of verteporfins in the subarachnoid space. Second, ablation is likely confined to the calvarium due to low penetration of light in the skull base, which only represents one anatomical subpopulation of meningeal lymphatic vessels. Thus, a critical need still exists for a targeted approach to ablating the meningeal lymphatic vasculature throughout the cranium.

To target the meningeal lymphatic vasculature in a minimally-invasive manner, we crossed the inducible diphtheria toxin receptor (iDTR) mouse (Buch et al., 2005), which conditionally expresses the DTR in a cre recombinase-dependent manner, with the LYVE1-cre mouse, thereby inducing the expression of DTR in LYVE1+ cells. In a previous study, systemic treatment of diphtheria toxin (DT) in the iDTR;LYVE1-cre mouse via intraperitoneal injection resulted in septicemia associated with loss of intestinal lymphatic lacteals (Gardenier et al., 2016). To avoid systemic side effects, we administered a relatively

low dose of DT (10-100 ng) into the subarachnoid space via injection into the cisterna magna. Previous studies suggested that lymphatic ablation occurs within 24 hours of systemic administration. Thus, in early pilot trials we sacrificed mice 24 hours after intracisternal infusion and examined the meningeal lymphatic vasculature, deep cervical lymph nodes, and jejunum using conventional confocal microscopy. We found that this novel approach produces robust ablation of the meningeal lymphatic vasculature (Figure 25), and planned a subsequent survival study to ensure that mice recovered from the infusion without significant weight loss or neurological deficits (Figure 25A). Despite treatment with perioperative buprenorphine and fluids, and soft food, mice consistently demonstrated weight loss and anecdotal gait instability when treated with a dose of DT that effectively ablated LYVE1+ cells in the meninges (Figure 25C and Figure 25D). Interestingly, we did not note disruption of the jejunal lymphatic lacteals in these mice as previously reported. It is possible that the acute ablation of the meningeal lymphatic vasculature induced hydrocephalus in mice, however ventricular volume and intracranial pressure was not systematically assessed in these mice. Chronic lymphatic insufficiency, such as that modeled by the K14-VEGFR-3-Ig mouse developed by Mäkinen and colleagues, does not result in gait instability and weight loss. This suggests either that developmental compensation for the loss of lymphatic vessels prevents these pathological developments or that ablation of the meningeal lymphatic vasculature is not the underlying cause of the symptoms observed in iDTR;LYVE1-cre mice treated with intracisternal DT.

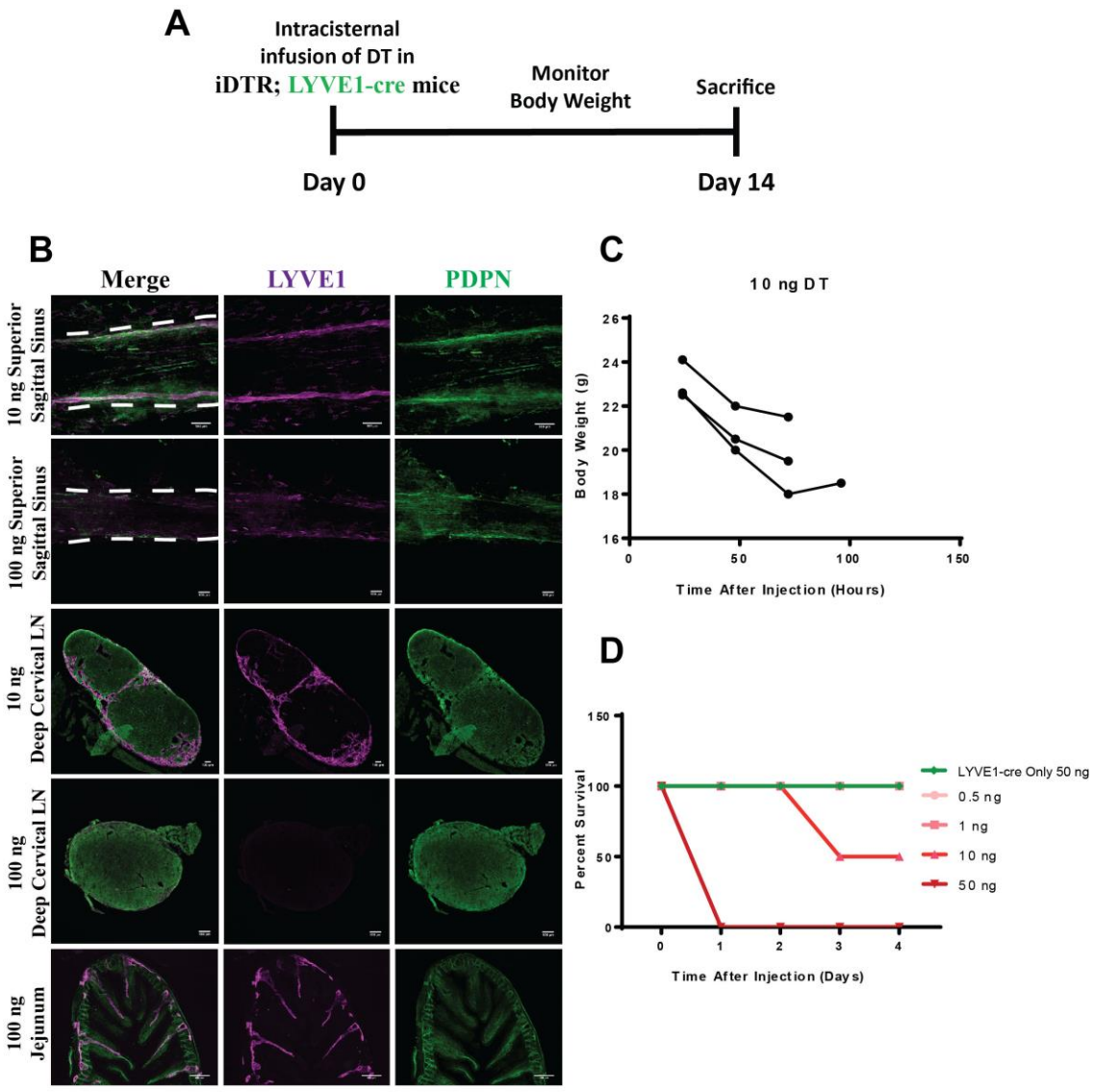

Figure 25. Ablation of meningeal lymphatic vessels in the mouse with intracisternal diphtheria toxin results in fatal weight loss.

A. Experimental time course for survival study. B. Representative images of meningeal lymphatic vessels, deep cervical lymph nodes, and jejunums stained with LYVE1 and PDPN after intracisternal infusion of DT. C. Time course of weight loss in mice treated with 10 ng DT. D. Survival analysis of LYVE1;iDTR and LYVE1cre- only mice treated with varying doses of intracisternal DT.

Inducing lymphangiogenesis in the meninges

Similar to the rationale for ablation of the meningeal lymphatic vasculature, future study of these lymphatic vessels requires the development of specific tools to augment function of lymphatic vessels in these meninges. In 2015, Louveau and colleagues reported that the meningeal lymphatic vessels responded to a single infusion of intracisternal infusion of recombinant human vascular endothelial growth factor C mutant C156S (VEGF-C^{C156S}), as measured by an increase in lymphatic capillary diameter (Louveau et al., 2015). This is presumably accomplished through direct effects of VEGF-C^{C156S} on the transmembrane tyrosine kinase receptor, VEGFR3, of lymphatic endothelial cells. However, this was a transient effect and was lost several weeks after infusion. Therefore, we reasoned that chronic overexpression of VEGF-C^{C156S} in the brain may achieve CSF concentrations of VEGF-C^{C156S} that are sufficient to induce meningeal lymphangiogenesis.

To increase the likelihood that cells transduced with VEGF-C^{C156S} would secrete this cytokine into the ISF, we interrogated a publicly-available RNASeq database of cell-specific gene expression throughout the CNS for cells that express VEGF-A. We assumed that cells that express and secrete VEGF-A would contain the cellular machinery required for post-transcriptional processing and secretion of VEGF-C^{C156S}. We found that astrocytes are responsible for expressing most of the VEGF-A found in the brain, which agonizes the VEGFR receptor on vascular endothelium (Figure 26A). This query also confirmed very low endogenous expression of VEGF-C and VEGFR3 in the CNS, which minimizes the risk of off-target effects of VEGF-C^{C156S}(Figure 26B). Therefore, to achieve astrocytic specificity, we generated a vector driven under the truncated glial fibrillary acidic protein (GFAP) promoter, GFAABC1D, followed by a P2A and enhanced green fluorescent protein (eGFP)

sequence to measure cellular expression in vitro. Transfection of this vector into primary murine astrocytes demonstrated effective astrocytic expression of the vector as measured by eGFP expression in cells (Figure 27A). Subsequent analysis of the conditioned media using enzyme-linked immunosorbent assay (ELISA) specific to the human VEGF-C^{C156S} mutant confirmed secretion of VEGF-C^{C156S} into the media (Figure 27A). These results suggested that introduction of the construct into murine astrocytes would result in robust expression of VEGF-C^{C156S}.

To avoid potential cytotoxic effects of long-term overexpression of eGFP in murine astrocytes, we generated two contructs: an experimental vector containing VEGF-C^{C156S} and a control vector containing eGFP only (Ansari et al., 2016; Kalyanaraman and Zielonka, 2017). These constructs were packaged into the adeno-associated virus 9 variant PHP.B, which has demonstrably superior transduction efficiency of CNS targets compared to other serotypes that were currently available (Deverman et al., 2016). Combined with a sham transduction group, this would provide insight into effects of brain-wide overexpression of VEGF-C^{C156S} on the meningeal lymphatic vasculature and approximate transduction efficiency in the brain. We inoculated mice with $2.35x10^{12}$ vector genomes via retro-orbital injection and sacrificed them 4 weeks after inoculation. Samples of CSF, brain tissue, and the calvarium were collected at the time of sacrifice. Using confocal microscopy and immunofluorescence, we noted expression of eGFP in astrocytes throughout the brain, including cortical regions without high expression of GFAP (Figure 27B). Interestingly, despite the widespread expression of VEGF-C^{C156S}, we did not detect elevated levels of VEGF-C^{C156S} in the CSF of mice inoculated with the experimental vector compared to the control vector and sham transduced mice (Figure 27C). Considering the meningeal lymphatic

vasculature in the calvarium of these mice, we did not detect any changes in the diameter, branching, or total number of lymphatic capillaries in the experimental group compared to the eGFP control (Figure 27D). Because the experimental construct did not contain eGFP and failed to increase VEGF-C^{C156S} in the CSF, expression of VEGF-C^{C156S} in the brain was confirmed by reverse transcriptase polymerase chain reaction (data not shown).

This experiment failed to demonstrate proof of principle for brain-wide expression of VEGF-C^{C156S} as a means of inducing lymphangiogenesis in the meninges. It is important to note that we did not measure lymphatic absorption of solutes in the CSF after viral transduction. Given the previous evidence that injection or overexpression of VEGF-C^{C156S} results in structural changes in lymphatic capillaries throughout the body, we anticipated that structural readouts would be sufficient to detect lymphangiogenesis (Cao et al., 1998; Veikkola et al., 2001). However, it is possible that brain-wide astrocytic overexpression of VEGF-C^{C156S} increases lymphatic uptake of solutes from the CSF in the absence of structural changes. We consider this possibility unlikely, but may be easily ruled out by measuring lymphatic efflux of fluorescent or superparamagnetic tracers in future experiments.

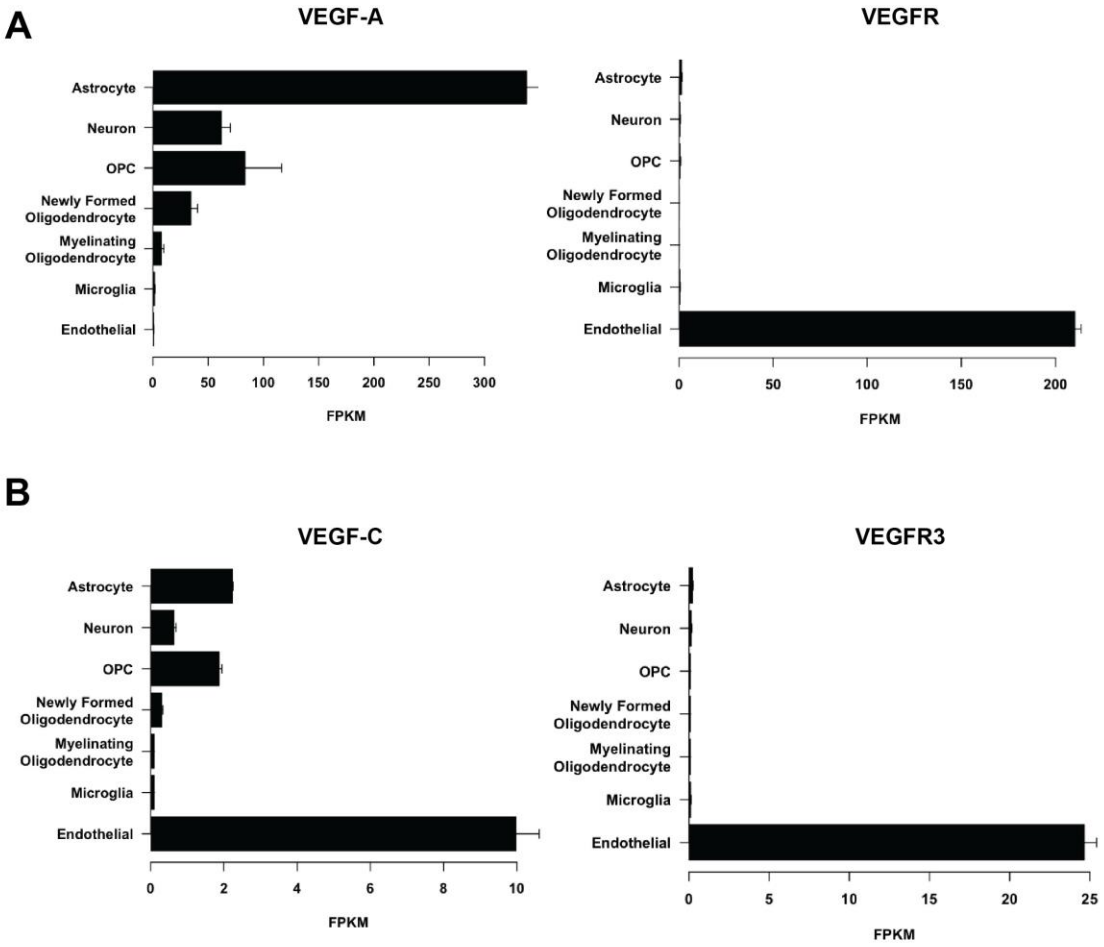

Figure 26. Expression of VEGF and VEGFR proteins throughout the CNS.
A. Expression of VEGF-A and VEGFR stratified by CNS cell-type. B. Expression of VEGF-C and VEGFR3 stratified by CNS cell type. Data are sourced from the publically-available Brain RNASeq database (Zhang et al., 2014).

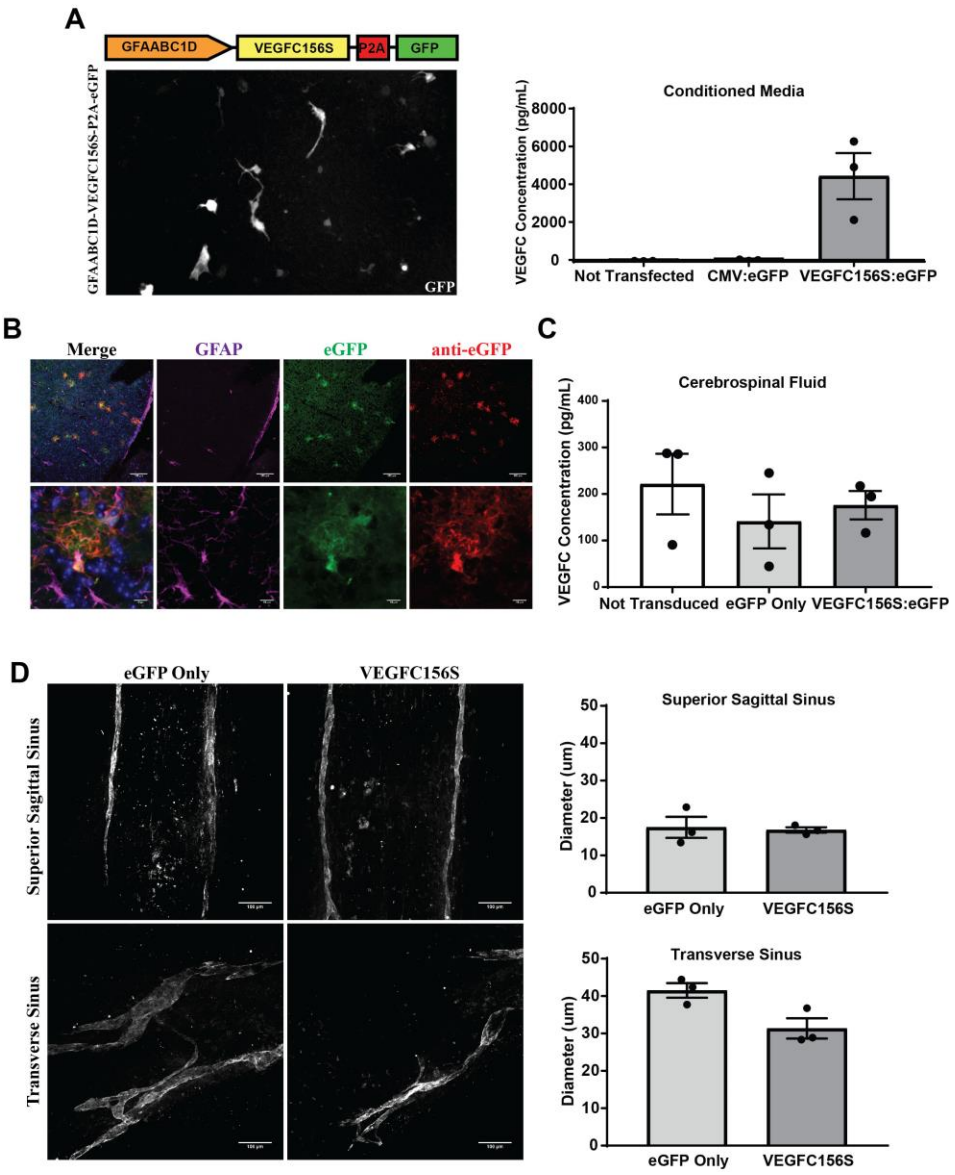

Figure 27. Brain-wide astrocytic overexpression of VEGFC156S is insufficient to induce meningeal lymphangiogenesis.

A. Left, Vector construct and expression of eGFP in primary murine astrocytes after transfection. Right, quantification of VEGFC156S protein in conditioned media 72 hours after transfection. B. Representative images of cortical astrocytes expressing eGFP 4 weeks after transduction with AAV9 PHP.B. C. Quantification of VEGFC156S in the CSF 4 weeks after transduction. D. Left, representative images of meningeal lymphatic vessels associated with the superior sagittal sinus and transverse sinus. Right, quantification of meningeal lymphatic vessel diameter in mice transduced with virus containing experimental and control vectors

Measuring solute trafficking in the CSF with dynamic contrast-enhanced magnetic resonance imaging

One of the greatest technical limitations of the experiments described in this dissertation is the reliance of fluorescent tracers for measurements of solute trafficking in the CSF. The inherent problem with this approach is that detection of the fluorescent tracer in vivo requires complex surgical approaches, such as thin skull preparation for multiphoton microscopy (Figure 4) or surgical dissection of the anterior cervical region to visualize the deep cervical lymph nodes. Even with these solutions, visualization of fluorescent tracers can only currently be measured in one region at a time. A more desirable approach would facilitate measurement of tracer distribution in multiple compartments of the intact animal such as the entire brain, ventricular system, cisterns, nasal turbinates, spinal cord, and deep cervical lymph nodes. Were this approach quantitative, this would enable a more complete scientific understanding of how solutes behave once introduced into the brain or CSF. To generate proof of principle for one such approach we coupled the use of ultra high-field 12T MRI and contrast-enhanced cisternography using gadolinium and ferumoxytol, two tracers with different paramagnetic properties. We optimized acquisition sequences that facilitated the collection of three-dimensional T1-weighted images with exceptional resolution of the mouse and rat head and neck every 5-10 minutes.

Gadolinium, which is an FDA-approved MRI contrast agent, increases the signal intensity of T1-weighted voxels. Because gadolinium is a relatively small contrast agent, it is readily exchanged into the interstitial fluid of the brain. Therefore, measurements can be made from the same dataset to compare the rate of tracer influx into brain subregions, efflux pathways, and other intracranial compartments in a noninvasive manner. Theoretically this

would also allow for the development of rate constants for solute transition between these compartments. First, to demonstrate that average changes in voxel intensity can be made simultaneously using this approach, gadolinium contrast was infused into the cisterna magna and the mouse head was repeatedly imaged for 80 minutes. This approach facilitated the simultaneous measurement of changes in three dimensional voxel intensity in multiple regions of interest, including the brain, ventricles, and nasal turbinates. Indeed, we measured the relative enhancement of tracer efflux into the nasal turbinates relative to its distribution in the ventricles (Figure 28).

Unlike gadolinium, which is a much smaller agent, ferumoxytol is a superparamagnetic oxide molecule that is encased by a polyglucose sorbitol carboxymethylether, extending its hydrodynamic radius to 17-31 nm, which generally prevents its exchange from the perivascular space into the brain parenchyma in rodent models. Ferumoxytol potently reduces the signal intensity of T2 and T2*-weighted MR imaging, and the resultant intensity reduction can be measured as the contrast agent is distributed throughout the central nervous system (Figure 29). Contrary to T2 and T2*-weighted images, ferumoxytol appears hyperintense in T1-weighted images at low concentrations, and hypointense at higher concentrations (Figure 29). In a similar experiment, we infused ferumoxytol into the cisterna magna of rats in an effort to measure lymphatic uptake and cisternal distribution of the tracer with respect to time. In these data, we were able to measure distribution of ferumoxytol into the basal cisterns (Figure 29) and deep cervical lymph nodes (Figure 30).

Considering these pilot experiments, we believe that use of dynamic contrast-enhanced MRI will enable more sophisticated measurement of solute trafficking throughout

the CNS. This will be particularly useful when examining relevant pathways for extracranial solute efflux, physiological conditions that may affect intracranial solute distribution including adrenergic tone, hypoxia and hypercapnia, as well as different ventilation states. Furthermore, the unique properties of gadolinium and ferumoxytol contrast agents can be exploited to interrogate a variety of scientific questions related to this space in addition to the behavior of different sized molecules.

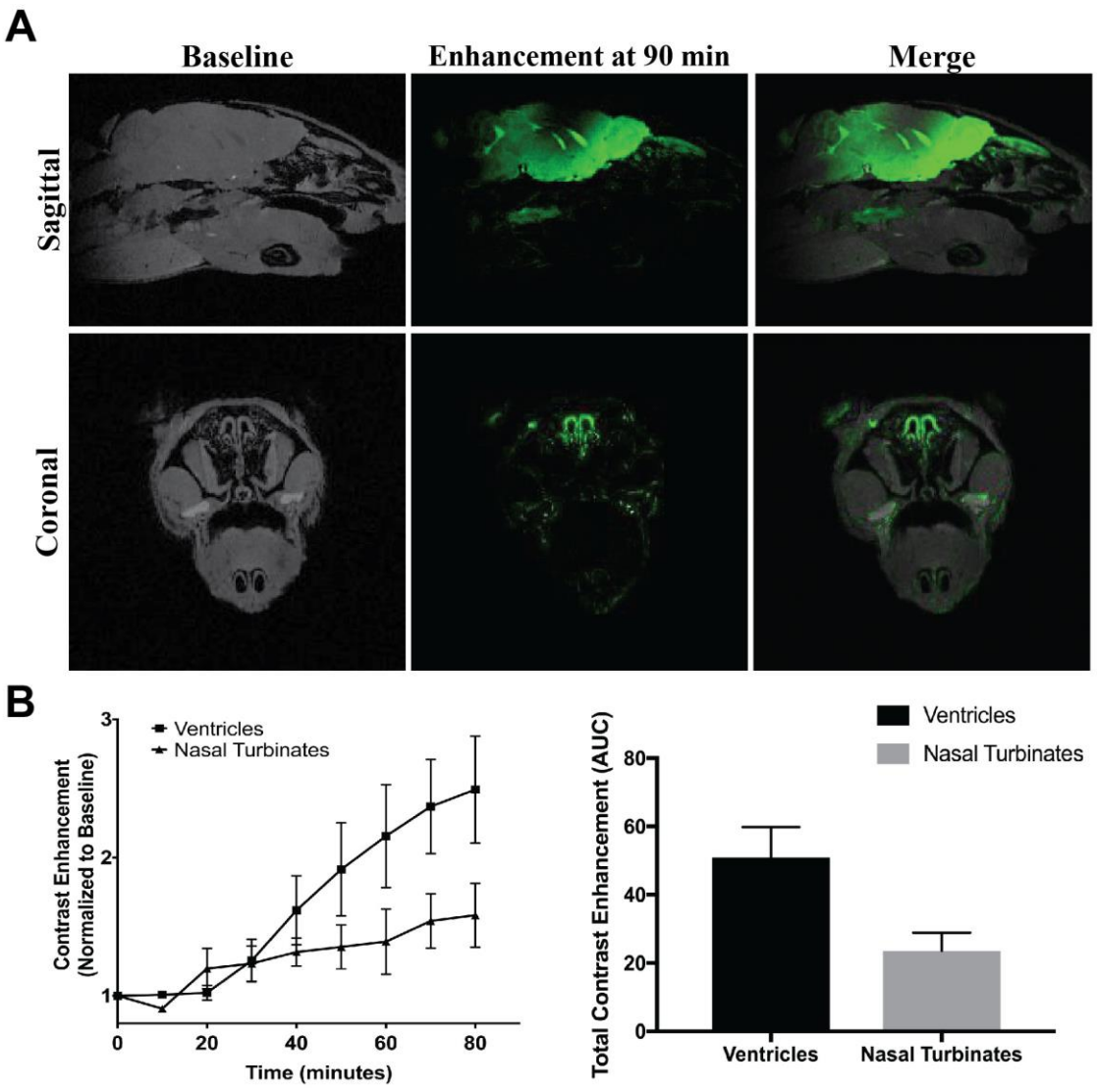

Figure 28. 12 Tesla dynamic contrast enhanced MRI cisternography with intracisternal gadolinium reveals solute efflux across the anterior skull base and absorption in the nasopharyngeal mucosa.

A. Representative sagittal and coronal sections at baseline and 90 minutes after intracisternal contrast (green). B. Left, time course of contrast enhancement of the ventricles and nasal turbinates after intracisternal gadolinium. Values are normalized to baseline. Right, total contrast enhancement across the experiment, as measured by the integrating the area under the curve.

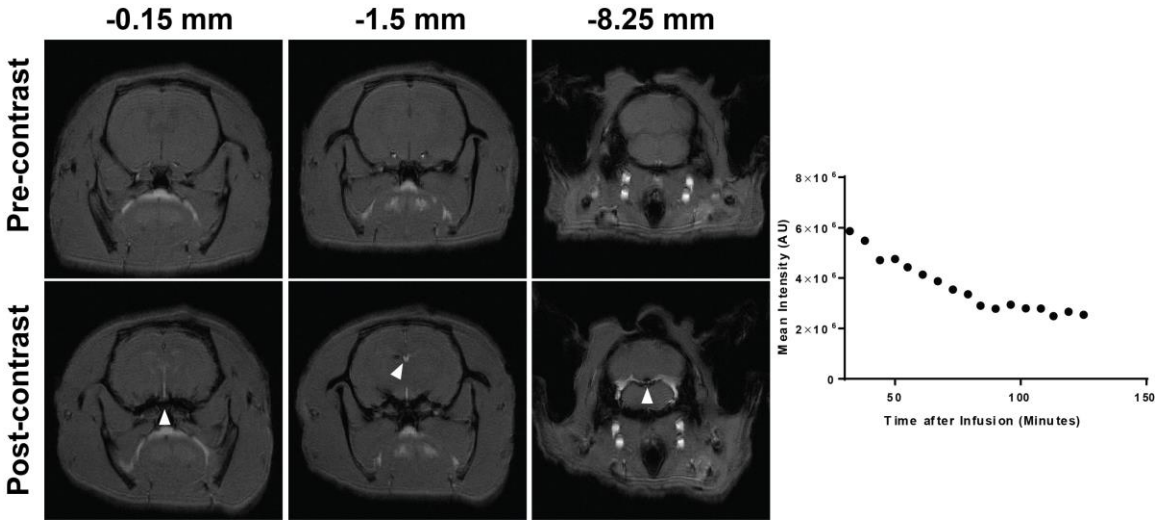

Figure 29. 12 Tesla dynamic contrast enhanced MRI cisternography with ferumoxytol. Left, representative T1-weighed coronal sections showing intracranial distribution of ferumoxytol tracer in the CSF. Arrows indicate cisternal and ventricular compartments displaying changes in signal intensity. Right, proof of principle for dynamic cisternal distribution of ferumoxytol after injection of ferumoxytol in the cisterna magna.

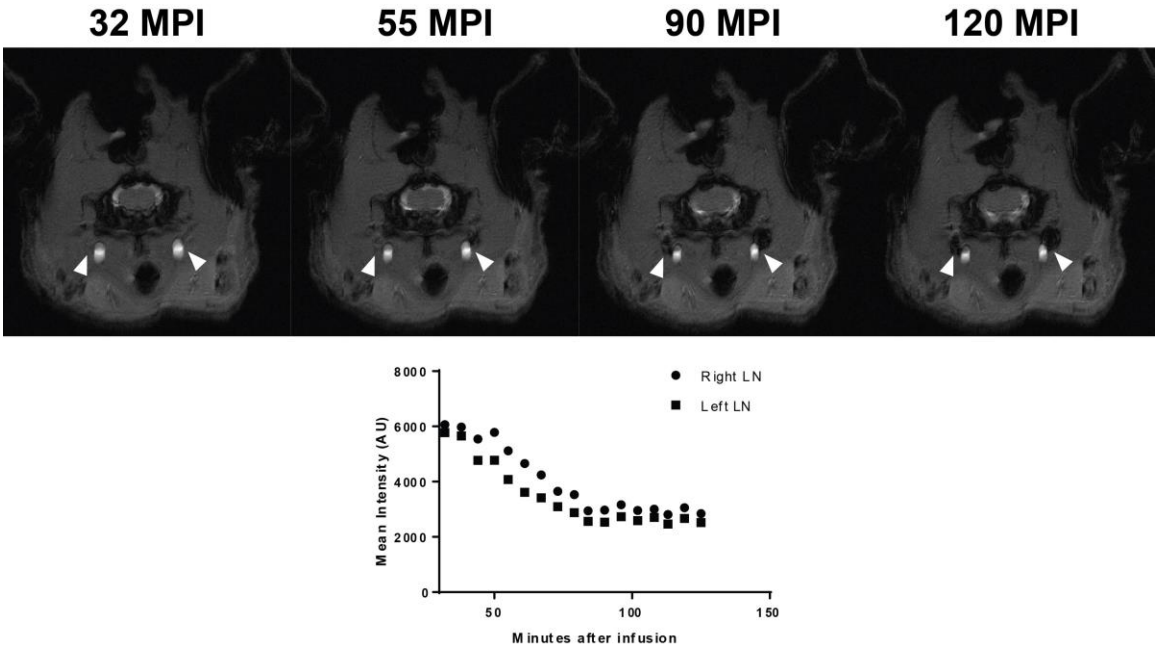

Figure 30. Dynamic measurement of lymphatic drainage of ferumoxytol from the CSF, measured with 12T MRI.

Top, T1-weighted coronal sections of the cervical region in a rat after intracisternal infusion of ferumoxytol. Arrows indicate approximate location of the deep cervical lymph nodes lateral to the hyperintense common carotid artery. Bottom, quantification of ferumoxytol efflux from the CSF into the cervical lymphatic vasculature measured by reduction in signal intensity.

Exploring potential mechanisms of lymph propagation in the meningeal lymphatic vasculature

As described in Chapter 1, the directional propagation of lymph requires several structural features. In lymphatic capillaries, transient structural deformation of endothelial cells results in a gap formation that facilitates fluid movement from the ISF into the lumen of lymphatic capillaries. In lymphatic collecting vessels, physical valvular structures analogous to those in veins define boundaries in lymphangions and prevent reflux of fluid during contraction and relaxation of the lymphatic wall. The general lack of valvular structures in meningeal lymphatic vessels in the calvarium led many to conclude that these vessels are likely lymphatic capillaries, not collecting vessels (Aspelund et al., 2015; Louveau et al., 2015). Although rarely documented in the literature, pericytes can surround lymphatic capillaries in abnormal developmental and pathological contexts(Petrova et al., 2004). Recently reports suggest that pericytes contribute to the tone of blood vessels, which raises the possibility that lymphatic tone may also be, in part, generated by pericytes. To investigate this possibility, we used immunolabeling and confocal microscopy to evaluate whether lymphatic vessels in the meninges were associated with pericytes. To label pericytes, we harvested dural samples from NG2-DsRed mice, which robustly express the fluorescent DsRed protein in oligodendrocytes and pericytes (Zhu et al., 2007) and labeled lymphatic capillaries with LYVE1 or VEGFR3.

To our surprise, we observed that some VEGFR3-positive lymphatic vessels in the meninges which did not express LYVE1 appeared to be ensheathed with pericytes (Figure 31). Although the majority of lymphatic vessels did not appear to be invested with pericytes, it is possible that lymphatic function differs between vessels ensheathed by perciytes and

those that are not. Subsequent attempts to reproduce these findings and investigate functional differences between vessels were unsuccessful. One possible explanation for the lack of reproducibility in this observation is technical failure of the approach. We predicted that this inconsistency may be due to the degradation of the VEGFR3 antibody (AF743, R&D Systems); however upon testing new antibody from the same company, we were still unable to identify $VEGFR3^{+}LYVE1^{-}$ lymphatic vessels in the dura mater of NG2-DsRed mice. This antibody is polyclonal, therefore another possibility is that the original antibody used was comprised of clonal antibody species that recognized different epitopes on the $VEGFR3^{+}LYVE1^{-}$ lymphatic vessels. Another possibility is that the VEGFR3 antibody used to produce this initial observation contained clonal species that recognized VEGFR or VEGFR2, and that the immunoreactivity around $VEGFR3^{+}LYVE1^{-}$ vessels actually represents blood vessel capillaries. However, the structure of the $VEGFR3^{+}LYVE1^{-}$ vessels more closely resembles lymphatic capillary morphology than blood vessel morphology. Nonetheless, this could be easily ruled out by colabeling the vessels with PDPN and CD31, which are expressed by meningeal lymphatic vessels and blood vessels, respectively. Further investigation in this area may provide interesting insight into the mechanisms that govern movement of lymph through intracranial lymphatic capillary networks.

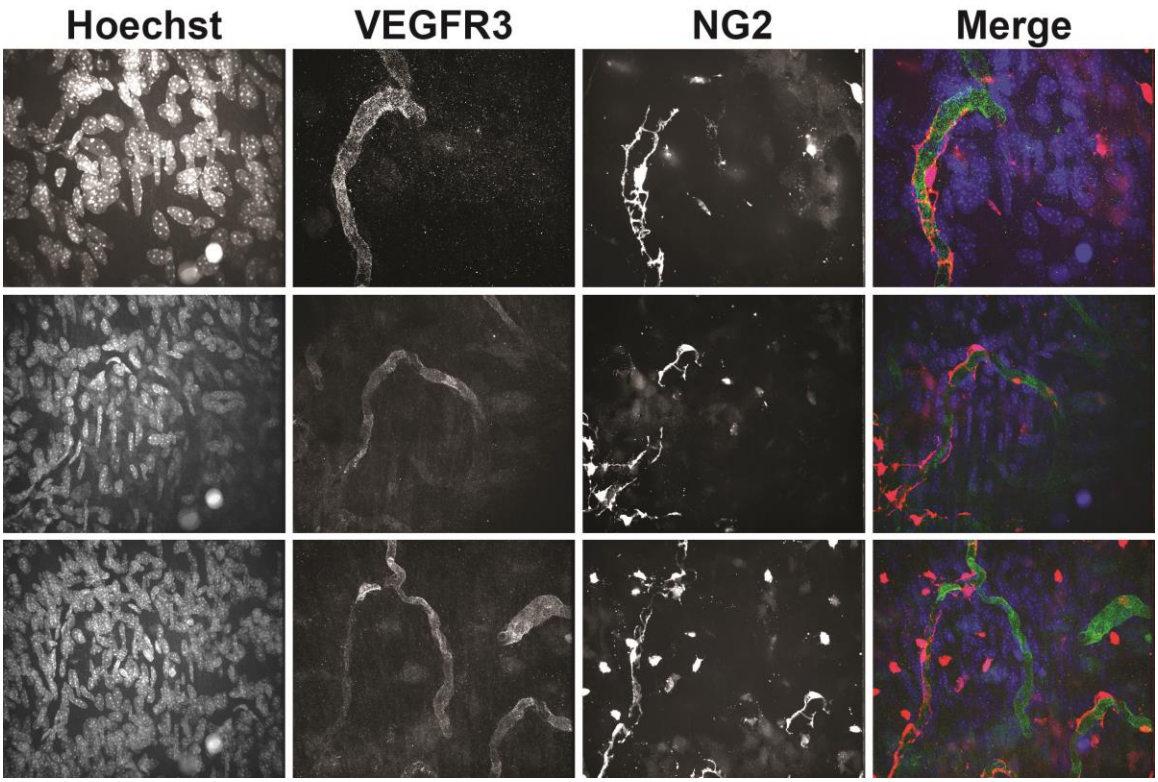

Figure 31. Pericytes ensheathe subpopulations of VEGFR3-positive vessels in the meninges. Immunofluorescence reveals that some lymphatic vessels in the dura mater of the calvarium are invested with pericytes. Lymphatic vessels are denoted by VEGFR3-positivity and pericytes are denoted by NG2-positivity.

Bibliography

Abbott, N.J., Pizzo, M.E., Preston, J.E., Janigro, D., Thorne, R.G., 2018. The role of brain barriers in fluid movement in the CNS: is there a 'glymphatic' system? Acta Neuropathol. 135, 387–407. https://doi.org/10.1007/s00401-018-1812-4

Absinta, M., Ha, S.-K., Nair, G., Sati, P., Luciano, N.J., Palisoc, M., Louveau, A., Zaghloul, K.A., Pittaluga, S., Kipnis, J., Reich, D.S., 2017. Human and nonhuman primate meninges harbor lymphatic vessels that can be visualized noninvasively by MRI. Elife 6, e29738. https://doi.org/10.7554/eLife.29738

Aho, L., Pikkarainen, M., Hiltunen, M., Leinonen, V., Alafuzoff, I., 2010. Immunohistochemical Visualization of Amyloid-β Protein Precursor and Amyloid-β in Extra- and Intracellular Compartments in the Human Brain. J. Alzheimer's Dis. 20, 1015–1028. https://doi.org/10.3233/JAD-2010-091681

Ansari, A.M., Ahmed, A.K., Matsangos, A.E., Lay, F., Born, L.J., Marti, G., Harmon, J.W., Sun, Z., 2016. Cellular GFP Toxicity and Immunogenicity: Potential Confounders in in Vivo Cell Tracking Experiments. Stem Cell Rev. Reports 12, 553–559. https://doi.org/10.1007/s12015-016-9670-8

Antila, S., Karaman, S., Nurmi, H., Airavaara, M., Voutilainen, M.H., Mathivet, T., Chilov, D., Li, Z., Koppinen, T., Park, J.-H., Fang, S., Aspelund, A., Saarma, M., Eichmann, A., Thomas, J.-L., Alitalo, K., 2017. Development and plasticity of meningeal lymphatic vessels. J. Exp. Med. jem.20170391. https://doi.org/10.1084/jem.20170391

Armstrong, J.K., Wenby, R.B., Meiselman, H.J., Fisher, T.C., 2004. The hydrodynamic radii of macromolecules and their effect on red blood cell aggregation. Biophys. J. 87, 4259–70. https://doi.org/10.1529/biophysj.104.047746

Asgari, M., de Zélicourt, D., Kurtcuoglu, V., 2016. Glymphatic solute transport does not require bulk flow. Sci. Rep. 6, 38635.

Aspelund, a., Antila, S., Proulx, S.T., Karlsen, T. V., Karaman, S., Detmar, M., Wiig, H., Alitalo, K., 2015. A dural lymphatic vascular system that drains brain interstitial fluid and macromolecules. J. Exp. Med. 212, 991–9. https://doi.org/10.1084/jem.20142290

Bairamian, D., Johanson, C.E., Parmelee, J.T., Epstein, M.H., 1991. Potassium cotransport with sodium and chloride in the choroid plexus. J. Neurochem. 56, 1623–9.

Basser, P.J., Mattiello, J., LeBihan, D., 1994. MR diffusion tensor spectroscopy and imaging. Biophys. J. 66, 259–267. https://doi.org/10.1016/S0006-3495(94)80775-1

Basser, P.J., Pierpaoli, C., 1996. Microstructural and physiological features of tissues elucidated by quantitative-diffusion-tensor MRI. J. Magn. Reson. B 111, 209–19.

Bateman, R.J., Munsell, L.Y., Morris, J.C., Swarm, R., Yarasheski, K.E., Holtzman, D.M., 2006. Human amyloid-beta synthesis and clearance rates as measured in cerebrospinal fluid in vivo. Nat. Med. 12, 856–61. https://doi.org/10.1038/nm1438

Beasley, M.G., Blau, J.N., Gosling, R.G., 1979. Changes in Internal Carotid Artery Flow Velocities with Cerebral Vasodilation and Constriction 331, Stroke.

Bedussi, B., van der Wel, N.N., de Vos, J., van Veen, H., Siebes, M., VanBavel, E., Bakker, E.N., 2017. Paravascular channels, cisterns, and the subarachnoid space in the rat brain: A single compartment with preferential pathways. J. Cereb. Blood Flow Metab. 37, 1374–1385. https://doi.org/10.1177/0271678X16655550

Bode, D.C., Baker, M.D., Viles, J.H., 2017. Ion Channel Formation by Amyloid-β42 Oligomers but Not Amyloid-β40 in Cellular Membranes. J. Biol. Chem. 292, 1404–1413. https://doi.org/10.1074/jbc.M116.762526

Boon, A.J.W., Tans, J.T.J., Delwel, E.J., Egeler-Peerdeman, S.M., Hanlo, P.W., Wurzer, H.A.L., Avezaat, C.J.J., de Jong, D.A., Gooskens, R.H.J.M., Hermans, J., 1997. Dutch Normal-Pressure Hydrocephalus Study: prediction of outcome after shunting by resistance to outflow of cerebrospinal fluid. J. Neurosurg. 87, 687–693. https://doi.org/10.3171/jns.1997.87.5.0687

Boulton, M., Armstrong, D., Flessner, M., Hay, J., Szalai, J.P., Johnston, M., 1998. Raised intracranial pressure increases CSF drainage through arachnoid villi and extracranial lymphatics. Am. J. Physiol. 275, R889–R896.

Boulton, M., Flessner, M., Armstrong, D., Mohamed, R., Hay, J., Johnston, M., 1999. Contribution of extracranial lymphatics and arachnoid villi to the clearance of a CSF tracer in the rat. Am. J. Physiol. 276, R818-23.

Braak, H., Braak, E., 1995. Staging of Alzheimer's disease-related neurofibrillary changes. Neurobiol. Aging 16, 271–8; discussion 278-84.

Brace, R.A., Taylor, A.E., Guyton, A.C., 1977. Time course of lymph protein concentration in the dog. Microvasc. Res. 14, 243–249. https://doi.org/10.1016/0026-2862(77)90023-1

Bradbury, M.W., Cole, D.F., 1980. The role of the lymphatic system in drainage of cerebrospinal fluid and aqueous humour. J. Physiol. 299, 353–365. https://doi.org/10.1113/jphysiol.1980.sp013129

Bradbury, M.W., Cserr, H.F., Westrop, R.J., 1981. Drainage of cerebral interstitial fluid into deep cervical lymph of the rabbit. Am. J. Physiol. Physiol. 240, F329–F336. https://doi.org/10.1152/ajprenal.1981.240.4.F329

Bradbury, M.W., Westrop, R.J., 1983. Factors influencing exit of substances from cerebrospinal fluid into deep cervical lymph of the rabbit. J. Physiol. 339, 519–534. https://doi.org/10.1113/jphysiol.1983.sp014731

Bradley, K.C., 1970a. Cerebrospinal fluid pressure. J. Neurol. Neurosurg. Psychiat 33, 387–397. https://doi.org/10.1136/jnnp.33.3.387

Bradley, K.C., 1970b. Cerebrospinal fluid pressure. J. Neurol. Neurosurg. Psychiat 33, 387–397. https://doi.org/10.1136/jnnp.33.3.387

Buch, T., Heppner, F.L., Tertilt, C., Heinen, T.J.A.J., Kremer, M., Wunderlich, F.T., Jung, S., Waisman, A., 2005. A Cre-inducible diphtheria toxin receptor mediates cell lineage ablation after toxin administration. Nat. Methods 2, 419–26. https://doi.org/10.1038/nmeth762

Cai, R., Pan, C., Ghasemigharagoz, A., Todorov, M.I., Foerstera, B., Zhao, S., Bhatia, H.S., Mrowka, L., Theodorou, D., Rempfler, M., Xavier, A., Kress, B.T., Benakis, C., Liesz, A., Menze, B., Kerschensteiner, M., Nedergaard, M., Erturk, A., 2018. Panoptic vDISCO imaging reveals neuronal connectivity, remote trauma effects and meningeal vessels in intact transparent mice. bioRxiv 374785. https://doi.org/10.1101/374785

Cao, Y., Linden, P., Farnebo, J., Cao, R., Eriksson, A., Kumar, V., Qi, J.-H., Claesson-Welsh, L., Alitalo, K., 1998. Vascular endothelial growth factor C induces angiogenesis in vivo. Proc. Natl. Acad. Sci. 95, 14389–14394. https://doi.org/10.1073/pnas.95.24.14389

Carare, R.O., Bernardes-Silva, M., Newman, T.A., Page, A.M., Nicoll, J.A.R., Perry, V.H., Weller, R.O., 2008. Solutes, but not cells, drain from the brain parenchyma along

basement membranes of capillaries and arteries: significance for cerebral amyloid angiopathy and neuroimmunology. Neuropathol. Appl. Neurobiol. 34, 131–144. https://doi.org/10.1111/j.1365-2990.2007.00926.x
Carrion, E., Hertzog, J.H., Medlock, M.D., Hauser, G.J., Dalton, H.J., 2001. Use of acetazolamide to decrease cerebrospinal fluid production in chronically ventilated patients with ventriculopleural shunts. Arch. Dis. Child. 84, 68–71. https://doi.org/10.1136/ADC.84.1.68
Casley-Smith, J.R., Sims, M.A., 1976. Protein concentrations in regions with fenestrated and continuous blood capillaries and in initial and collecting lymphatics. Microvasc. Res. 12, 245–257. https://doi.org/10.1016/0026-2862(76)90024-8
Chevalier, S., Ferland, G., Tuchweber, B., 1996. Lymphatic absorption of retinol in young, mature, and old rats: influence of dietary restriction. FASEB J. 10, 1085–90.
Cselényi, Z., Jönhagen, M.E., Forsberg, A., Halldin, C., Julin, P., Schou, M., Johnström, P., Varnäs, K., Svensson, S., Farde, L., 2012. Clinical validation of 18F-AZD4694, an amyloid-β-specific PET radioligand. J. Nucl. Med. 53, 415–24. https://doi.org/10.2967/jnumed.111.094029
Cserr, H.F., 1983. Flow of Brain Interstitial Fluid and Drainage into Cerebrospinal Fluid and Lymph, in: Intracranial Pressure V. Springer Berlin Heidelberg, Berlin, Heidelberg, pp. 618–621. https://doi.org/10.1007/978-3-642-69204-8_105
Cserr, H.F., 1971. Physiology of the choroid plexus. Physiol. Rev. 51, 273–311. https://doi.org/10.1152/physrev.1971.51.2.273
Cserr, H.F., Cooper, D.N., Milhorat, T.H., 1977. Flow of cerebral interstitial fluid as indicated by the removal of extracellular markers from rat caudate nucleus. Exp. Eye Res. 25, 461–473. https://doi.org/10.1016/S0014-4835(77)80041-9
Cserr, H.F., Cooper, D.N., Suri, P.K., Patlak, C.S., 1981. Efflux of radiolabeled polyethylene glycols and albumin from rat brain.
Cserr, H.F., Harling-Berg, C.J., Knopf, P.M., 1992. Drainage of Brain Extracellular Fluid into Blood and Deep Cervical Lymph and its Immunological Significance. Brain Pathol. 2, 269–276. https://doi.org/10.1111/j.1750-3639.1992.tb00703.x
Cserr, H.F., Knopf, P.M., 1992. Cervical lymphatics, the blood-brain barrier and the immunoreactivity of the brain: a new view. Immunol. Today 13, 507–512. https://doi.org/10.1016/0167-5699(92)90027-5
Cushing, H., 1914. STUDIES ON THE CEREBRO-SPINAL FLUID.*. J. Med. Res. XXVI, 1–19.
Czosnyka, M., Czosnyka, Z., Momjian, S., Schmidt, E., 2003. Calculation of the resistance to CSF outflow. J. Neurol. Neurosurg. Psychiatry 74, 1354; author reply 1354-5. https://doi.org/10.1136/jnnp.74.9.1354
Czosnyka, M., Richards, H.K., Whitehouse, H.E., Pickard, J.D., 1996. Relationship between transcranial Doppler-determined pulsatility index and cerebrovascular resistance: an experimental study. J. Neurosurg. 84, 79–84. https://doi.org/10.3171/jns.1996.84.1.0079
Da Mesquita, S., Louveau, A., Vaccari, A., Smirnov, I., Cornelison, R.C., Kingsmore, K.M., Contarino, C., Onengut-Gumuscu, S., Farber, E., Raper, D., Viar, K.E., Powell, R.D., Baker, W., Dabhi, N., Bai, R., Cao, R., Hu, S., Rich, S.S., Munson, J.M., Lopes, M.B., Overall, C.C., Acton, S.T., Kipnis, J., 2018. Functional aspects of meningeal lymphatics in ageing and Alzheimer's disease. Nature 560, 185–191.

https://doi.org/10.1038/s41586-018-0368-8
Dandy, W.E., 1929. WHERE IS CEREBROSPINAL FLUID ABSORBED? J. Am. Med. Assoc. 92, 2012. https://doi.org/10.1001/jama.1929.02700500024008
Dandy, W.E., Blackfan, K., 1913. AN EXPERIMENTAL AND CLINICAL STUDY OF INTERNAL HYDROCEPHALUS. JAMA J. Am. Med. Assoc. 61, 2216. https://doi.org/10.1001/jama.1913.04350260014006
Daulatzai, M.A., 2015. Evidence of neurodegeneration in obstructive sleep apnea: Relationship between obstructive sleep apnea and cognitive dysfunction in the elderly. J. Neurosci. Res. 93, 1778–1794. https://doi.org/10.1002/jnr.23634
Davson, H., Segal, M.B., 1970. The effects of some inhibitors and accelerators of sodium transport on the turnover of ^{22} Na in the cerebrospinal fluid and the brain. J. Physiol. 209, 131–153. https://doi.org/10.1113/jphysiol.1970.sp009159
de Leon, M.J., Li, Y., Okamura, N., Tsui, W.H., Saint Louis, L.A., Glodzik, L., Osorio, R.S., Fortea, J., Butler, T., Pirraglia, E., Fossati, S., Kim, H.-J., Carare, R.O., Nedergaard, M., Benveniste, H., Rusinek, H., 2017. CSF clearance in Alzheimer Disease measured with dynamic PET. J. Nucl. Med. jnumed.116.187211. https://doi.org/10.2967/jnumed.116.187211
Deverman, B.E., Pravdo, P.L., Simpson, B.P., Kumar, S.R., Chan, K.Y., Banerjee, A., Wu, W.-L., Yang, B., Huber, N., Pasca, S.P., Gradinaru, V., 2016. Cre-dependent selection yields AAV variants for widespread gene transfer to the adult brain. Nat. Biotechnol. 34, 204–9. https://doi.org/10.1038/nbt.3440
Doody, R.S., Raman, R., Farlow, M., Iwatsubo, T., Vellas, B., Joffe, S., Kieburtz, K., He, F., Sun, X., Thomas, R.G., Aisen, P.S., Siemers, E., Sethuraman, G., Mohs, R., 2013. A Phase 3 Trial of Semagacestat for Treatment of Alzheimer's Disease. N. Engl. J. Med. 369, 341–350. https://doi.org/10.1056/NEJMoa1210951
Dovey, H.F., John, V., Anderson, J.P., Chen, L.Z., De Saint Andrieu, P., Fang, L.Y., Freedman, S.B., Folmer, B., Goldbach, E., Holsztynska, E.J., Hu, K.L., Johnson-Wood, K.L., Kennedy, S.L., Kholodenko, D., Knops, J.E., Latimer, L.H., Lee, M., Liao, Z., Lieberburg, I.M., Motter, R.N., Mutter, L.C., Nietz, J., Quinn, K.P., Sacchi, K.L., Seubert, P.A., Shopp, G.M., Thorsett, E.D., Tung, J.S., Wu, J., Yang, S., Yin, C.T., Schenk, D.B., May, P.C., Altstiel, L.D., Bender, M.H., Boggs, L.N., Britton, T.C., Clemens, J.C., Czilli, D.L., Dieckman-McGinty, D.K., Droste, J.J., Fuson, K.S., Gitter, B.D., Hyslop, P.A., Johnstone, E.M., Li, W.Y., Little, S.P., Mabry, T.E., Miller, F.D., Ni, B., Nissen, J.S., Porter, W.J., Potts, B.D., Reel, J.K., Stephenson, D., Su, Y., Shipley, L.A., Whitesitt, C.A., Yin, T., Audia, J.E., 2001. Functional gamma-secretase inhibitors reduce beta-amyloid peptide levels in brain. J. Neurochem. 76, 173–181. https://doi.org/10.1046/j.1471-4159.2001.00012.x
Dreha-Kulaczewski, S., Joseph, A.A., Merboldt, K.-D., Ludwig, H.-C., Gärtner, J., Frahm, J., 2015. Inspiration is the major regulator of human CSF flow. J. Neurosci. 35, 2485–91. https://doi.org/10.1523/JNEUROSCI.3246-14.2015
Egan, M.F., Kost, J., Tariot, P.N., Aisen, P.S., Cummings, J.L., Vellas, B., Sur, C., Mukai, Y., Voss, T., Furtek, C., Mahoney, E., Harper Mozley, L., Vandenberghe, R., Mo, Y., Michelson, D., 2018. Randomized Trial of Verubecestat for Mild-to-Moderate Alzheimer's Disease. N. Engl. J. Med. 378, 1691–1703. https://doi.org/10.1056/NEJMoa1706441
Eide, P., 2016. The correlation between pulsatile intracranial pressure and indices of

intracranial pressure-volume reserve capacity: results from ventricular infusion testing. J. Neurosurg. 125, 1493–1503.
Eide, P.K., Ringstad, G., 2018. Delayed clearance of cerebrospinal fluid tracer from entorhinal cortex in idiopathic normal pressure hydrocephalus: A glymphatic magnetic resonance imaging study. J. Cereb. Blood Flow Metab. 0271678X1876097. https://doi.org/10.1177/0271678X18760974
Eide, P.K., Ringstad, G., 2015. MRI with intrathecal MRI gadolinium contrast medium administration: a possible method to assess glymphatic function in human brain. Acta Radiol. Open 4, 205846011560963. https://doi.org/10.1177/2058460115609635
Eide, P.K., Vatnehol, S.A.S., Emblem, K.E., Ringstad, G., 2018. Magnetic resonance imaging provides evidence of glymphatic drainage from human brain to cervical lymph nodes. Sci. Rep. 8, 7194. https://doi.org/10.1038/s41598-018-25666-4
Ekstedt, J., 1978. CSF hydrodynamic studies in man. 2 . Normal hydrodynamic variables related to CSF pressure and flow. J. Neurol. Neurosurg. Psychiatry 41, 345–53. https://doi.org/10.1136/JNNP.41.4.345
Elias, A., Cummins, T., Tyrrell, R., Lamb, F., Dore, V., Williams, R., Rosenfeld, J.V., Hopwood, M., Villemagne, V.L., Rowe, C.C., 2018. Risk of Alzheimer's Disease in Obstructive Sleep Apnea Syndrome: Amyloid-β and Tau Imaging. J. Alzheimer's Dis. 66, 733–741. https://doi.org/10.3233/JAD-180640
Elman, R., 1923. Spinal arachnoid granulations with special reference to the cerebrospinal fluid. Johns Hopkins Hosp Bull 34, 99–104.
Erten-Lyons, D., Woltjer, R., Kaye, J., Mattek, N., Dodge, H.H., Green, S., Tran, H., Howieson, D.B., Wild, K., Silbert, L.C., 2013. Neuropathologic basis of white matter hyperintensity accumulation with advanced age. Neurology 81, 977–83. https://doi.org/10.1212/WNL.0b013e3182a43e45
Faghih, M.M., Sharp, M.K., 2018. Is bulk flow plausible in perivascular, paravascular and paravenous channels? Fluids Barriers CNS 15, 17. https://doi.org/10.1186/s12987-018-0103-8
Faraci, F.M., Mayhan, W.G., Heistad, D.D., 1990. Vascular effects of acetazolamide on the choroid plexus. J. Pharmacol. Exp. Ther. 254, 23–7.
Faubel, R., Westendorf, C., Bodenschatz, E., Eichele, G., 2016. Cilia-based flow network in the brain ventricles. Science 353, 176–8. https://doi.org/10.1126/science.aae0450
Fenstermacher, J., Rapoport, S., 1984. Blood-brain barrier, in: Renkin, E., Michel, C. (Eds.), Handbook of Physiology. American Physiological Society, pp. 969–1000.
Gaberel, T., Gakuba, C., Goulay, R., Martinez De Lizarrondo, S., Hanouz, J.-L., Emery, E., Touze, E., Vivien, D., Gauberti, M., 2014. Impaired glymphatic perfusion after strokes revealed by contrast-enhanced MRI: a new target for fibrinolysis? Stroke 45, 3092–6. https://doi.org/10.1161/STROKEAHA.114.006617
Gakuba, C., Gaberel, T., Goursaud, S., Bourges, J., Di Palma, C., Quenault, A., de Lizarrondo, S.M., Vivien, D., Gauberti, M., 2018. General Anesthesia Inhibits the Activity of the "Glymphatic System." Theranostics 8, 710–722. https://doi.org/10.7150/thno.19154
Galie, P., Spilker, R.L., 2009. A Two-Dimensional Computational Model of Lymph Transport Across Primary Lymphatic Valves. J. Biomech. Eng. 131, 111004. https://doi.org/10.1115/1.3212108
Garai, K., Sahoo, B., Sengupta, P., Maiti, S., 2008. Quasihomogeneous nucleation of amyloid

beta yields numerical bounds for the critical radius, the surface tension, and the free energy barrier for nucleus formation. J. Chem. Phys. 128, 045102. https://doi.org/10.1063/1.2822322
Gardenier, J.C., Hespe, G.E., Kataru, R.P., Savetsky, I.L., Torrisi, J.S., Nores, G.D.G., Dayan, J.J., Chang, D., Zampell, J., Martínez-Corral, I., Ortega, S., Mehrara, B.J., 2016. Diphtheria toxin-mediated ablation of lymphatic endothelial cells results in progressive lymphedema. JCI insight 1, e84095. https://doi.org/10.1172/jci.insight.84095
Gashev, A.A., Chatterjee, V., 2013. Aged Lymphatic Contractility: Recent Answers and New Questions. Lymphat. Res. Biol. 11, 2–13. https://doi.org/10.1089/lrb.2013.0003
Gashev, A.A., Davis, M.J., Delp, M.D., Zawieja, D.C., 2004. Regional variations of contractile activity in isolated rat lymphatics. Microcirculation 11, 477–492. https://doi.org/10.1080/10739680490476033
Ghorani, V., Boskabady, M.H., Khazdair, M.R., Kianmeher, M., 2017. Experimental animal models for COPD: a methodological review. Tob. Induc. Dis. 15, 25. https://doi.org/10.1186/s12971-017-0130-2
Glabe, C.C., 2005. Amyloid Accumulation and Pathogensis of Alzheimer's Disease: Significance of Monomeric, Oligomeric and Fibrillar Aβ, in: Alzheimer's Disease. Springer US, pp. 167–177. https://doi.org/10.1007/0-387-23226-5_8
Gomez, D.G., Potts, D.G., 1974. The Surface Characteristics of Arachnoid Granulations. Arch. Neurol. 31, 88. https://doi.org/10.1001/archneur.1974.00490380036003
Gomez, D.G., Potts, D.G., Deonarine, V., 1974a. Arachnoid Granulations of the Sheep. Arch. Neurol. 30, 169. https://doi.org/10.1001/archneur.1974.00490320057008
Gomez, D.G., Potts, D.G., Deonarine, V., 1974b. Arachnoid Granulations of the Sheep. Arch. Neurol. 30, 169. https://doi.org/10.1001/archneur.1974.00490320057008
Goodman, J.R., Adham, Z.O., Woltjer, R.L., Lund, A.W., Iliff, J.J., 2018. Characterization of dural sinus-associated lymphatic vasculature in human Alzheimer's dementia subjects. Brain. Behav. Immun. 73. https://doi.org/10.1016/j.bbi.2018.07.020
Goulay, R., Flament, J., Gauberti, M., Naveau, M., Pasquet, N., Gakuba, C., Emery, E., Hantraye, P., Vivien, D., Aron-Badin, R., Gaberel, T., 2017. Subarachnoid Hemorrhage Severely Impairs Brain Parenchymal Cerebrospinal Fluid Circulation in Nonhuman Primate. Stroke 48, 2301–2305. https://doi.org/10.1161/STROKEAHA.117.017014
Greenbaum, A., Chan, K.Y., Dobreva, T., Brown, D., Balani, D.H., Boyce, R., Kronenberg, H.M., McBride, H.J., Gradinaru, V., 2017. Bone CLARITY: Clearing, imaging, and computational analysis of osteoprogenitors within intact bone marrow. Sci. Transl. Med. 9, eaah6518. https://doi.org/10.1126/scitranslmed.aah6518
Groothuis, D.R., Vavra, M.W., Schlageter, K.E., Kang, E.W.-Y., Itskovich, A.C., Hertzler, S., Allen, C. V, Lipton, H.L., 2007. Efflux of Drugs and Solutes from Brain: The Interactive Roles of Diffusional Transcapillary Transport, Bulk Flow and Capillary Transporters. J. Cereb. Blood Flow Metab. 27, 43–56. https://doi.org/10.1038/sj.jcbfm.9600315
Haberkern, C.M., Bland, R.D., 1981. Effect of hypercapnia on net filtration of fluid in the lungs of awake newborn lambs. J. Appl. Physiol. 51, 423–427. https://doi.org/10.1152/jappl.1981.51.2.423
Habgood, M.D., 1995. The nature of increased blood-cerebrospinal fluid barrier exchange during CO2 inhalation in newborn and adult rats. Exp. Physiol. 80, 117–28.
Hammerstad, J., Lorenzo, A., Cutler, R., 1969. Iodide transport from the spinal

subarachnoid fluid in the cat. Am. J. Physiol. 216, 353–358.
Hardy, J.A., Higgins, G.A., 1992. Alzheimer's disease: the amyloid cascade hypothesis. Science 256, 184–5.
Heisey, S.R., Held, D., Pappenheimer, J.R., 1962. Bulk flow and diffusion in the cerebrospinal fluid system of the goat. Am. J. Physiol. Content 203, 775–781. https://doi.org/10.1152/ajplegacy.1962.203.5.775
Hill, L., 1896. The physiology and pathology of the cerebral circulation : an experimental research : Hill, Leonard, Sir, b. 1866 : Free Download, Borrow, and Streaming : Internet Archive. London: J & A Churchill.
Hladky, S.B., Barrand, M.A., 2016. Fluid and ion transfer across the blood–brain and blood–cerebrospinal fluid barriers; a comparative account of mechanisms and roles. Fluids Barriers CNS 13, 19. https://doi.org/10.1186/s12987-016-0040-3
Holter, K.E., Kehlet, B., Devor, A., Sejnowski, T.J., Dale, A.M., Omholt, S.W., Ottersen, O.P., Nagelhus, E.A., Mardal, K.-A., Pettersen, K.H., 2017a. Interstitial solute transport in 3D reconstructed neuropil occurs by diffusion rather than bulk flow. Proc. Natl. Acad. Sci. 114, 9894–9899. https://doi.org/10.1073/pnas.1706942114
Holter, K.E., Kehlet, B., Devor, A., Sejnowski, T.J., Dale, A.M., Omholt, S.W., Ottersen, O.P., Nagelhus, E.A., Mardal, K.-A., Pettersen, K.H., 2017b. Interstitial solute transport in 3D reconstructed neuropil occurs by diffusion rather than bulk flow. Proc. Natl. Acad. Sci. 114, 9894–9899. https://doi.org/10.1073/pnas.1706942114
Honig, L.S., Vellas, B., Woodward, M., Boada, M., Bullock, R., Borrie, M., Hager, K., Andreasen, N., Scarpini, E., Liu-Seifert, H., Case, M., Dean, R.A., Hake, A., Sundell, K., Poole Hoffmann, V., Carlson, C., Khanna, R., Mintun, M., DeMattos, R., Selzler, K.J., Siemers, E., 2018. Trial of Solanezumab for Mild Dementia Due to Alzheimer's Disease. N. Engl. J. Med. 378, 321–330. https://doi.org/10.1056/NEJMoa1705971
Hsiao, K., Chapman, P., Nilsen, S., Eckman, C., Harigaya, Y., Younkin, S., Yang, F., Cole, G., 1996. Correlative memory deficits, Abeta elevation, and amyloid plaques in transgenic mice. Science 274, 99–102. https://doi.org/10.1126/SCIENCE.274.5284.99
Huang, Y., Potter, R., Sigurdson, W., Santacruz, A., Shih, S., Ju, Y.-E., Kasten, T., Morris, J.C., Mintun, M., Duntley, S., Bateman, R.J., 2012. Effects of Age and Amyloid Deposition on Aβ Dynamics in the Human Central Nervous System. Arch. Neurol. 69, 51. https://doi.org/10.1001/archneurol.2011.235
Hyman, B.T., Phelps, C.H., Beach, T.G., Bigio, E.H., Cairns, N.J., Carrillo, M.C., Dickson, D.W., Duyckaerts, C., Frosch, M.P., Masliah, E., Mirra, S.S., Nelson, P.T., Schneider, J.A., Thal, D.R., Thies, B., Trojanowski, J.Q., Vinters, H. V., Montine, T.J., 2012. National Institute on Aging–Alzheimer's Association guidelines for the neuropathologic assessment of Alzheimer's disease. Alzheimer's Dement. 8, 1–13. https://doi.org/10.1016/J.JALZ.2011.10.007
Iaccarino, H.F., Singer, A.C., Martorell, A.J., Rudenko, A., Gao, F., Gillingham, T.Z., Mathys, H., Seo, J., Kritskiy, O., Abdurrob, F., Adaikkan, C., Canter, R.G., Rueda, R., Brown, E.N., Boyden, E.S., Tsai, L.-H., 2016. Gamma frequency entrainment attenuates amyloid load and modifies microglia. Nature 540, 230–235. https://doi.org/10.1038/nature20587
Ichimura, T., Fraser, P.A., Cserr, H.F., 1991. Distribution of extracellular tracers in perivascular spaces of the rat brain. Brain Res. 545, 103–13.
Iliff, J., Wang, M., Zeppenfeld, D.M., Venkataraman, A., Plog, B.A., Liao, Y., Deane, R.,

Nedergaard, M., 2013. Cerebral arterial pulsation drives paravascular CSF-interstitial fluid exchange in the murine brain. J. Neurosci. 33, 18190–9. https://doi.org/10.1523/JNEUROSCI.1592-13.2013

Iliff, J.J., Chen, M.J., Plog, B.A., Zeppenfeld, D.M., Soltero, M., Yang, L., Singh, I., Deane, R., Nedergaard, M., 2014. Impairment of Glymphatic Pathway Function Promotes Tau Pathology after Traumatic Brain Injury. J. Neurosci. 34, 16180–16193. https://doi.org/10.1523/JNEUROSCI.3020-14.2014

Iliff, J.J., Goldman, S.A., Nedergaard, M., 2015. Implications of the discovery of brain lymphatic pathways. Lancet Neurol. 14, 977–979. https://doi.org/10.1016/s1474-4422(15)00221-5

Iliff, J.J., Lee, H., Yu, M., Feng, T., Logan, J., Nedergaard, M., Benveniste, H., 2013. Brain-wide pathway for waste clearance captured by contrast-enhanced MRI. J. Clin. Invest. 123, 1299–1309. https://doi.org/10.1172/JCI67677

Iliff, J.J., Wang, M., Liao, Y., Plogg, B.A., Peng, W., Gundersen, G.A., Benveniste, H., Vates, G.E., Deane, R., Goldman, S.A., Nagelhus, E.A., Nedergaard, M., 2012. A paravascular pathway facilitates CSF flow through the brain parenchyma and the clearance of interstitial solutes, including amyloid β. Sci. Transl. Med. 4, 147ra111-147ra111. https://doi.org/10.1126/scitranslmed.3003748

Jaraj, D., Rabiei, K., Marlow, T., Jensen, C., Skoog, I., Wikkelsø, C., 2014. Prevalence of idiopathic normal-pressure hydrocephalus. Neurology 82, 1449–54. https://doi.org/10.1212/WNL.0000000000000342

Jeltsch, M., Kaipainen, A., Joukov, V., Meng, X., Lakso, M., Rauvala, H., Swartz, M., Fukumura, D., Jain, R.K., Alitalo, K., 1997. Hyperplasia of lymphatic vessels in VEGF-C transgenic mice. Science 276, 1423–5.

Jin, B.-J., Smith, A.J., Verkman, A.S., 2016. Spatial model of convective solute transport in brain extracellular space does not support a "glymphatic" mechanism. J. Gen. Physiol. 148, 489–501. https://doi.org/10.1085/jgp.201611684

Johnson, L.A., Prevo, R., Clasper, S., Jackson, D.G., 2007. Inflammation-induced uptake and degradation of the lymphatic endothelial hyaluronan receptor LYVE-1. J. Biol. Chem. 282, 33671–33680. https://doi.org/10.1074/jbc.M702889200

Johnston, M., Zakharov, A., Papaiconomou, C., Salmasi, G., Armstrong, D., 2004. Evidence of connections between cerebrospinal fluid and nasal lymphatic vessels in humans, non-human primates and other mammalian species. Cerebrospinal Fluid Res. 1, 2. https://doi.org/10.1186/1743-8454-1-2

Joukov, V., Kumar, V., Sorsa, T., Arighi, E., Weich, H., Saksela, O., Alitalo, K., 1998. A recombinant mutant vascular endothelial growth factor-C that has lost vascular endothelial growth factor receptor-2 binding, activation, and vascular permeability activities. J. Biol. Chem. 273, 6599–602. https://doi.org/10.1074/JBC.273.12.6599

Joyce, R.R., McGee, W.T., 2011. Hypercapnic cerebral edema presenting in a woman with asthma: a case report. J. Med. Case Rep. 5, 192. https://doi.org/10.1186/1752-1947-5-192

Kalaria, R.N., Ballard, C., 1999. Overlap between pathology of Alzheimer disease and vascular dementia. Alzheimer Dis. Assoc. Disord. https://doi.org/10.1097/00002093-199912003-00017

Kalyanaraman, B., Zielonka, J., 2017. Green fluorescent proteins induce oxidative stress in cells: A worrisome new wrinkle in the application of the GFP reporter system to

biological systems? Redox Biol. 12, 755–757. https://doi.org/10.1016/j.redox.2017.03.019
Kanekiyo, T., Cirrito, J.R., Liu, C.-C., Shinohara, M., Li, J., Schuler, D.R., Shinohara, M., Holtzman, D.M., Bu, G., 2013. Neuronal Clearance of Amyloid- by Endocytic Receptor LRP1. J. Neurosci. 33, 19276–19283. https://doi.org/10.1523/JNEUROSCI.3487-13.2013
Kang, J.-H., Irwin, D.J., Chen-Plotkin, A.S., Siderowf, A., Caspell, C., Coffey, C.S., Waligórska, T., Taylor, P., Pan, S., Frasier, M., Marek, K., Kieburtz, K., Jennings, D., Simuni, T., Tanner, C.M., Singleton, A., Toga, A.W., Chowdhury, S., Mollenhauer, B., Trojanowski, J.Q., Shaw, L.M., Parkinson's Progression Markers Initiative, 2013. Association of Cerebrospinal Fluid β-Amyloid 1-42, T-tau, P-tau $_{181}$, and α-Synuclein Levels With Clinical Features of Drug-Naive Patients With Early Parkinson Disease. JAMA Neurol. 70, 1277–87. https://doi.org/10.1001/jamaneurol.2013.3861
Kayed, R., Head, E., Sarsoza, F., Saing, T., Cotman, C.W., Necula, M., Margol, L., Wu, J., Breydo, L., Thompson, J.L., Rasool, S., Gurlo, T., Butler, P., Glabe, C.G., 2007. Fibril specific, conformation dependent antibodies recognize a generic epitope common to amyloid fibrils and fibrillar oligomers that is absent in prefibrillar oligomers. Mol. Neurodegener. 2, 18. https://doi.org/10.1186/1750-1326-2-18
Keep, R.F., Xiang, J., Betz, A.L., 1994. Potassium cotransport at the rat choroid plexus. Am. J. Physiol. Physiol. 267, C1616–C1622. https://doi.org/10.1152/ajpcell.1994.267.6.C1616
Kennedy, M.E., Stamford, A.W., Chen, X., Cox, K., Cumming, J.N., Dockendorf, M.F., Egan, M., Ereshefsky, L., Hodgson, R.A., Hyde, L.A., Jhee, S., Kleijn, H.J., Kuvelkar, R., Li, W., Mattson, B.A., Mei, H., Palcza, J., Scott, J.D., Tanen, M., Troyer, M.D., Tseng, J.L., Stone, J.A., Parker, E.M., Forman, M.S., 2016. The BACE1 inhibitor verubecestat (MK-8931) reduces CNS β-amyloid in animal models and in Alzheimer's disease patients. Sci. Transl. Med. 8, 363ra150. https://doi.org/10.1126/scitranslmed.aad9704
Kety, S.S., Schmidt, C.F., 1948. The Effects of Altered Arterial Tensions of Carbon Dioxide and Oxygen on Cerebral Blood Flow and Cerebral Oxygen Consumption of Normal Young Men. J. Clin. Invest. 27, 484–492. https://doi.org/10.1172/JCI101995
Key, A., Retzius, G., 1875. Studien in der Anatomie des Nervensystems und des Bindegewebes. Norstedt & Söner.
Kida, S., Pantazis, A., Weller, R.O., 1993. CSF drains directly from the subarachnoid space into nasal lymphatics in the rat. Anatomy, histology and immunological significance. Neuropathol. Appl. Neurobiol. 19, 480–8. https://doi.org/10.1111/j.1365-2990.1993.tb00476.x
Koo, E.H., Sisodia, S.S., Archer, D.R., Martin, L.J., Weidemann, A., Beyreuther, K., Fischer, P., Masters, C.L., Price, D.L., 1990. Precursor of amyloid protein in Alzheimer disease undergoes fast anterograde axonal transport. Proc. Natl. Acad. Sci. U. S. A. 87, 1561–5.
Koo, E.H., Squazzo, S.L., 1994. Evidence that production and release of amyloid beta-protein involves the endocytic pathway. J. Biol. Chem. 269, 17386–9.
Kress, B.T., Iliff, J.J., Xia, M., Wang, M., Wei, H.S., Zeppenfeld, D., Xie, L., Kang, H., Xu, Q., Liew, J.A., Plog, B.A., Ding, F., Deane, R., Nedergaard, M., 2014. Impairment of paravascular clearance pathways in the aging brain. Ann. Neurol. 76, 845–861. https://doi.org/10.1002/ana.24271

Lai, F., Williams, R.S., 1989. A Prospective Study of Alzheimer Disease in Down Syndrome. Arch. Neurol. 46, 849–853. https://doi.org/10.1001/archneur.1989.00520440031017
Lam, M.A., Hemley, S.J., Najafi, E., Vella, N.G.F., Bilston, L.E., Stoodley, M.A., 2017. The ultrastructure of spinal cord perivascular spaces: Implications for the circulation of cerebrospinal fluid. Sci. Rep. 7, 12924. https://doi.org/10.1038/s41598-017-13455-4
Leak, L. V, Burke, J.F., 1968. Ultrastructural studies on the lymphatic anchoring filaments. J. Cell Biol. 36, 129–49.
Lee, H., Xie, L., Yu, M., Kang, H., Feng, T., Deane, R., Logan, J., Nedergaard, M., Benveniste, H., 2015. The Effect of Body Posture on Brain Glymphatic Transport. J. Neurosci. 35, 11034–44. https://doi.org/10.1523/JNEUROSCI.1625-15.2015
Leston, J., Harthé, C., Brun, J., Mottolese, C., Mertens, P., Sindou, M., Claustrat, B., 2010. Melatonin is released in the third ventricle in humans. A study in movement disorders. Neurosci. Lett. 469, 294–297. https://doi.org/10.1016/j.neulet.2009.12.008
Li, S., Jin, M., Koeglsperger, T., Shepardson, N.E., Shankar, G.M., Selkoe, D.J., 2011. Soluble Amyloid Beta Oligomers Inhibit Long-Term Potentiation through a Mechanism Involving Excessive Activation of Extrasynaptic NR2B-Containing NMDA Receptors. J. Neurosci. 31, 6627–6638. https://doi.org/10.1523/JNEUROSCI.0203-11.2011
Lichtenthaler, S.F., 2012. Alpha-secretase cleavage of the amyloid precursor protein: proteolysis regulated by signaling pathways and protein trafficking. Curr. Alzheimer Res. 9, 165–77.
Liu, C.-C., Hu, J., Zhao, N., Wang, J., Wang, N., Cirrito, J.R., Kanekiyo, T., Holtzman, D.M., Bu, G., 2017. Astrocytic LRP1 Mediates Brain Aβ Clearance and Impacts Amyloid Deposition. J. Neurosci. 37, 4023–4031. https://doi.org/10.1523/JNEUROSCI.3442-16.2017
Liu, P., Paulson, J.B., Forster, C.L., Shapiro, S.L., Ashe, K.H., Zahs, K.R., 2015. Characterization of a Novel Mouse Model of Alzheimer's Disease—Amyloid Pathology and Unique β-Amyloid Oligomer Profile. PLoS One 10, e0126317. https://doi.org/10.1371/journal.pone.0126317
Lokmic, Z., Ng, E.S., Burton, M., Stanley, E.G., Penington, A.J., Elefanty, A.G., 2015. Isolation of human lymphatic endothelial cells by multi-parameter fluorescence-activated cell sorting. J. Vis. Exp. e52691. https://doi.org/10.3791/52691
Louveau, A., Da Mesquita, S., Kipnis, J., 2016. Lymphatics in Neurological Disorders: A Neuro-Lympho-Vascular Component of Multiple Sclerosis and Alzheimer's Disease? Neuron 91, 957–973. https://doi.org/10.1016/j.neuron.2016.08.027
Louveau, A., Plog, B.A., Antila, S., Alitalo, K., Nedergaard, M., Kipnis, J., 2017. Understanding the functions and relationships of the glymphatic system and meningeal lymphatics. J. Clin. Invest. 127, 3210–3219. https://doi.org/10.1172/JCI90603
Louveau, A., Smirnov, I., Keyes, T.J., Eccles, J.D., Rouhani, S.J., Peske, J.D., Derecki, N.C., Castle, D., Mandell, J.W., Lee, K.S., Harris, T.H., Kipnis, J., 2015. Structural and functional features of central nervous system lymphatic vessels. Nature 523, 337–341. https://doi.org/10.1038/nature14432
Lund, A.W., Medler, T.R., Leachman, S.A., Coussens, L.M., 2016. Lymphatic Vessels, Inflammation, and Immunity in Skin Cancer. Cancer Discov. 6, 22–35. https://doi.org/10.1158/2159-8290.CD-15-0023
Ma, Q., Ineichen, B. V., Detmar, M., Proulx, S.T., 2017. Outflow of cerebrospinal fluid is

predominantly through lymphatic vessels and is reduced in aged mice. Nat. Commun. 8, 1434. https://doi.org/10.1038/s41467-017-01484-6
Ma, Q., Ries, M., Decker, Y., Müller, A., Riner, C., Bücker, A., Fassbender, K., Detmar, M., Proulx, S.T., 2019. Rapid lymphatic efflux limits cerebrospinal fluid flow to the brain. Acta Neuropathol. 137, 151–165. https://doi.org/10.1007/s00401-018-1916-x
Manzoni, T., 1998. The cerebral ventricles, the animal spirits and the dawn of brain localization of function. Arch. Ital. Biol. 136, 103–52.
Markwalder, T.-M., Grolimund, P., Seiler, R.W., Roth, F., Aaslid, R., 1984. Dependency of Blood Flow Velocity in the Middle Cerebral Artery on End-Tidal Carbon Dioxide Partial Pressure—A Transcranial Ultrasound Doppler Study. J. Cereb. Blood Flow Metab. 4, 368–372. https://doi.org/10.1038/jcbfm.1984.54
Massey, C.A., Richerson, G.B., 2017. Isoflurane, ketamine-xylazine, and urethane markedly alter breathing even at subtherapeutic doses. J. Neurophysiol. 118, 2389–2401. https://doi.org/10.1152/jn.00350.2017
Mattsson, N., Zetterberg, H., Hansson, O., Andreasen, N., Parnetti, L., Jonsson, M., Herukka, S.-K., van der Flier, W.M., Blankenstein, M.A., Ewers, M., Rich, K., Kaiser, E., Verbeek, M., Tsolaki, M., Mulugeta, E., Rosén, E., Aarsland, D., Visser, P.J., Schröder, J., Marcusson, J., de Leon, M., Hampel, H., Scheltens, P., Pirttilä, T., Wallin, A., Jönhagen, M.E., Minthon, L., Winblad, B., Blennow, K., 2009. CSF Biomarkers and Incipient Alzheimer Disease in Patients With Mild Cognitive Impairment. JAMA 302, 385. https://doi.org/10.1001/jama.2009.1064
Mawuenyega, K.G., Sigurdson, W., Ovod, V., Munsell, L., Kasten, T., Morris, J.C., Yarasheski, K.E., Bateman, R.J., 2010. Decreased Clearance of CNS -Amyloid in Alzheimer's Disease. Science (80-.). 330, 1774–1774. https://doi.org/10.1126/science.1197623
Mendoza, E., Schmid-Schönbein, G.W., 2003. A model for mechanics of primary lymphatic valves. J. Biomech. Eng. 125, 407–14.
Mirra, S.S., Heyman, A., McKeel, D., Sumi, S.M., Crain, B.J., Brownlee, L.M., Vogel, F.S., Hughes, J.P., van Belle, G., Berg, L., 1991. The Consortium to Establish a Registry for Alzheimer's Disease (CERAD). Part II. Standardization of the neuropathologic assessment of Alzheimer's disease. Neurology 41, 479–86.
Morita, S., Furube, E., Mannari, T., Okuda, H., Tatsumi, K., Wanaka, A., Miyata, S., 2016. Heterogeneous vascular permeability and alternative diffusion barrier in sensory circumventricular organs of adult mouse brain. Cell Tissue Res. 363, 497–511. https://doi.org/10.1007/s00441-015-2207-7
Morris, A.W.J., Carare, R.O., Schreiber, S., Hawkes, C.A., 2014. The Cerebrovascular Basement Membrane: Role in the Clearance of β-amyloid and Cerebral Amyloid Angiopathy. Front. Aging Neurosci. 6, 251. https://doi.org/10.3389/fnagi.2014.00251
Murphy, V.A., Johanson, C.E., 1989. Alteration of sodium transport by the choroid plexus with amiloride. Biochim. Biophys. Acta 979, 187–92.
Nabeshima, S., Reese, T.S., Landis, D.M.D., Brightman, M.W., 1975. Junctions in the meninges and marginal glia. J. Comp. Neurol. 164, 127–169. https://doi.org/10.1002/cne.901640202
Nag, S., Sarkar, B., Bandyopadhyay, A., Sahoo, B., Sreenivasan, V.K.A., Kombrabail, M., Muralidharan, C., Maiti, S., 2011. Nature of the amyloid-beta monomer and the monomer-oligomer equilibrium. J. Biol. Chem. 286, 13827–33.

https://doi.org/10.1074/jbc.M110.199885
Nagai, T., Bridenbaugh, E.A., Gashev, A.A., 2011. Aging-associated alterations in contractility of rat mesenteric lymphatic vessels. Microcirculation 18, 463–473. https://doi.org/10.1111/j.1549-8719.2011.00107.x
Nicholson, C., Phillips, J.M., 1981. Ion diffusion modified by tortuosity and volume fraction in the extracellular microenvironment of the rat cerebellum. J. Physiol. 321, 225–57.
Nielsen, S., Smith, B.L., Christensen, E.I., Agre, P., 1993. Distribution of the aquaporin CHIP in secretory and resorptive epithelia and capillary endothelia. Proc. Natl. Acad. Sci. U. S. A. 90, 7275–9. https://doi.org/10.1073/PNAS.90.15.7275
Nilsson, C., Lindvall-Axelsson, M., Owman, C., 1992a. Neuroendocrine regulatory mechanisms in the choroid plexus-cerebrospinal fluid system. Brain Res. Brain Res. Rev. 17, 109–138. https://doi.org/10.1016/0165-0173(92)90011-A
Nilsson, C., Stahlberg, F., Thomsen, C., Henriksen, O., Herning, M., Owman, C., 1992b. Circadian variation in human cerebrospinal fluid production measured by magnetic resonance imaging. Am. J. Physiol. Integr. Comp. Physiol. 262, R20–R24. https://doi.org/10.1152/ajpregu.1992.262.1.R20
Noguchi-Shinohara, M., Tokuda, T., Yoshita, M., Kasai, T., Ono, K., Nakagawa, M., El-Agnaf, O.M.A., Yamada, M., 2009. CSF α-synuclein levels in dementia with Lewy bodies and Alzheimer's disease. Brain Res. 1251, 1–6. https://doi.org/10.1016/j.brainres.2008.11.055
Oakley, H., Cole, S.L., Logan, S., Maus, E., Shao, P., Craft, J., Guillozet-Bongaarts, A., Ohno, M., Disterhoft, J., Van Eldik, L., Berry, R., Vassar, R., 2006. Intraneuronal beta-Amyloid Aggregates, Neurodegeneration, and Neuron Loss in Transgenic Mice with Five Familial Alzheimer's Disease Mutations: Potential Factors in Amyloid Plaque Formation. J. Neurosci. 26, 10129–10140. https://doi.org/10.1523/JNEUROSCI.1202-06.2006
Ono, K., Condron, M.M., Teplow, D.B., 2009. Structure-neurotoxicity relationships of amyloid -protein oligomers. Proc. Natl. Acad. Sci. 106, 14745–14750. https://doi.org/10.1073/pnas.0905127106
Oshio, K., Watanabe, H., Song, Y., Verkman, A.S., Manley, G.T., 2005. Reduced cerebrospinal fluid production and intracranial pressure in mice lacking choroid plexus water channel Aquaporin-1. FASEB J. 19, 76–78. https://doi.org/10.1096/fj.04-1711fje
Pappolla, M., Sambamurti, K., Vidal, R., Pacheco-Quinto, J., Poeggeler, B., Matsubara, E., 2014. Evidence for lymphatic Aβ clearance in Alzheimer's transgenic mice. Neurobiol. Dis. 71, 215–219. https://doi.org/10.1016/j.nbd.2014.07.012
Patterson, B.W., Elbert, D.L., Mawuenyega, K.G., Kasten, T., Ovod, V., Ma, S., Xiong, C., Chott, R., Yarasheski, K., Sigurdson, W., Zhang, L., Goate, A., Benzinger, T., Morris, J.C., Holtzman, D., Bateman, R.J., 2015. Age and amyloid effects on human central nervous system amyloid-beta kinetics. Ann. Neurol. 78, 439–453. https://doi.org/10.1002/ana.24454
Petrova, T. V, Karpanen, T., Norrmén, C., Mellor, R., Tamakoshi, T., Finegold, D., Ferrell, R., Kerjaschki, D., Mortimer, P., Ylä-Herttuala, S., Miura, N., Alitalo, K., 2004. Defective valves and abnormal mural cell recruitment underlie lymphatic vascular failure in lymphedema distichiasis. Nat. Med. 10, 974–981. https://doi.org/10.1038/nm1094

Piper, I., 1997. Intracranial Pressure and Elastance, in: Reilly, P., Bullock, R. (Eds.), Head Injury. Chapman & Hall, London, pp. 121–120.
Pizzo, M.E., Wolak, D.J., Kumar, N.N., Brunette, E., Brunnquell, C.L., Hannocks, M.-J., Abbott, N.J., Meyerand, M.E., Sorokin, L., Stanimirovic, D.B., Thorne, R.G., 2018. Intrathecal antibody distribution in the rat brain: surface diffusion, perivascular transport and osmotic enhancement of delivery. J. Physiol. 596, 445–475. https://doi.org/10.1113/JP275105
Podgrabinska, S., Braun, P., Velasco, P., Kloos, B., Pepper, M.S., Skobe, M., Skobe, M., 2002. Molecular characterization of lymphatic endothelial cells. Proc. Natl. Acad. Sci. U. S. A. 99, 16069–74. https://doi.org/10.1073/pnas.242401399
Pollay, M., Curl, F., 1967. Secretion of cerebrospinal fluid by the ventricular ependyma of the rabbit. Am. J. Physiol. Content 213, 1031–1038. https://doi.org/10.1152/ajplegacy.1967.213.4.1031
Pollay, M., Hisey, B., Reynolds, E., Tomkins, P., Stevens, F.A., Smith, R., 1985. Choroid plexus Na+/K+-activated adenosine triphosphatase and cerebrospinal fluid formation. Neurosurgery 17, 768–72.
Praetorius, J., Nejsum, L.N., Nielsen, S., 2004. A SCL4A10 gene product maps selectively to the basolateral plasma membrane of choroid plexus epithelial cells. Am. J. Physiol. Physiol. 286, C601–C610. https://doi.org/10.1152/ajpcell.00240.2003
Proulx, S.T., Ma, Q., Andina, D., Leroux, J.-C., Detmar, M., 2017. Quantitative measurement of lymphatic function in mice by noninvasive near-infrared imaging of a peripheral vein. JCI Insight 2, 362–365. https://doi.org/10.1172/jci.insight.90861
Rak, M., Del Bigio, M.R., Mai, S., Westaway, D., Gough, K., 2007. Dense-core and diffuse Aβ plaques in TgCRND8 mice studied with synchrotron FTIR microspectroscopy. Biopolymers 87, 207–217. https://doi.org/10.1002/bip.20820
Ramanathan, A., Nelson, A.R., Sagare, A.P., Zlokovic, B. V, 2015. Impaired vascular-mediated clearance of brain amyloid beta in Alzheimer's disease: the role, regulation and restoration of LRP1. Front. Aging Neurosci. 7, 136. https://doi.org/10.3389/fnagi.2015.00136
Raper, D., Louveau, A., Kipnis, J., 2016. How Do Meningeal Lymphatic Vessels Drain the CNS? Trends Neurosci. 39, 581–586. https://doi.org/10.1016/j.tins.2016.07.001
Ray, L., Iliff, J.J., Heys, J.J., 2019. Analysis of convective and diffusive transport in the brain interstitium. Fluids Barriers CNS 16. https://doi.org/10.1186/s12987-019-0126-9
Rennels, M.L., Blaumanis, O.R., Grady, P.A., 1990. Rapid solute transport throughout the brain via paravascular fluid pathways. Adv. Neurol. 52, 431–9.
Rennels, M.L., Gregory, T.F., Blaumanis, O.R., Fujimoto, K., Grady, P.A., 1985. Evidence for a 'Paravascular' fluid circulation in the mammalian central nervous system, provided by the rapid distribution of tracer protein throughout the brain from the subarachnoid space. Brain Res. 326, 47–63. https://doi.org/10.1016/0006-8993(85)91383-6
Rhoton, A.L., 2002. The lateral and third ventricles. Neurosurgery 51, S207-71.
Ringstad, G., Vatnehol, S.A.S., Eide, P.K., 2017. Glymphatic MRI in idiopathic normal pressure hydrocephalus. Brain 140, 2691–2705. https://doi.org/10.1093/brain/awx191
Rinne, J.O., Brooks, D.J., Rossor, M.N., Fox, N.C., Bullock, R., Klunk, W.E., Mathis, C.A., Blennow, K., Barakos, J., Okello, A.A., de LIano, S.R.M., Liu, E., Koller, M., Gregg, K.M., Schenk, D., Black, R., Grundman, M., 2010. 11C-PiB PET assessment of change in fibrillar amyloid-β load in patients with Alzheimer's disease treated with

bapineuzumab: a phase 2, double-blind, placebo-controlled, ascending-dose study. Lancet Neurol. 9, 363–372. https://doi.org/10.1016/S1474-4422(10)70043-0
Rivera, B., Miller, S.R., Brown, E.M., 2005. A Novel Method for Endotracheal Intubation of Mice 44, 3–6.
Roh, D., Merkler, A.E., Al-Mufti, F., Morris, N., Agarwal, S., Claassen, J., Park, S., 2016. Global cerebral edema from hypercapnic respiratory acidosis and response to hyperosmolar therapy. Neurology 86, 1556–8. https://doi.org/10.1212/WNL.0000000000002584
Roh, J.H., Huang, Y., Bero, A.W., Kasten, T., Stewart, F.R., Bateman, R.J., Holtzman, D.M., 2012. Disruption of the sleep-wake cycle and diurnal fluctuation of β-amyloid in mice with Alzheimer's disease pathology. Sci. Transl. Med. 4, 150ra122. https://doi.org/10.1126/scitranslmed.3004291
Román, G.C., Verma, A.K., Zhang, Y.J., Fung, S.H., 2018. Idiopathic normal-pressure hydrocephalus and obstructive sleep apnea are frequently associated: A prospective cohort study. J. Neurol. Sci. 395, 164–168. https://doi.org/10.1016/j.jns.2018.10.005
Rosenberg, G.A., Kyner, W.T., 1980. Gray and white matter brain-blood transfer constants by steady-state tissue clearance in cat. Brain Res. 193, 59–66.
Rosenberg, G.A., Kyner, W.T., Estrada, E., 1980. Bulk flow of brain interstitial fluid under normal and hyperosmolar conditions. Am. J. Physiol. Physiol. 238, F42–F49. https://doi.org/10.1152/ajprenal.1980.238.1.F42
Rothe, C.F., Maass-Moreno, R., Flanagan, A.D., 1990. Effects of hypercapnia and hypoxia on the cardiovascular system: vascular capacitance and aortic chemoreceptors. Am. J. Physiol. Circ. Physiol. 259, H932–H939. https://doi.org/10.1152/ajpheart.1990.259.3.h932
Rusanen, M., Ngandu, T., Laatikainen, T., Tuomilehto, J., Soininen, H., Kivipelto, M., 2013. Chronic obstructive pulmonary disease and asthma and the risk of mild cognitive impairment and dementia: a population based CAIDE study. Curr. Alzheimer Res. 10, 549–55.
Salloway, S., Sperling, R., Fox, N.C., Blennow, K., Klunk, W., Raskind, M., Sabbagh, M., Honig, L.S., Porsteinsson, A.P., Ferris, S., Reichert, M., Ketter, N., Nejadnik, B., Guenzler, V., Miloslavsky, M., Wang, D., Lu, Y., Lull, J., Tudor, I.C., Liu, E., Grundman, M., Yuen, E., Black, R., Brashear, H.R., 2014. Two Phase 3 Trials of Bapineuzumab in Mild-to-Moderate Alzheimer's Disease. N. Engl. J. Med. 370, 322–333. https://doi.org/10.1056/NEJMoa1304839
Sato, O., Asai, T., Amano, Y., Hara, M., Tsugane, R., Yagi, M., 1972. Extraventricular origin of the cerebrospinal fluid: formation rate quantitatively measured in the spinal subarachnoid space of dogs. J. Neurosurg. 36, 276–282. https://doi.org/10.3171/jns.1972.36.3.0276
Schubert, J.J., Veronese, M., Marchitelli, L., Bodini, B., Tonietto, M., Stankoff, B., Brooks, D.J., Bertoldo, A., Edison, P., Turkheimer, F., 2019. Dynamic 11C-PiB PET shows cerebrospinal fluid flow alterations in Alzheimer's disease and multiple sclerosis. J. Nucl. Med. jnumed.118.223834. https://doi.org/10.2967/jnumed.118.223834
Scott, D., Krobisch-Dudley, G., Paull, W., Kozlowski, G., 1977. The ventricular system in neuroendocrine mechanisms. Cell Tissue Res. 179, 235–254. https://doi.org/10.1007/BF00219799
Selkoe, D.J., 2001a. Alzheimer's disease results from the cerebral accumulation and

cytotoxicity of amyloid beta-protein. J. Alzheimers. Dis. 3, 75–80.
Selkoe, D.J., 2001b. Alzheimer's Disease: Genes, Proteins, and Therapy. Physiol. Rev. 81, 741–766. https://doi.org/10.1152/physrev.2001.81.2.741
Serra-Batiste, M., Ninot-Pedrosa, M., Bayoumi, M., Gairí, M., Maglia, G., Carulla, N., 2016. Aβ42 assembles into specific β-barrel pore-forming oligomers in membrane-mimicking environments. Proc. Natl. Acad. Sci. U. S. A. 113, 10866–71. https://doi.org/10.1073/pnas.1605104113
Shabo, A., Maxwell, D., 1968. The Morphology of the Arachnoid Villi: A Light and Electron Microscopic Study in the Monkey. J. Neurosurg. 29, 451–463.
Sharifi, M., Ciołkowski, M., Krajewski, P., Ciszek, B., 2005. The choroid plexus of the fourth ventricle and its arteries. Folia Morphol. (Warsz). 64, 194–8.
Shibata, H., Saitoh, Y., Takahashi, H., Okubo, T., 1976. The apparent buffer value of cerebrospinal fluid in acute hypercapnia. Bull. Eur. Physiopathol. Respir. 12, 297–315.
Skinner, D.C., Malpaux, B., 1999. High Melatonin Concentrations in Third Ventricular Cerebrospinal Fluid Are Not due to Galen Vein Blood Recirculating through the Choroid Plexus [1]. Endocrinology 140, 4399–4405. https://doi.org/10.1210/endo.140.10.7074
Smith, A.J., Yao, X., Dix, J.A., Jin, B.-J., Verkman, A.S., 2017. Test of the "glymphatic" hypothesis demonstrates diffusive and aquaporin-4-independent solute transport in rodent brain parenchyma. Elife 6. https://doi.org/10.7554/eLife.27679
Stinson, D.A., Taylor, P.M., Rees, E.P., Boonyaprakob, U., 1977. Hypercapnia and right-duct lymph flow in pups and adult dogs. Am. J. Physiol. Circ. Physiol. 232, H236–H240. https://doi.org/10.1152/ajpheart.1977.232.3.H236
Storck, S.E., Meister, S., Nahrath, J., Meißner, J.N., Schubert, N., Di Spiezio, A., Baches, S., Vandenbroucke, R.E., Bouter, Y., Prikulis, I., Korth, C., Weggen, S., Heimann, A., Schwaninger, M., Bayer, T.A., Pietrzik, C.U., 2015. Endothelial LRP1 transports amyloid-β1–42 across the blood-brain barrier. J. Clin. Invest. 126, 123–136. https://doi.org/10.1172/JCI81108
Swanson, A.G., Rosengren, H., 1962. Cerebrospinal fluid buffering during acute experimental respiratory acidosis. J. Appl. Physiol. 17, 812–814. https://doi.org/10.1152/jappl.1962.17.5.812
Sweet, W.H., Selverstone, B., Soloway, S., Stetten, D., 1950. Studies of formation, flow and absorption of cerebrospinal fluid. II. Studies with heavy water in the normal man. Surg. Forum 376–81.
Sweetman, B., Linninger, A.A., 2011. Cerebrospinal Fluid Flow Dynamics in the Central Nervous System. Ann. Biomed. Eng. 39, 484–496. https://doi.org/10.1007/s10439-010-0141-0
Tarasoff-Conway, J.M., Carare, R.O., Osorio, R.S., Glodzik, L., Butler, T., Fieremans, E., Axel, L., Rusinek, H., Nicholson, C., Zlokovic, B. V, Frangione, B., Blennow, K., Ménard, J., Zetterberg, H., Wisniewski, T., de Leon, M.J., 2015. Clearance systems in the brain-implications for Alzheimer disease. Nat. Rev. Neurol. 11, 457–70. https://doi.org/10.1038/nrneurol.2015.119
Thorne, R.G., Lakkaraju, A., Rodriguez-Boulan, E., Nicholson, C., 2008. In vivo diffusion of lactoferrin in brain extracellular space is regulated by interactions with heparan sulfate. Proc. Natl. Acad. Sci. U. S. A. 105, 8416–21. https://doi.org/10.1073/pnas.0711345105

Thorne, R.G., Nicholson, C., 2006. In vivo diffusion analysis with quantum dots and dextrans predicts the width of brain extracellular space. Proc. Natl. Acad. Sci. 103, 5567–5572. https://doi.org/10.1073/pnas.0509425103

Tomlinson, J.J., Shutinoski, B., Dong, L., Meng, F., Elleithy, D., Lengacher, N.A., Nguyen, A.P., Cron, G.O., Jiang, Q., Roberson, E.D., Nussbaum, R.L., Majbour, N.K., El-Agnaf, O.M., Bennett, S.A., Lagace, D.C., Woulfe, J.M., Sad, S., Brown, E.G., Schlossmacher, M.G., 2017. Holocranohistochemistry enables the visualization of α-synuclein expression in the murine olfactory system and discovery of its systemic anti-microbial effects. J. Neural Transm. 124, 721–738. https://doi.org/10.1007/s00702-017-1726-7

Tourtelloutte, W., 1968. Pathology of the Nervous System I. McGraw-Hill Book Co.: New York.

Trumbore, C.N., 2016. Shear-Induced Amyloid Formation in the Brain: I. Potential Vascular and Parenchymal Processes. J. Alzheimer's Dis. 54, 457–470. https://doi.org/10.3233/JAD-160027

Trzewik, J., Mallipattu, S.K., Artmann, G.M., Delano, F.A., Schmid-Schönbein, G.W., 2001. Evidence for a second valve system in lymphatics: endothelial microvalves. FASEB J. 15, 1711–7.

Tubbs, R.S., Louis, R.G., Wartmann, C.T., Loukas, M., Shoja, M.M., Apaydin, N., Oakes, W.J., 2008. The velum interpositum revisited and redefined. Surg. Radiol. Anat. 30, 131–135. https://doi.org/10.1007/s00276-007-0293-2

Tully, H.M., Dobyns, W.B., 2014. Infantile hydrocephalus: A review of epidemiology, classification and causes. Eur. J. Med. Genet. 57, 359–368. https://doi.org/10.1016/j.ejmg.2014.06.002

Uldall, M., Botfield, H., Jansen-Olesen, I., Sinclair, A., Jensen, R., 2017. Acetazolamide lowers intracranial pressure and modulates the cerebrospinal fluid secretion pathway in healthy rats. Neurosci. Lett. 645, 33–39. https://doi.org/10.1016/j.neulet.2017.02.032

Unno, N., Tanaka, H., Suzuki, M., Yamamoto, N., Mano, Y., Sano, M., Saito, T., Konno, H., 2011. INFLUENCE OF AGE AND GENDER ON HUMAN LYMPHATIC PUMPING PRESSURE IN THE LEG. Lymphology 44, 113–120.

Upton, M., Weller, R., 1985. The morphology of cerebrospinal fluid drainage pathways in human arachnoid granulations. J. Neurosurg. 63, 867–875.

Vandenabeele, F., Creemers, J., Lambrichts, I., 1996. Ultrastructure of the human spinal arachnoid mater and dura mater, J. Anat.

Vassar, R., Bennett, B.D., Babu-Khan, S., Kahn, S., Mendiaz, E.A., Denis, P., Teplow, D.B., Ross, S., Amarante, P., Loeloff, R., Luo, Y., Fisher, S., Fuller, J., Edenson, S., Lile, J., Jarosinski, M.A., Biere, A.L., Curran, E., Burgess, T., Louis, J.C., Collins, F., Treanor, J., Rogers, G., Citron, M., 1999. Beta-secretase cleavage of Alzheimer's amyloid precursor protein by the transmembrane aspartic protease BACE. Science 286, 735–41. https://doi.org/10.1126/SCIENCE.286.5440.735

Vastola, E.F., 1980. CSF Formation and Absorption Estimates by Constant Flow Infusion Method. Arch. Neurol. 37, 150–154. https://doi.org/10.1001/archneur.1980.00500520048007

Veikkola, T., Jussila, L., Makinen, T., Karpanen, T., Jeltsch, M., Petrova, T. V., Kubo, H., Thurston, G., McDonald, D.M., Achen, M.G., Stacker, S.A., Alitalo, K., 2001. Signalling via vascular endothelial growth factor receptor-3 is sufficient for

lymphangiogenesis in transgenic mice. EMBO J. 20, 1223–1231. https://doi.org/10.1093/emboj/20.6.1223
Venegas, C., Kumar, S., Franklin, B.S., Dierkes, T., Brinkschulte, R., Tejera, D., Vieira-Saecker, A., Schwartz, S., Santarelli, F., Kummer, M.P., Griep, A., Gelpi, E., Beilharz, M., Riedel, D., Golenbock, D.T., Geyer, M., Walter, J., Latz, E., Heneka, M.T., 2017. Microglia-derived ASC specks cross-seed amyloid-β in Alzheimer's disease. Nature 552, 355–361. https://doi.org/10.1038/nature25158
Wagshul, M.E., Eide, P.K., Madsen, J.R., 2011. The pulsating brain: A review of experimental and clinical studies of intracranial pulsatility. Fluids Barriers CNS 8, 5. https://doi.org/10.1186/2045-8118-8-5
Walsh, D.M., Klyubin, I., Fadeeva, J. V., Cullen, W.K., Anwyl, R., Wolfe, M.S., Rowan, M.J., Selkoe, D.J., 2002. Naturally secreted oligomers of amyloid β protein potently inhibit hippocampal long-term potentiation in vivo. Nature 416, 535–539. https://doi.org/10.1038/416535a
Wang, L., Zhang, Y., Zhao, Y., Marshall, C., Wu, T., Xiao, M., 2019. Deep cervical lymph node ligation aggravates AD-like pathology of APP/PS1 mice. Brain Pathol. 29, 176–192. https://doi.org/10.1111/bpa.12656
Wang, M., Ding, F., Deng, S., Guo, X., Wang, W., Iliff, J.J., Nedergaard, M., 2017. Focal Solute Trapping and Global Glymphatic Pathway Impairment in a Murine Model of Multiple Microinfarcts. J. Neurosci. 37, 2870–2877. https://doi.org/10.1523/JNEUROSCI.2112-16.2017
Weed, L.H., 1938. Meninges and Cerebrospinal Fluid. J. Anat. 72, 181–215.
Weed, L.H., 1917. An anatomical consideration of the cerebro-spinal fluid. Anat. Rec. 12, 461–496. https://doi.org/10.1002/ar.1090120405
Weed, L.H., 1914a. Studies on Cerebro-Spinal Fluid. No. III : The pathways of escape from the Subarachnoid Spaces with particular reference to the Arachnoid Villi. J. Med. Res. 31, 51–91.
Weed, L.H., 1914b. Studies on Cerebro-Spinal Fluid. No. II : The Theories of Drainage of Cerebro-Spinal Fluid with an Analysis of the Methods of Investigation. J. Med. Res. 31, 21–49.
Weller, R.O., Subash, M., Preston, S.D., Mazanti, I., Carare, R.O., 2007. SYMPOSIUM: Clearance of Aβ from the Brain in Alzheimer's Disease: Perivascular Drainage of Amyloid-β Peptides from the Brain and Its Failure in Cerebral Amyloid Angiopathy and Alzheimer's Disease. Brain Pathol. 18, 253–266. https://doi.org/10.1111/j.1750-3639.2008.00133.x
Willis, C.L., Garwood, C.J., Ray, D.E., 2007. A size selective vascular barrier in the rat area postrema formed by perivascular macrophages and the extracellular matrix. Neuroscience 150, 498–509. https://doi.org/10.1016/j.neuroscience.2007.09.023
Wisniewski, K.E., Wisniewski, H.M., Wen, G.Y., 1985. Occurrence of neuropathological changes and dementia of Alzheimer's disease in Down's syndrome. Ann. Neurol. 17, 278–282. https://doi.org/10.1002/ana.410170310
Xie, L., Kang, H., Xu, Q., Chen, M.J., Liao, Y., Thiyagarajan, M., O'Donnell, J., Christensen, D.J., Nicholson, C., Iliff, J.J., Takano, T., Deane, R., Nedergaard, M., 2013. Sleep Drives Metabolite Clearance from the Adult Brain. Science (80-.). 342, 373–377. https://doi.org/10.1126/science.1241224
Xu, Z., Xiao, N., Chen, Y., Huang, H., Marshall, C., Gao, J., Cai, Z., Wu, T., Hu, G., Xiao,

M., 2015. Deletion of aquaporin-4 in APP/PS1 mice exacerbates brain Aβ accumulation and memory deficits. Mol. Neurodegener. 10, 58. https://doi.org/10.1186/s13024-015-0056-1

Yang, B., Treweek, J.B., Kulkarni, R.P., Deverman, B.E., Chen, C.-K., Lubeck, E., Shah, S., Cai, L., Gradinaru, V., 2014. Single-Cell Phenotyping within Transparent Intact Tissue through Whole-Body Clearing. https://doi.org/10.1016/j.cell.2014.07.017

Yang, L., Kress, B.T., Weber, H.J., Thiyagarajan, M., Wang, B., Deane, R., Benveniste, H., Iliff, J.J., Nedergaard, M., 2013. Evaluating glymphatic pathway function utilizing clinically relevant intrathecal infusion of CSF tracer. J. Transl. Med. 11, 107. https://doi.org/10.1186/1479-5876-11-107

Yuede, C.M., Lee, H., Restivo, J.L., Davis, T.A., Hettinger, J.C., Wallace, C.E., Young, K.L., Hayne, M.R., Bu, G., Li, C.-Z., Cirrito, J.R., 2016. Rapid in vivo measurement of β-amyloid reveals biphasic clearance kinetics in an Alzheimer's mouse model. J. Exp. Med. 213, 677–85. https://doi.org/10.1084/jem.20151428

Zakharov, A., Papaiconomou, C., Koh, L., Djenic, J., Bozanovic-Sosic, R., Johnston, M., 2004. Integrating the roles of extracranial lymphatics and intracranial veins in cerebrospinal fluid absorption in sheep. Microvasc. Res. 67, 96–104. https://doi.org/10.1016/j.mvr.2003.08.004

Zawieja, D.C., Barber, B.J., 1987. Lymph protein concentration in initial and collecting lymphatics of the rat. Am. J. Physiol. 252, G602-6. https://doi.org/10.1152/ajpgi.1987.252.5.G602

Zhang, E.T., Inman, C.B., Weller, R.O., 1990. Interrelationships of the pia mater and the perivascular (Virchow-Robin) spaces in the human cerebrum. J. Anat. 170, 111–23.

Zhang, Y., Chen, K., Sloan, S.A., Bennett, M.L., Scholze, A.R., O'Keeffe, S., Phatnani, H.P., Guarnieri, P., Caneda, C., Ruderisch, N., Deng, S., Liddelow, S.A., Zhang, C., Daneman, R., Maniatis, T., Barres, B.A., Wu, J.Q., 2014. An RNA-sequencing transcriptome and splicing database of glia, neurons, and vascular cells of the cerebral cortex. J. Neurosci. 34, 11929–47. https://doi.org/10.1523/JNEUROSCI.1860-14.2014

Zhu, X., Bergles, D.E., Nishiyama, A., 2007. NG2 cells generate both oligodendrocytes and gray matter astrocytes. Development 135, 145–157. https://doi.org/10.1242/dev.004895

Zlokovic, B. V, Mackic, J.B., Wang, L., McComb, J.G., McDonough, A., 1993. Differential expression of Na,K-ATPase alpha and beta subunit isoforms at the blood-brain barrier and the choroid plexus. J. Biol. Chem. 268, 8019–8025.

Zohdi, A., Elkheshin, S., 2012. Endoscopic anatomy of the velum interpositum: A sequential descriptive anatomical study. Asian J. Neurosurg. 7, 12–6. https://doi.org/10.4103/1793-5482.95689